

FACILE ROUTE TO PURIFICATION AND SEPARATION OF HIGH ASPECT RATIO
SINGLE-WALLED CARBON NANOTUBES AND IT'S APPLICATIONS IN
ELECTRONICS

by

NIDHI BHATT

(Under the Direction of Marcus D. Lay)

ABSTRACT

The work presented herein develops a new method for purification and separation of high aspect ratio single-walled carbon nanotubes (SWNTs). Regardless of the growth methods, purification of SWNTs is required to enhance their properties especially in electronics. By forming SWNT network, the electrical properties of metallic tubes and semiconducting tubes can be tuned in a device by changing the density of the network. This dissertation discusses different purification techniques and its application in electronics using self-assembled monolayers (SAMs).

The first part demonstrates a new technique of bulk purification and enrichment of SWNTs with average lengths in excess of $2\mu\text{m}$ by using iterative cycles at low g centrifugation. The effect of processing time on the purification of as produced (AP) soot by density gradient was discussed. Scanning and spectroscopic probe studies show non-destructive, non-oxidizing purification methods are effective in order to obtain unbundled, high aspect ratio SWNTs. The second part discusses the effect of sucrose density gradient on the purity and length of SWNTs. A single step purification using sucrose gradient showed similar level of purification with higher yield as

compared to the iterative cycles. Finally, the formation of SWNT network by Laminar Flow Deposition (LFD) was investigated by depositing carbon nanotubes on different self-assembled monolayers. SWNT network with aminosilanes favor semiconducting nanotubes, whereas phenyl terminated silanes favor metallic nanotubes. This was confirmed by transistor response curves showing higher I_{on}/I_{off} ratios for aminosilanes vs. lower I_{on}/I_{off} ratios for phenyl terminated silane.

INDEX WORDS: Single-walled Carbon Nanotube (SWNT), Sodium dodecyl sulfate (SDS), sonication, centrifugation, purification, sucrose density gradient, Laminar Flow Deposition (LFD), network density, Atomic Force Microscopy, Raman Microscopy, Metal Vapor Deposition, Field-effect transistor, Self-assembled monolayers (SAMs).

FACILE ROUTE TO PURIFICATION AND SEPARATION OF HIGH ASPECT RATIO
SINGE-WALLED CARBON NANOTUBES AND IT'S APPLICATIONS IN ELECTRONICS

by

NIDHI BHATT

BS in Chemistry, University of Georgia, USA, 2010

A Dissertation Submitted to the Graduate Faculty of The University of Georgia in Partial

Fulfillment of the Requirements for the Degree

DOCTOR OF PHILOSOPHY

ATHENS, GEORGIA

2016

© 2016

Nidhi Bhatt

All Rights Reserved

FACILE ROUTE TO PURIFICATION AND SEPARATION OF HIGH ASPECT RATIO
SINGE-WALLED CARBON NANOTUBES AND IT'S APPLICATIONS IN ELECTRONICS

by

NIDHI BHATT

Major Professor: Marcus D. Lay
Committee: Tina Salguero
Jin Xie

Electronic Version Approved:

Suzanne Barbour
Dean of the Graduate School
The University of Georgia
May 2016

DEDICATION

To my parents

ACKNOWLEDGEMENTS

I would like to thank and acknowledge my parents for their unconditional support and assistance throughout my academic career. I would also like to express my gratitude to my major professor, Dr. Marcus D. Lay for his guidance, assistance, support, encouragement, and giving me the opportunity to explore the world of single-walled carbon nanotubes. Without him, none of this would have been possible. I would like to thank my other committee members, Dr. Tina Salguero and Dr. Jin Xie for serving on my committee, and for all of their inputs and advice. I would like to thank all of the current and former members of Lay Research group for providing constant motivation to work harder. I would like to thank my family and friends for their support. Lastly, I would like to thank The University of Georgia for offering me this opportunity to pursue and to obtain the degree of Doctorate of Philosophy within the Chemistry Department.

TABLE OF CONTENTS

	Page
ACKNOWLEDGEMENTS	v
LIST OF TABLES	viii
LIST OF FIGURES	ix
CHAPTER	
1 INTRODUCTION AND LITERATURE REVIEW	1
2 BULK PURIFICATION AND DEPOSITON METHODS FOR SELECTIVE ENRICHMENT OF HIGH ASPECT SINGLE-WALLED CARBON NANOTUBES	35
2.1 ABSTRACT.....	36
2.2 INTRODUCTION	37
2.3 EXPERIMENTAL PROCEDURE.....	41
2.4 RESULTS AND DISCUSSION.....	44
2.5 CONCLUSIONS.....	51
2.6 REFERENCES	67
3 EFFECT OF SUCROSE GRADIENT ON THE LENGTH, DENISTY, AND PURITY OF SINGLE-WALLED CARBON NANOTUBES.....	72
3.1 ABSTRACT.....	73
3.2 INTRODUCTION	74
3.3 EXPERIMENTAL PROCEDURE	77

3.3	RESULTS AND DISCUSSION	79
3.4	CONCLUSIONS.....	86
3.5	REFERENCES	88
4	EFFECT OF SELF-ASSEMBLED MONOLAYERS (SAMs) ON ELECTRICAL PROPERTIES OF SINGLE-WALLED CARBON NANOTUBE NETWORK.....	120
4.1	ABSTRACT.....	121
4.2	INTRODUCTION	122
4.3	EXPERIMENTAL PROCEDURE.....	124
4.4	RESULTS AND DISCUSSION.....	127
4.5	CONCLUSIONS.....	132
4.6	REFERENCES	133
5	EFFECT OF SONICATION ENERGY ON AQUEOUS SUSPENSIONS OF SINGLE WALED CARBON NANOTUBES (SWNTs)	149
5.1	ABSTRACT.....	150
5.2	INTRODUCTION	151
5.3	EXPERIMENTAL PROCEDURE.....	153
5.4	RESULTS AND DISCUSSION.....	155
5.5	CONCLUSIONS.....	157
5.6	REFERENCES	159
6	CONCLUSIONS AND FUTURE WORK.....	166
6.1	CONCLUSIONS.....	167
6.2	FUTURE WORK.....	169

LIST OF TABLES

	Page
Table 2.1: AFM analysis of the effect of iterative processing steps on low-density SWNT deposits	65
Table 3.1: I_G/I_D ratios of SWNT deposits and suspension at 1mg/mL	103
Table 3.2: I_G/I_D ratios of SWNT deposits and suspension at 0.5mg/mL	104
Table 3.3: I_G/I_D ratios of SWNT deposits and suspension at 0.1mg/mL	105
Table 3.4a: AFM analysis of sucrose density gradients at 1mg/mL	118
Table 3.4b: AFM analysis of sucrose density gradients at 0.5mg/mL	118
Table 3.4c: AFM analysis of sucrose density gradients at 0.1mg/mL	119
Table 4.1: Average I_G/I_D ratios for SWNT suspensions using different SAMs	145
Table 4.2: Average I_G/I_D ratios for SWNT deposits and suspensions at varying pH	146
Table 4.3: AFM analysis of the effect of SAMs on low density SWNT network	147
Table 4.4: AFM analysis and I_{on}/I_{off} ratios for different SAMs	148
Table 5.1: I_G/I_D ratios of SWNT deposit at different sonication power	164

LIST OF FIGURES

	Page
Figure 1.1: Schematic representation of single graphene layer	21
Figure 1.2: Schematic representation of SWNT chirality.....	22
Figure 1.3: Schematic of an electric-arc discharge chamber	23
Figure 1.4: Schematic of laser ablation technique	24
Figure 1.5: Schematic of Chemical Vapor Deposition apparatus.....	25
Figure 1.6: Schematic Diagram for synthesizing HiPCO carbon nanotubes.....	26
Figure 1.7a-b: TEM images of SWNTs before purification	27
Figure 1.7c-d: TEM images of SWNTs after two purification cycles	27
Figure 1.8: Schematic representation of Self-assembled monolayer (SAM) structure	28
Figure 2.1a: Schematic for experimental approach for suspensions treated with centrifugation at 18,000G for 45 or 90min	52
Figure 2.1b: Schematic for experimental approach where upper 50% supernatant was removed after six 45min centrifugation cycles	52
Figure 2.1c: Low densities of unbundled SWNTs deposited via rapid evaporation	52
Figure 2.2a: The absorbance in UV region for aliquots after one 45 min step.....	54
Figure 2.2b: The absorbance in UV region for aliquots after one 90 min step.....	54
Figure 2.3a: NIR spectra for semiconducting SWNTs for aliquots for 45 min step	55
Figure 2.3b: NIR spectra for semiconducting SWNTs for aliquots for 90 min step	55
Figure 2.4: Relative assessment of purity of SWNTs at 45 min and 90 min	57

Figure 2.5a: Representative Raman spectra obtained after 90 min processing periods for SWNT suspensions	58
Figure 2.5b: Representative Raman spectra obtained after 90 min processing periods for SWNT deposits	58
Figure 2.6a: Average I_G/I_D ratios for SWNT suspensions and deposits at 45 min	59
Figure 2.6b: Average I_G/I_D ratios for SWNT suspensions and deposits at 90 min	59
Figure 2.7 a-b: AFM images for SWNT deposits at 45 min for aliquots A and E respectively ...	60
Figure 2.7 c-d: AFM images for SWNT deposits at 90 min for aliquots A and E respectively ...	60
Figure 2.8: RMS roughness values for 45 and 90 min processing times	61
Figure 2.9: Relative purity of SWNTs for iterative cycles	62
Figure 2.10a: AFM image for deposits formed from an unprocessed suspension.....	63
Figure 2.10b: AFM image for deposits formed after first processing iteration	63
Figure 2.10c: AFM image for deposits formed after third processing iteration	63
Figure 2.10d: AFM image for deposits formed after sixth processing suspension	63
Figure 2.11: Raman I_G/I_D ratios for suspensions and deposits over six processing iterations.....	66
Figure 3.1: Schematic showing sucrose density gradient with SWNT suspension centrifuged at 10,000G for 60 min.....	91
Figure 3.2a: Absorbance in UV region at 1mg/mL concentration from 5% to 25%	92
Figure 3.2b: Absorbance in NIR region at 1mg/mL concentration from 5% to 25%.....	92
Figure 3.3a: Absorbance in UV region at 0.5mg/mL concentration from 5% to 25%	93
Figure 3.3b: Absorbance in NIR region at 0.5mg/mL concentration from 5% to 25%.....	93
Figure 3.4a: Absorbance in UV region at 0.1mg/mL concentration from 5% to 25%	94
Figure 3.4b: Absorbance in NIR region at 0.1mg/mL concentration from 5% to 25%.....	94

Figure 3.5a: NIR spectra showing M_{11} transitions at 1mg/mL SWNT concentration.....95

Figure 3.5b: NIR spectra showing M_{11} transitions at 0.5mg/mL SWNT concentration.....95

Figure 3.5c: NIR spectra showing M_{11} transitions at 0.1mg/mL SWNT concentration.....96

Figure 3.6a: UV-vis spectra with sucrose and SDS (5%-25%) at 1mg/mL.....97

Figure 3.6b: NIR spectra with sucrose and SDS (5%-25%) at 1mg/mL97

Figure 3.7a: UV-vis spectra with sucrose and SDS (15%-25%) at 1mg/mL.....98

Figure 3.7b: NIR spectra with sucrose and SDS (15%-75%) at 1mg/mL98

Figure 3.8a: Effect of SWNT concentration at 5%-25% with SDS and water at 1mg/mL99

Figure 3.8b: Effect of SWNT concentration at 5%-25% with SDS and water at 0.5mg/mL99

Figure 3.8c: Effect of SWNT concentration at 5%-25% with SDS and water at 0.1mg/mL100

Figure 3.9a: Effect of SWNT concentration at 15%-75% with SDS and water at 1mg/mL101

Figure 3.9b: Effect of SWNT concentration at 15%-75% with SDS and water at 0.5mg/mL ...101

Figure 3.9c: Effect of SWNT concentration at 15%-75% with SDS and water at 0.1mg/mL ...102

Figure 3.10a: RBM spectra for sucrose density 5%-25% at 1mg/mL106

Figure 3.10b: RBM spectra for sucrose density 5%-25% at 0.5mg/mL106

Figure 3.10c: RBM spectra for sucrose density 5%-25% at 0.1mg/mL107

Figure 3.11a: RBM spectra indicating peak shifts for 5% at 1, 0.5, and 0.1mg/mL108

Figure 3.11b: RBM spectra indicating peak shifts for 20% at 1, 0.5, and 0.1mg/mL108

Figure 3.11c: RBM spectra indicating peak shifts for bottom layer at 1, 0.5, and 0.1mg/mL109

Figure 3.12a: AFM image for SWNTs with sucrose and water at 1mg/mL at 5%.....110

Figure 3.12b: AFM image for SWNTs with sucrose and water at 1mg/mL at 15%110

Figure 3.12a: AFM image for SWNTs with sucrose and water at 1mg/mL at bottom layer.....110

Figure 3.13a: AFM image for SWNTs with sucrose and water at 0.5mg/mL at 5%.....112

Figure 3.13b: AFM image for SWNTs with sucrose and water at 0.5mg/mL at 15%	112
Figure 3.13c: AFM image for SWNTs with sucrose and water at 0.5mg/mL at bottom layer....	112
Figure 3.14a: AFM image for SWNTs with sucrose and water at 0.1mg/mL at 5%.....	113
Figure 3.14b: AFM image for SWNTs with sucrose and water at 0.1mg/mL at 15%	113
Figure 3.14c: AFM image for SWNTs with sucrose and water at 0.1mg/mL at bottom layer....	113
Figure 3.15a: AFM image for SWNTs with sucrose and SDS at 0.1mg/mL at 5%	114
Figure 3.15b: AFM image for SWNTs with sucrose and SDS at 0.1mg/mL at 15%	114
Figure 3.15c: AFM image for SWNTs with sucrose and SDS at 0.1mg/mL at bottom layer	114
Figure 3.16a: AFM image for SWNTs with sucrose and SDS at 1mg/mL at 15%	116
Figure 3.16b: AFM image for SWNTs with sucrose and SDS at 1mg/mL at 45%	116
Figure 3.16c: AFM image for SWNTs with sucrose and SDS at 1mg/mL at bottom layer	116
Figure 4.1: Schematic representation of Laminar Flow Deposition of SWNT network	136
Figure 4.2: Schematic representation showing Titanium deposition on Silicon substrate	137
Figure 4.3a: The absorbance in UV region for acid and basic SWNT suspension.....	138
Figure 4.3b: NIR region for semiconducting SWNTs	138
Figure 4.4a: AFM image of pristine SWNT deposit.....	139
Figure 4.4b: AFM image of acidic SWNT deposit.....	139
Figure 4.4c: AFM image of basic SWNT deposit	139
Figure 4.5a: AFM image of pristine SWNT suspension on OTS substrate.....	140
Figure 4.5b: AFM image of pristine SWNT suspension on n-propyl substrate	140
Figure 4.5c: AFM image of pristine SWNT suspension on phenyl substrate	140
Figure 4.6a: I_{on}/I_{off} ratios for purified suspension using OTS.....	141
Figure 4.6b: I_{on}/I_{off} ratios for purified suspension using phenyltriethoxysilane	141

Figure 4.6c: I_{on}/I_{off} ratios for purified suspension using n-propyltriethoxysilane.....	142
Figure 4.6a: I_{on}/I_{off} ratios for purified suspension using 3-APTES.....	142
Figure 4.7a: AFM image of SWNT network using OTS.....	143
Figure 4.7b: AFM image of SWNT network using n-propyltriethoxysilane.....	143
Figure 4.7c: AFM image of SWNT network using phenyltriethoxysilane.....	143
Figure 4.7c: AFM image of SWNT network using 3-APTES.....	143
Figure 5.1a: The absorbance in UV-region at various sonication power	161
Figure 5.1b: NIR region for semiconducting SWNTs at various sonication power	161
Figure 5.2: Plot of concentration of purified SWNTs vs. uncentrifuge.....	162
Figure 5.3: D band of Raman spectra at different sonication power	163
Figure 5.4: Calibration curve of purified suspension and as produced (AP) soot	165

CHAPTER 1
INTRODUCTION AND LITERATURE REVIEW

1.1 Introduction

Nanotechnology is the field of science and manipulation of atoms and molecules which builds new materials and devices down to nanometer scale. It manipulates matter in the range of 0.1A to 1000A or 0.1nm to 100nm. It is not just a study of technology but also involves the combination of chemistry, physics, material science, and engineering. The materials include are quantum dots (zero dimensional), nanowires, (one dimensional), nanotubes, thin films (two dimensional) etc. Nanotechnology can be described using two approaches: Top down methods and bottom up methods. In top down method, larger materials are carve out to make nanomaterials (e.g.: lithographic patterning). Whereas in bottom up methods larger structures are build up from atoms and molecules (e.g.: Self-assembled monolayers, nanotubes). In this growing field of nanotechnology, carbon nanotubes draws great attention.

Carbon Nanotubes were first described as “worm like carbon structures” formed during the reaction of CO and Fe at 450⁰C in 1953.¹ In 1978, Wiles and Abrahamson² observed the formation of bundles of “carbon fibers” on graphitic electrodes in arc discharge experiments. Although they were observed several decades ago, it was not until 1991, that Ijima’s³ famous paper documenting his observation of “Helical microtubules of graphitic carbon”, the research on carbon nanotubes started trending. In 1991, Ijima and coworkers discovered MWNTs. It was not until 1993, that Ijima as well as Bethune⁴ and coworkers report 1.37nm SWNTs and in 1995, Smalley and his group use laser vaporization to grow SWNTs in high yields.⁵

Carbon Nanotubes are allotropes of carbon with a cylindrical nanostructure⁶ composed of 6 membered rings of sp² hybridized carbon atoms. Because of the sp² hybridization, they have interesting electrical and physical properties. They are hollow cylindrical molecules closed at their extremities. They are part of the fullerene family, the third known allotropic form of carbon after

graphite and diamond. There are two main types of carbon nanotubes: single-walled carbon nanotubes (SWNTs) and multi-walled carbon nanotubes (MWNTs). SWNT is a sp^2 bonded graphene sheet seamlessly rolled into a cylinder (Figure 1.1) making sure that the hexagonal rings are joined coherently. In SWNT, every atom is a surface atom. MWNTs are concentric layers of a rolled up graphene sheet consisting of several single-walled carbon nanotubes. Each MWNT has its own SWNT for structural support and are hold together by π - π interactions. Strong van der Waals attraction between them causes nanotube bundling.

1.2 Properties of SWNTs

Single-walled carbon nanotubes are hollow tubes with one atomic layer wall. The diameter ranges from 0.5nm to 1nm, whereas length can reach hundreds of microns. So they are considered to be one-dimensional nanostructures. The electronic, structural, and physical properties vary according to how the graphene sheet is formed (chirality). Chirality is in the form of (n, m) , where n and m are integers; it is defined as how or at what angle the graphene sheet is rolled up to form tubes.^{8,9} This direction is called the chiral vector. There are three geometric possibilities based on the chiral vector: armchair, zigzag, or chiral geometries. If the graphene sheet is rolled up along the vector greater than the chiral angle, “zigzag” SWNTs are formed. The sheets are rolled up in a way that a zigzag pattern in formed. They show semi-conductive behavior where the band gap varies inversely with the tube of the diameter. If the graphene sheet is rolled up along the vector smaller than chiral angle, “armchair” SWNTs are formed. In this formation, the graphene sheets show a cis formation defining the pattern. They show metallic behavior with no band gap between the conductance and the valence band. Chiral geometry is seen when the graphene sheet is rolled up on the vector, which means it is formed between the zigzag and armchair formation shown in Fig 1.2 and has both metallic and semiconducting properties. In simpler terms, if $n = m$, the

nanotube has arm chair structure while for m or $n = 0$, the nanotube has a zig zag structure and while others values of m and n , nanotube has a chiral structure. It is observed that if $n-m= 3Q$ (Q is an integer), SWNTs appear as metallic and are semiconducting for $n-m \neq 3Q$. SWNTs normally consists of 1/3 metallic and 2/3 semiconducting.^{10, 11} SWNTs can be either metals or semiconductors, with band gaps that are relatively large (~ 0.5 eV for typical diameter of 1.5 nm) or small (~ 10 meV), for identical diameters.¹²

SWNTs are highly elastic, exhibit largest tensile strength due to the covalent sp^2 bonds between individual carbon atoms, and can withstand larger strains. It can bend at large angles without damage. The Young's Modulus is a measure of elasticity. The Young Modulus for SWNTs is about 1.2T Pa which is 100 times higher than compared to 210 Gpa for steel.^{9, 13} They can be stretched over five times their original strength. They are good conductors of heat and their thermal stability is excellent in inert spheres, where they remain stable at 1200° C.¹⁴ They are stable up to 2800° C in vacuum and 750° C in air.¹⁵ They are used as stationary phase in chromatography due to the thermal property. As mentioned earlier, carbon nanotubes can show both metallic and semiconducting behavior, which means they can be used in transistors as well as nanoscale circuits. The current carrying capacity is estimated at 1 billion amps per square centimeter as compared to copper wires which burn out at 1 million amps per square centimeter.¹⁵ As semiconductors, carbon nanotubes offer flexibility by varying the band gap according to its diameter and chirality. Due to the 2:1 ratio of semi conductive to metallic nanotubes, it's quite obvious to isolate the semiconducting nanotubes from the metallic ones especially due to its growing popularity amongst transistors.

SWNTs are hydrophobic in nature due to the non-polar bonds and higher length to diameter ratio. This results in forming aggregates of SWNTs in the solution. This tendency to remain in

aggregates is a major hurdle and is due to the van der Waals forces between the nanotubes, in combination with the high surface area and high aspect ratio leading to agglomeration.¹⁶ The insolubility in water makes them difficult to purify and characterize. This can be overcome by dispersing SWNTs in an aqueous medium by adding a chemical modifier called surfactant.¹⁷ SWNTs show solubility in organic solvents such as dimethyl formamide, dimethyl acetamide and dimethyl pyrrolidone.¹⁷ They can also be functionalized inserting different functional groups since they can be modified covalently.¹⁸ SWNTs show field emission behavior when the nanotubes are fabricated by means of direct current plasma-enhanced chemical vapor deposition.¹⁹ This property results in ability of SWNTs to carry large electric current with minimal resistance.

1.3 Growth Methods for SWNTs

The most common methods used for synthesis of carbon nanotubes include, arc-discharge,^{20, 21} laser-ablation,^{22, 23} and chemical vapor deposition.²⁴ All the different growth techniques have two points in common: high temperature (1000 K-6000K) and used of graphene as a carbon source. In electric arc-discharge set up, the carbon nanotubes is created through arc vaporization of two graphite electrodes each separated by 1 mm as shown in Fig 1.3.²⁵ Cathode rod is a graphite rod and the anode rod is filled with metal catalyst powder (eg: Yiridium, nickel, cobalt) in a ~500 Torr Helium atmosphere. The inert gas is meant for cooling/condensation of the sample. The arc discharge was created by a current of 100A with a potential difference of 30V, which creates high temperature discharger between two electrodes.²⁶ The discharge vaporizes on one end of the electrode and forms small rod shape deposit on the other surface. Higher yield of carbon nanotube depends on the uniformity of plasma arc and the temperature of the deposit. However, the initial work of arc-discharge method was first reported by Ijima in 1991.³

In 1995, Smalley²⁷ and his group were the first ones to use laser ablation to grow high quality nanotubes. They produced high yield (~60-80%) of SWNTs via this technique. It involves a quartz chamber, an inert gas (helium or argon ~500 Torr) which flows through the chamber to carry the nanotubes to the copper collector, and small amount of catalytic metals (Ni or Co)²⁸ as shown in Fig 1.4. In the laser ablation process, a pulsed laser vaporizes a graphite target at high-temperature of 1200°C while an inert gas is inserted into the reactor. Nanotubes develop on the cooler surfaces of the reactor as the vaporized carbon condenses. Two laser pulses are used: one is to minimize the amount of carbon deposited as soot and the other breaks the large particles ablated by the laser and feeds to the nanotube structure. The average diameter and size can be varied using the varying temperature growth and catalyst composition.

Chemical Vapor Deposition (CVD)²⁹ synthesizes carbon nanotubes at lower temperatures as compared to arc discharge and laser ablation methods, hence this technique is useful for carbon synthesis in electronics. CVD uses hydrocarbon gases such as methane, ethanol, and acetylene as sources for carbon atoms and metal catalyst particles such Ni, Fe, and Co as seeds for CNT growth.³⁰ These methods produce high-quality, almost perfect nanotube structures despite the large amounts of byproducts also formed in the process. It produces high yield by catalytic decomposition of H₂/CH₄ mixture, where H₂ works as a reducing agent. The substrate covered with metal catalyst is heated at 700°C to decompose the hydrocarbon (Figure 1.5). Carbon nanotubes grow on the catalysts in the tube furnace, which are collected after the system is cooled to room temperature. CVD is a versatile technique which can produce hydrocarbons in any state (solid, liquid or gas), and allow carbon nanotube growth in any form such as powder, thin films, aligned, orthogonal, coiled etc.



In 1999, Smalley and his group³¹ developed a high pressure carbon monoxide method called HiPco for synthesis of carbon nanotubes. In this method, $\text{Fe}(\text{CO})_5$ or $\text{Ni}(\text{CO})_4$ acts as a catalyst and is injected into the reactor along with a stream of carbon monoxide (CO) gas at 900 ~ 1100°C with a pressure of 30~50 atm which acts as a feedback stock³² as shown in Fig 1.6. With this method, the high quality SWNTs, with few defects were achieved. The product yield is as high as 97% and purification yield is 90%.³²

1.4 Purification and Separation techniques of SWNTs

Regardless of the growth method, there are always significant amount of impurities present in SWNTs such as metal catalysts, fullerenes, amorphous carbon, and nanoparticles. These impurities have deleterious effect on the performance of different electronic device such as transistors,^{33,34} sensors etc. So developing a purification technique without damaging the SWNTs is crucial in obtaining a fundamental understanding of properties of individual SWNTs. In recent years, lot of progress has been made in removal of impurities and highly effective purification techniques without much damage to the SWNTs has been developed. A commonly followed purification method involves chemical³⁵ and/or acid oxidation treatment,³⁶ which creates defect sites on the side-walls SWNTs. To reduce the damage caused by direct oxidation, non-conventional methods have been studied such as filtration,³⁷ chromatography³⁸ and a combination of ultra-sonication and ultracentrifugation³⁹ etc.

Reported methods for purification such as gas or liquid phase oxidation, damage the pristine SWNTs. Oxidation reduces the electrical conductivity of SWNTs by introducing side wall defects in them. Zimmerman et al⁴⁰ has used the gas phase oxidation technique with the mixture of gases like oxygen, CO, CCl_4 , and COCl_2 at high temperatures in a tube furnace for removal of globular impurities. But no single gas was shown to offer any purification, but the dual gas

mixtures of chlorine and water were effective in etching the carbon. The unwanted carbon is selectively removed only if hydrogen chloride is added to the water and chlorine mixture. Since SWNTs consists entirely of carbon, the gas phase purification also etch the SWNTs by forming a functional group especially hydroxyl and chloride along the side walls of the nanotubes. These functional groups decrease the effectiveness of properties of nanotubes by introducing side wall defects. So gas phase technique has not yet proven successful for bulk purification of SWNTs.

A purification route involving the treatment of AP SWNT soot with liquid phase oxidizing media such as H_2SO_4 or nitric acid^{41, 42} is also used as an alternative for bulk purification of SWNT soot. Although this treatment is effective in removal of carbonaceous impurities and catalyst nanoparticles, the oxidation causes the chemical modification of SWNTs such as formation of carboxylic acid on the side walls. The use of oxidizing acids attacks the sp^2 structure of the SWNT interfering with their electronic properties.

As mentioned earlier, oxidation procedures are used as first step in the removal of impurities, and the most common technique used is by refluxing nitric acid on AP soot. Haddon and co-workers³⁶ reported results of treating SWNTs with refluxing 3, 7, and 16M nitric acid at varying times. They used SEM (scanning electron microscopy) and NIR and found that the refluxing not only removes metal catalysts, but also consumes significant portion of nanotubes. Nitric acid is a standard reagent for the purification of SWNTs and its major function is to remove metal catalysts and amorphous carbon. It also oxidizes the carbon atoms at the end of the SWNTs, while opening the ends and introducing carboxylic acids groups to the open ends and defects sites of SWNTs. Nitric acid combined with another strong acid like H_2SO_4 can reduce the length of the SWNTs. The residues of the nitric acid molecules leads to doping of the SWNTs, which destroys the electronic transitions of SWNTs observed via spectroscopic techniques. Overall, nitric acid is

suitable for removable of catalysts particles, but at the expense of the severe destruction to the SWNT structure.

Oxidation methods have an advantage of removing catalyst nanoparticles and amorphous carbon completely. They are cheap and can produce large quantity of purified SWNTs. But, the SWNTs are partially attacked due to the acid treatment and the loss of SWNTs is larger than the impurities. So development of non-destructive methods for the purification of SWNTs is of utmost importance. The most common mild purification methods involve using aqueous SWNT suspension in a surfactant and separating the impurities via filtration or centrifugation. Bandow et al.³⁷ have discussed a one-step SWNT purification procedure by microfiltration using a cationic surfactant (benzalkonium chloride). The purity of the SWNTs obtained was in excess of 90 wt % which was estimated by counting the number of tubes from the TEM image (Figure 1.7).⁴³ He also showed that SWNTs dispersed in 1% SDS can be purified by single centrifugation for 30 min.

An effective purification method that does not require covalent modification of carbon nanotubes, which can degrade the electronic, optical and mechanical properties, is ultracentrifugation. Conventional ultracentrifugation occurs in a density medium and separates SWNTs according to the sedimentation coefficient.⁷ The sedimentation coefficient depends on buoyant density and molecular weight of the SWNTs. But structural parameters like diameter and length, complicates sorting of SWNTs using the conventional ultracentrifugation. However, there is an exception where Smalley and his group³⁹ separated surfactant encapsulated SWNTs from the bundles in an aqueous solution. They obtained individual nanotubes, by dispersing in SDS at high sonication power of 540W and centrifuging at 122,000 g for 4h. This is an effective way of removal of carbonaceous and metallic impurities from the SWNT suspension. However due to the use of

centripetal force in excess of 100,000g, longer unbundled SWNTs are also removed producing nanotubes with lengths up to few hundred nanometers ~130nm.

Alternatively density gradient ultracentrifugation (DGU) is an established method which is used to sort SWNTs by buoyant density. In this method, SWNTs move towards the isopycnic point forming a density gradient in the centrifuge tube. It is also useful for separating SWNTs based on diameter and type of conductivity (metallic or semiconducting).⁷ In addition to using higher centripetal forces and yielding shorter nanotubes, it also involves reagents which are difficult to remove. It uses iodixanol as a gradient medium, which binds strongly to SWNTs and requires a separate dialysis treatment for removal. Also the iodine atoms work as an electron acceptor and increase the conductivity of the semiconducting SWNTs degrading their characteristics. Lastly having a higher molecular weight can make it difficult to remove from the solution which is important for electrical applications.⁴⁴

Low g centrifugation purification method has proved to be less destructive and harsh as compared to the other oxidation and or acid treatments mentioned earlier. Haddon and coworkers⁴⁵ showed that purification of nitric acid- treated SWNTs using centrifugation at 20,000 g for 60 min to remove carbon nanoparticles. They have shown that under these conditions, the SWNTs remain stable while carbon nanoparticles precipitate as sediment. The sediment is then removed by decantation of the supernatant and multiple cycles of centrifugation. As reported earlier, nitric acid leaves the carbon atoms at the ends and defect sides functionalized with carboxylic acids. This leads to shorter nanotubes in the process.

Therefore it is important to develop an effective method in reducing metal catalysts without damaging oxidative treatments and formation of stable suspension of unbundled high aspect ratio SWNTs. Lay group⁴⁶ has demonstrated that purification through low g centrifugation cycles

(18,000 g) is effective in removal of impurities and catalysts nanoparticles without increasing density of defects for SWNTs. This method can produce stable suspensions of SWNTs having lengths in excess of 2 μ m which will be discussed in detail in the next chapter. SWNT soot was dispersed in sodium dodecyl sulfate (SDS) via probe sonication. Since SDS has the lowest binding energy of all the surfactants, it is an important factor for post deposition removal of surfactants from the SWNT suspensions, especially for electrical applications.

1.5 Dispersion of SWNTs

SWNTs are known to be hydrophobic by nature and thus do not dissolve in water. The poor solubility of SWNTs in solvents can restrict the use of SWNTs and development of effective procedures for characterization. They are closed at the ends and interact with each other via van der Waals interactions and possess strong hydrophobicity. Due to this property they are not soluble in organic and aqueous solvents. However, surface functionalization of SWNTs has shown effective dispersion in both aqueous and organic media.¹⁸ There are two approaches for dispersing SWNTs: the non-covalent treatment^{47,48} or covalent treatment.⁴⁹ The non-covalent method has the advantage of adsorbing various groups on SWNT surface. They preserve the nanotubes conjugated π system and hence their electrical properties. Whereas, the covalent method like ultra-sonication can separate the nanotubes, however sonication done for extended time yields low aspect ratio nanotubes.⁵⁰

Surfactants disperse SWNTs in aqueous solutions through hydrophobic and hydrophilic interactions. The hydrophilic head consists of one or more hydrocarbon chains, associates with water.¹⁶ Whereas, the hydrophobic tail adsorbs on the surface of SWNT bundles. The adsorption depends on the characteristics of the particles, surfactant molecules, and the solvent. The driving force for the adsorption of surfactants on the charged surface is the formation of Columbic

attractions. Once the adsorption of surfactant molecules is achieved, they form micelles above the critical micelle concentration (CMC), where the performance is greatly improved. The surfactant is adsorbed on the surface by π - π interactions. The sonication unbundles the nanotubes by Columbic interactions and also overcomes the van der Waals forces among the individual nanotubes.⁵¹ Wang et al.¹⁶ came up with three different configurations for SWNT encapsulation: SWNTs can be encapsulated in cylindrical micelles, or covered with either hemispherical micelles or randomly adsorbed molecules. All these configurations are dependent on the surfactant concentration, and nanotube diameter.

Types of surfactants can be compared based on their ability to disperse in the presence of ring structures, different head groups, charges on the head group, length of an alkyl chain resonance ratios, and ionic or non-ionic surfactants. Resasco and Tan¹⁶ compared different types of surfactants and observed that benzene ring have high affinity towards SWNT surfaces and have high nanotubes dispersing ability. The π like stacking of benzene rings increase the binding and the surface coverage surfactant molecules to nanotube substrate. A higher charge on the head group strengthens the electrostatic repulsion of nanotubes, which prevents aggregation, resulting in more stable suspension.⁵² Longer alkyl chains improve surfactant energies, and this can be explained by the “unzippering mechanism”.⁵³ In this mechanism, the surfactant has to penetrate into the small spaces between the bundle and the tubes to compete with adsorption and exfoliate the nanotubes. The bulkier surfactant molecules (too long or too large hydrophobic groups) have difficulty entering the gaps between adjacent tubes. This leads to lower electrostatic charge reducing the debundling efficiency of a surfactant.

In order to overcome the problem of poor solubility, covalent and non-covalent functionalization has been studied to ensure efficient dispersion and debundling of nanotubes.

There are several methods to introduce side-wall functionalization of the tubes. Blau, et al.⁵⁴ reported functionalization of MWNTs using n-butyllithium and then covalently bonded to a chlorinated polypropylene. Haddon, et al.⁵⁵ in collaboration with Smalley observed functionalization of SWNTs with dichlorocarbene, but had difficulty distinguishing between the attachment to the walls of the SWNTs and its reaction with amorphous carbon. In another report by Haddon, metallic and semiconducting SWNTs were dissolved in organic solutions by deriving with thionylchloride and octadecylamine. Covalent functionalization has been successful in improving the solubility of SWNTs however, the intrinsic properties of SWNTs can be degraded by the disruption of π networks.

Non-covalent methods are the solutions to the problems caused by covalent methods. In this method, amphiphilic molecules such as surfactants, polymers etc. are frequently used. They can disperse and unbundle the SWNTs without disrupting their intrinsic properties. Yodh and his group⁵² reported a simple process to solubilize high weight fraction single-wall carbon nanotubes in water by physical adsorption of NaDDBS (sodium dodecylbenzene sulfonate). The most common surfactant used to suspend SWNTs in aqueous solution is SDS (sodium dodecyl sulfate). SDS has the lowest binding energy so it can be easily removed from the supernatant during the centrifugation process. At low level of CMC, SDS can encapsulate SWNTs. Significant progress has been made in recent years using SDS as a surfactant. O'Connell et al.³⁹ used ultracentrifugation process and remove SWNTs bundles using SDS. Whereas, Arnold et al.⁵⁶ went a step ahead and separate SWNTs using SDS and bile salts (sodium cholate) on the basis of diameter and chirality. Niyogi and coworkers,⁵⁷ showed that adding electrolytes to the SWNT-SDS solution enhances the density-gradient separations in SWNTs. The mechanism on how the surfactant self-assembles on the carbon nanotubes is not clear. It is assumed that SDS coats SWNTs with micelles, forming a

hydrophobic core and hydrophilic surface, forming homogenous mixture with water. After the addition of the surfactant, sonication is used to disperse SWNTs in the solution. After dispersing SWNTs and purifying them, depositing SWNTs on the substrate is important for their applications in electronics. Here, self-assembled monolayers play a crucial role in the deposition process.

1.6 Self-Assembled Monolayers (SAMs)

Self-assembled monolayers (SAMs) are being proposed as a route for surface modification for various number of applications, especially in electronics.⁵⁸ They have shown tremendous growth for modification of surfaces including SiO₂. The use of SAMs has made a significant impact on the electrical properties of thin-film transistors and SWNT FETs (field-effect transistor). However, it is interesting to know when did this all began. In 1946, Zisman is credited with originating the concept of SAMs.⁵⁹ He reported the preparation of self-assembly of a surfactant into a metal surface. But the major breakthrough was achieved in 1980, when Nuzzo and Allara studied SAMs of alkanethiols on gold.⁶⁰ This was prepared by adsorption of di-n-alkyl disulfides from dilute solutions. In the same year, Maoz and Sagiv⁶¹ studied SAMs of alkylsilanes on silicon oxide. These went on to become the most used combination in self-assembly.

Self-assembled monolayers is the assembly of atoms or molecules to form larger structures by H bond, π - π stacking, ionic interactions, and hydrophilic or hydrophobic interactions. They are ordered molecular structures formed by adsorption of a surfactant on a solid surface. SAMs present a versatile approach to surface functionalization due to simple instrumentation, high reproducibility, and reduced assembly time. The self-assembled monolayers are single layer of organic molecules adsorbed onto a solid substrate. Each molecule is divided into three parts: the polar head, backbone (non-polar alkyl chain), and the functional tail group as shown in Fig 1.8. The head group is responsible for anchoring the molecules to the substrate. The alkyl chain

stabilizes the monolayer due to the van der Waals interactions between the chains. The tail group modifies the surface properties by introducing chemical functionality into the monolayer. This functionalization provides the properties like adhesion, conductivity in controlled manner as it offers effective tuning of these properties.⁶²

As mentioned earlier, alkanethiols have contributed most to the self-assembling of molecules on the substrate. Alkanethiols SAMs are prepared by immersing a substrate into the solution of alkane thiol in ethanol for 12 hours at room temperature.⁶³ Thiol assembly occurs in two steps: formation of sulfur-gold bond, and arrangement of organic functional group stabilize by van der Waals interactions. SAMs acts as an adhesive for SWNT deposition on the substrate. Most deposits are formed on the Si/SiO₂ substrate. SAMs can also help synthesize high quality SWNTs by stabilizing the iron catalyst on the template, where the self-assembly was used as a supporting layer. They prevent the agglomeration of nanoparticle by reinforcing the catalytic layer.⁶⁴ Liu and his group showed a wet chemical approach for organizing tangled SWNTs on gold substrate. The assembly was made by chemical adsorption to gold via Au-S bonds. Nanotubes were organized on gold, forming a self-assembled monolayer structure with perpendicular orientation.⁶⁵ Fuji et al.⁶⁶ reported site selective deposition of SWNT films on Si/SiO₂ substrate using self-assembled monolayer. Another study involving SWNTs and self-assembled monolayer show a low temperature “chemical transfer” process to align carbon nanotubes onto the substrates. Firstly carbon nanotubes are functionalized during CVD process. Secondly, attaching the SWNT onto the gold substrate by forming covalent bonds with the self-assembled monolayer.⁶⁷ To form SWNT network on the substrate, SAMs play an important role. They have significant impact on the source drain current, transistor response curve, on/off ratios etc.^{58, 68} Therefore they are extensively used in areas of nanomaterials, sensors,⁶⁹ electronics etc.

1.7 SWNT networks

SWNTs are usually studied as individual nanotubes or as a network. However, individual SWNTs pose difficulties especially with implementing in large scale fabrication of devices. Depositing individual SWNTs on a larger scale remains a challenge. This can cause poor reproducibility in device performance. To overcome this challenge, alternative SWNT configurations consisting of either nanotube bundles or ropes of SWNTS, or nanotubes integrated matrix (film or composite) can be used.

SWNT networks have high conductivity field-effect mobility which creates possibility of electronic devices like diodes, sensors, field-effect transistors etc. They also have high flexibility, resistance, and can be fabricated at room temperature techniques. The formation of 2-D networks results from the deposition of individual SWNTs. It averages the properties of all SWNTs in the sample (greater reproducibility). SWNT network connects nanotubes in parallel, so they have increased current flow for sensors, and semiconductor devices. The low density networks behave as thin-film semiconductor and high density networks exhibit metallic behavior. In SWNT network, the 2:1 ratio of semiconducting to metallic SWNTs is assumed. The random network can be formed by depositing the 2:1 ratio of semi conductive to conductive SWNTs, which in turn can be used for electronic device studies. The electrical properties can be tuned from semiconducting to metallic by increasing the density of deposited SWNT network. 2-D networks can behave as a semiconductor above the percolation threshold for semiconducting nanotubes.

Percolation theory describes at what density the random SWNT network behaves as semiconducting. It describes the macroscopic conduction in random SWNT networks using a ‘conducting stick model’.^{70, 71} Lay and his group⁷² have shown that macroscopic electronic behavior of highly aligned SWNTs can be described using the percolation theory. At low density

of SWNT network, there is no percolation pathway and therefore no conductivity since electrons can't travel from one area to another. At high density, conductivity is observed. This can be explained by an important criterion of percolation theory called the critical density N_c . This is given by an equation:

$$N_c = 4.236^2 / l^2 * \pi$$

Where l is the length of SWNTs, π is the ratio of circumference to its diameter and N_c is the critical density. SWNT network behaves as a semiconductor above N_c for semiconducting nanotubes. Once the critical density of metallic nanotubes is reached, the network behaves more as a conductor than semiconductor.

1.8 Characterization

Spectroscopic techniques like UV-vis-NIR spectroscopy, Raman spectroscopy and Atomic force microscopy are used to characterize the SWNT suspensions and deposits on the substrate. In UV-vis-NIR region, SWNTs show characteristic peaks of adsorption due to the van Hove singularities in the optical spectra.⁷³ This is due to the active electronic transitions in the region. The interband transitions produce prominent features in UV-vis-NIR region and the spectrum shows peaks between 340nm and 1400nm. The M_{11} transitions of metallic nanotubes are seen in the visible range from 645nm to 440nm, S_{11} and S_{22} transitions of semiconducting nanotubes occur in the NIR region between 1600 to 900nm and 800 to 600 nm respectively.⁷⁴

Raman spectroscopy was used to characterize the degree of order on graphene lattice of the carbon nanotubes. Every band in the Raman spectrum corresponds to the vibrational frequency of a bond, consisting of sp^2 and sp^3 hybridized carbon atoms. The graphite band (G-band) which occurs near 1590cm^{-1} is a characteristic feature of graphite layers and corresponds to tangential vibration of carbon atoms. The disorder band (D-band), near 1370cm^{-1} is indicative of the presence

of disordered sp^2 carbon atoms, caused by impurities in C lattice.⁷⁵ The comparison of ratios (I_g/I_d) of these two peaks was used to measure the quality of purified SWNTs and removal of impurities. RBM (radial breathing mode) measures the contractions and expansions of SWNTs. They also determine the chirality and diameter of SWNT in a spectra.

AFM was used to describe the deposits made on the substrate. To make deposit on the SWNT surface, silicon wafers were functionalized with a self-assembled monolayer which acts as an adhesive and helps SWNT to adhere to the surface. AFM images were obtained via intermittent contact mode in air, in which the tip is raster scanned over a surface showing tubes and impurities on the surface. The images were analyzed using software WSxM, v.6.1⁷⁶ to determine the effect of separation process on the average height, length and also roughness of the SWNT substrate. This information can also help determine the density of SWNTs on the substrate. Probe station and a semi-conductor analyzer system was used to monitor network conductance and characterize transistor behaviors of SWNT network with different self-assembled monolayers.

1.9 Summary and Future Directions

Single-walled carbon nanotubes are emerging as potential candidates for wide range of applications due to their structural, mechanical, and electronic properties and particularly in electronic devices like thin-films, field emission sources and sensors. However, major hurdle must be overcome before many of these applications can be used, most importantly purification of as-produced carbon nanotube soot and also their tendency to aggregate into bundles. Various purification methods have been reported involving oxidative treatments, which are successful in removing the impurities, but by creating defects sites on the side walls of SWNTs. So it is very important to develop a non-oxidizing, non-destructive purification method for SWNTs. In Chapter 2, iterative process of low g centrifugation has been introduced for removing residual catalyst

nanoparticles and amorphous carbon without damaging them and secondly obtaining unbundled high aspect ratio SWNTs.

Other purification techniques involve use of agarose density gradient,⁷⁷ polymer wrapping,⁷⁸ capillary electrophoresis⁷⁹ etc. However these methods are effective in separating SWNTs based on conductivity, but the down side is that they use a lot additional reagents like DMF, which are hard to remove; a requirement for electrical applications. The presence of impurities in the gel column can be another hurdle in the purification process. So preparing a gradient for purifying nanotubes without reagents is important. In Chapter 3, sucrose gradient along with the sedimentation method has been introduced to purify nanotubes. The effect of sucrose in the suspension has been discussed. The effect of SDS molecules when sucrose is wrapped around the surfactant had been observed. The quality of purification and amount of yield produced after just one processing cycles has been compared.

SWNTs networks are important in field of electronics. SWNT network can be formed in a lot of different ways, however some currents methods produce SWNT in random networks. In Chapter 4, aligned and orthogonal SWNT networks have been formed on different self-assembled monolayers. The effect of different SAMs on the SWNT network has been investigated. SAMs can be used to control the purity of the deposit while measuring the electrical properties during the deposition process. The effect of pH treatment on the aminosilanes has been reported. Resistance, I_{on}/I_{off} ratios has been determined for different self-assembled monolayers.

As mentioned earlier, SWNTs are composed of bundles, ropes which are held together by van der Waals interaction. The ability to form suspensions is of importance in electrical applications. Control over concentration and length is an important factor in low density networks. In Chapter 5, sonication in the presence of a surfactant has been used to disperse SWNTs in the

suspension. The effect of varying sonication power on the SWNT suspension has been investigated. Multiple cycles of centrifugation with different SWNT concentration at different sonication power has been introduced and discussed.

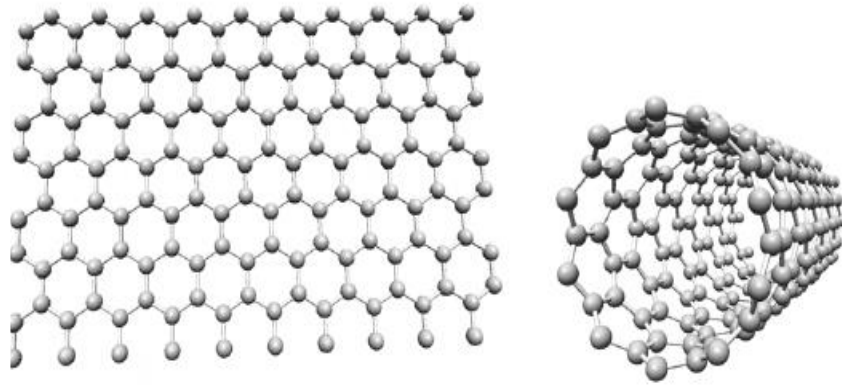


Figure 1.1: (Left) a single layer graphene sheet. This is a van der Waals material with covalent bonds in each graphene sheet, where each carbon atom is bound to 3 other carbon atoms and has one delocalized electron; (Right) a single-walled carbon nanotube resulting from rolled up graphene sheet.

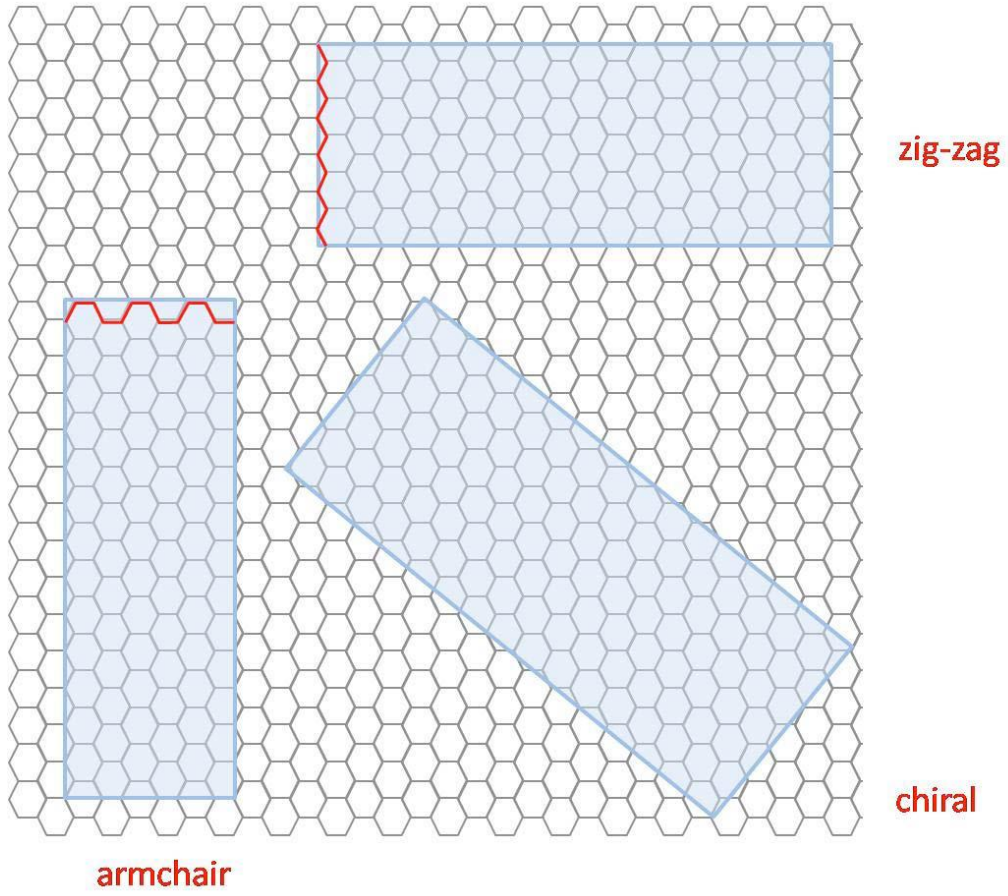


Figure 1.2: Schematic representation of SWNT chirality.

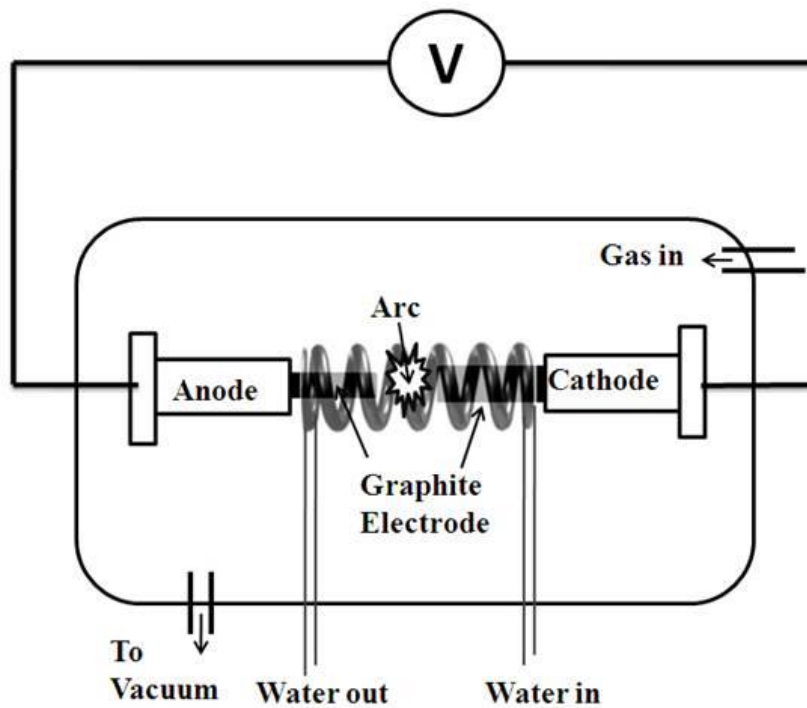


Figure 1.3: Schematic of an electric arc-discharge chamber.²⁵

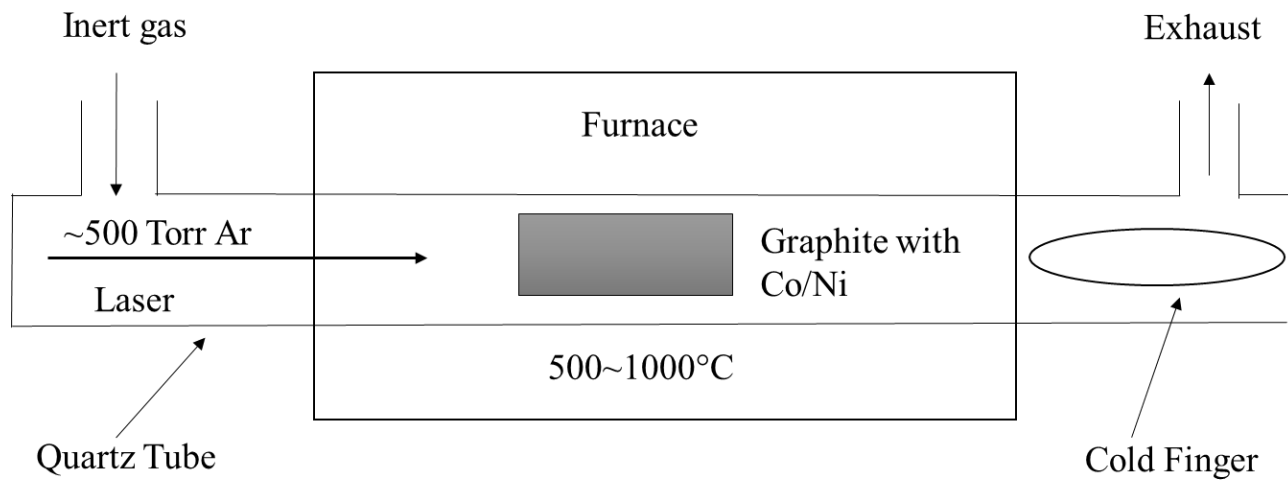


Figure 1.4: Schematic of laser-ablation technique.

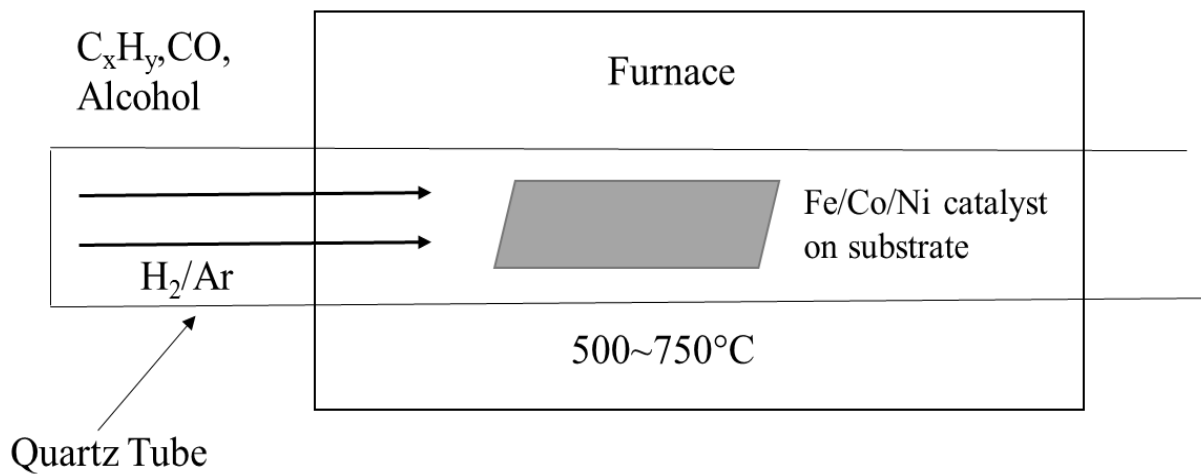


Figure 1.5: Schematic of Chemical Vapor Deposition apparatus.

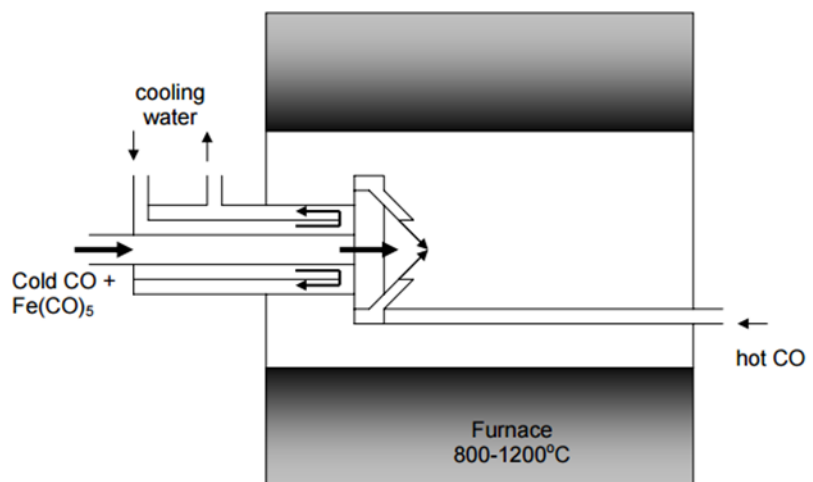


Figure 1.6: Schematic Diagram of apparatus for synthesizing HiPCO carbon nanotubes.³²

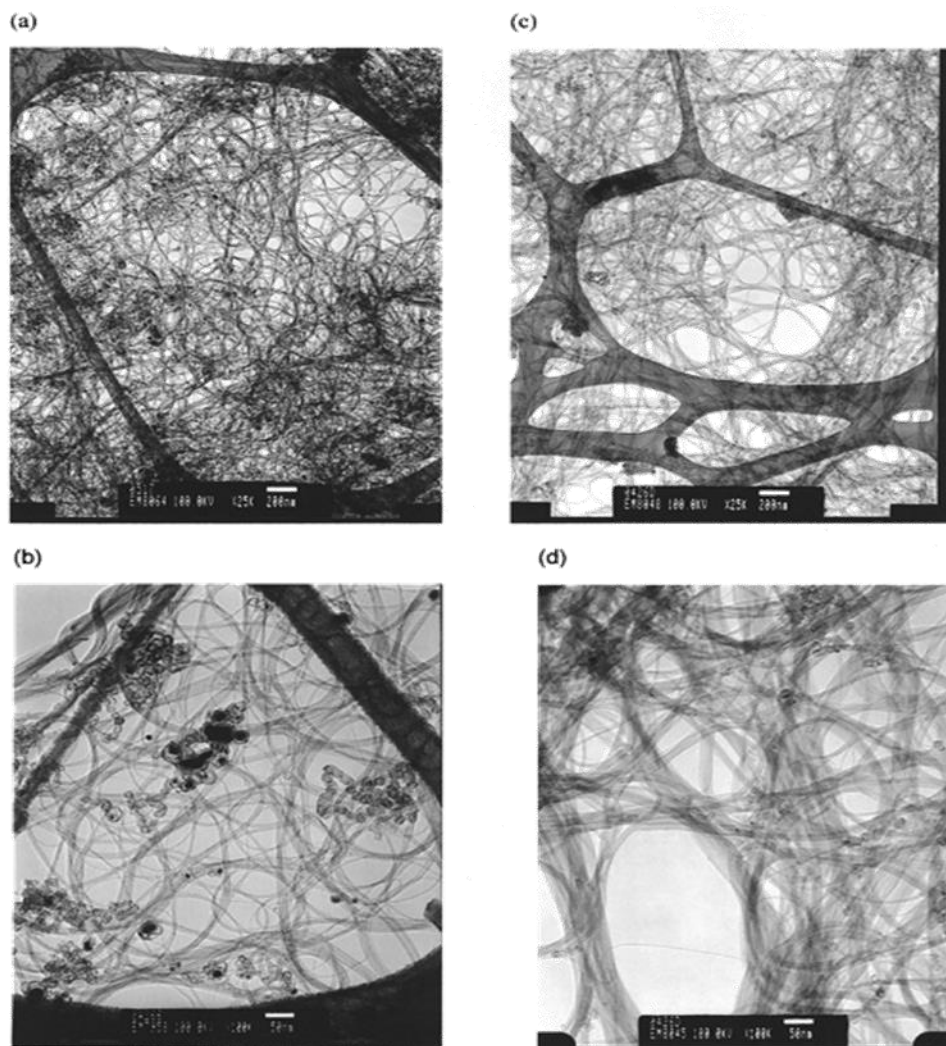


Figure 1.7 TEM images of SWNTs. Before purification a) and b); after two purification cycles c) and d).⁴³

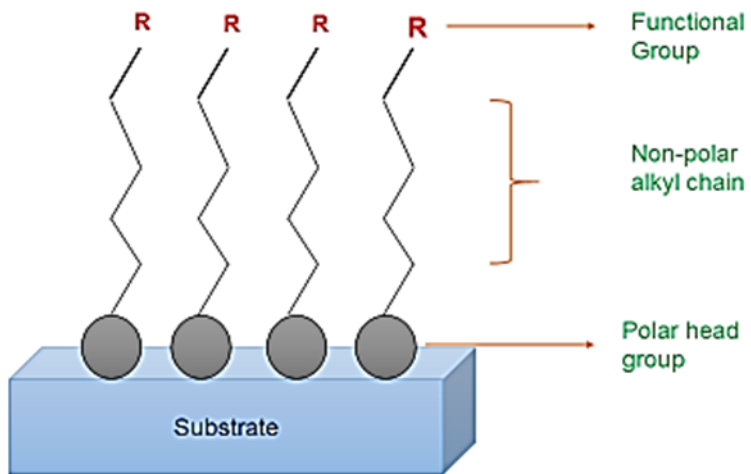


Figure 1.8: Schematic representation of Self-assembled monolayer (SAM) structure.

References

1. Davis, W. R.; Slawson, R. J.; Rigby, G. R. *Nature* **1953**, 171, (4356), 756-756.
2. Wiles, P. G.; Abrahamson, J. *Carbon* **1978**, 16, (5), 341-349.
3. Iijima, S. *Nature* **1991**, 354, (6348), 56-58.
4. Bethune, D.; Klang, C.; De Vries, M.; Gorman, G.; Savoy, R.; Vazquez, J.; Beyers, R. **1993**.
5. Guo, T.; Nikolaev, P.; Thess, A.; Colbert, D. T.; Smalley, R. E. *Chemical Physics Letters* **1995**, 243, (1-2), 49-54.
6. Wang, X.; Li, Q.; Xie, J.; Jin, Z.; Wang, J.; Li, Y.; Jiang, K.; Fan, S. *Nano Letters* **2009**, 9, (9), 3137-3141.
7. Hersam, M. C. *Nat Nano* **2008**, 3, (7), 387-394.
8. Venema, L. C.; Meunier, V.; Lambin, P.; Dekker, C. *Physical Review B* **2000**, 61, (4), 2991-2996.
9. Dai, H. *Accounts of Chemical Research* **2002**, 35, (12), 1035-1044.
10. O'connell, M. J., *Carbon nanotubes: properties and applications*. CRC press: 2006.
11. Popov, V. N. *Materials Science and Engineering: R: Reports* **2004**, 43, (3), 61-102.
12. Dresselhaus, M. S.; Dresselhaus, G.; Eklund, P. C., *Science of fullerenes and carbon nanotubes: their properties and applications*. Academic press: 1996.
13. Dai, H. *Surface Science* **2002**, 500, (1-3), 218-241.
14. Valcárcel, M.; Cárdenas, S.; Simonet, B. M. *Analytical Chemistry* **2007**, 79, (13), 4788-4797.
15. Collins, P. G.; Avouris, P. *Scientific American* **2000**, 283, (6), 62-9.
16. Wang, H. *Current Opinion in Colloid & Interface Science* **2009**, 14, (5), 364-371.

17. Vaisman, L.; Wagner, H. D.; Marom, G. *Advances in Colloid and Interface Science* **2006**, 128–130, (0), 37-46.
18. Georgakilas, V.; Kordatos, K.; Prato, M.; Guldi, D. M.; Holzinger, M.; Hirsch, A. *Journal of the American Chemical Society* **2002**, 124, (5), 760-761.
19. Jang, H. S.; Lee, H.-R.; Kim, D.-H. *Thin Solid Films* **2006**, 500, (1–2), 124-128.
20. Kim, H. H.; Kim, H. J. *Materials Science and Engineering: B* **2006**, 133, (1–3), 241-244.
21. Iijima, S.; Ichihashi, T. *Nature* **1993**, 363, (6430), 603-605.
22. Arepalli, S. *Journal of Nanoscience and Nanotechnology* **2004**, 4, (4), 317-325.
23. Guo, T.; Nikolaev, P.; Thess, A.; Colbert, D.; Smalley, R. *Chemical physics letters* **1995**, 243, (1), 49-54.
24. Su, M.; Zheng, B.; Liu, J. *Chemical Physics Letters* **2000**, 322, (5), 321-326.
25. Choudhary, V.; Singh, B. P.; Mathur, R. B., *Carbon Nanotubes and Their Composites*. 2013.
26. Journet, C.; Maser, W. K.; Bernier, P.; Loiseau, A.; de la Chapelle, M. L.; Lefrant, S.; Deniard, P.; Lee, R.; Fischer, J. E. *Nature* **1997**, 388, (6644), 756-758.
27. Thess, A.; Lee, R.; Nikolaev, P.; Dai, H.; Petit, P.; Robert, J.; Xu, C.; Lee, Y. H.; Kim, S. G.; Rinzler, A. G. *Science-AAAS-Weekly Paper Edition* **1996**, 273, (5274), 483-487.
28. Henley, S.; Anguita, J.; Silva, S. R., Synthesis of Carbon Nanotubes. In *Encyclopedia of Nanotechnology*, Bhushan, B., Ed. Springer Netherlands: 2012; pp 2615-2621.
29. Kumar, M.; Ando, Y. *Journal of nanoscience and nanotechnology* **2010**, 10, (6), 3739-3758.
30. Brukh, R.; Mitra, S. *Chemical Physics Letters* **2006**, 424, (1–3), 126-132.

31. Nikolaev, P.; Bronikowski, M. J.; Bradley, R. K.; Rohmund, F.; Colbert, D. T.; Smith, K. A.; Smalley, R. E. *Chemical Physics Letters* **1999**, 313, (1–2), 91-97.
32. Bronikowski, M. J.; Willis, P. A.; Colbert, D. T.; Smith, K. A.; Smalley, R. E. *Journal of Vacuum Science & Technology A* **2001**, 19, (4), 1800-1805.
33. Bradley, K.; Gabriel, J.-C. P.; Grüner, G. *Nano Letters* **2003**, 3, (10), 1353-1355.
34. Ozel, T.; Gaur, A.; Rogers, J. A.; Shim, M. *Nano Letters* **2005**, 5, (5), 905-911.
35. Robinson, J. A.; Snow, E. S.; Bădescu, Ș. C.; Reinecke, T. L.; Perkins, F. K. *Nano Letters* **2006**, 6, (8), 1747-1751.
36. Hu, H.; Zhao, B.; Itkis, M. E.; Haddon, R. C. *The Journal of Physical Chemistry B* **2003**, 107, (50), 13838-13842.
37. Bandow, S.; Rao, A. M.; Williams, K. A.; Thess, A.; Smalley, R. E.; Eklund, P. C. *The Journal of Physical Chemistry B* **1997**, 101, (44), 8839-8842.
38. Duesberg, G. S.; Muster, J.; Krstic, V.; Burghard, M.; Roth, S. *AIP Conference Proceedings* **1998**, 442, (1), 39-43.
39. O'connell, M. J.; Bachilo, S. M.; Huffman, C. B.; Moore, V. C.; Strano, M. S.; Haroz, E. H.; Rialon, K. L.; Boul, P. J.; Noon, W. H.; Kittrell, C. *Science* **2002**, 297, (5581), 593-596.
40. Zimmerman, J. L.; Bradley, R. K.; Huffman, C. B.; Hauge, R. H.; Margrave, J. L. *Chemistry of Materials* **2000**, 12, (5), 1361-1366.
41. Suri, A.; Coleman, K. S. *Carbon* **2011**, 49, (9), 3031-3038.
42. Monthieux, M.; Smith, B. W.; Burteaux, B.; Claye, A.; Fischer, J. E.; Luzzi, D. E. *Carbon* **2001**, 39, (8), 1251-1272.
43. Chiang, I. W.; Brinson, B. E.; Smalley, R. E.; Margrave, J. L.; Hauge, R. H. *The Journal of Physical Chemistry B* **2001**, 105, (6), 1157-1161.

44. Yanagi, K.; Iitsuka, T.; Fujii, S.; Kataura, H. *The Journal of Physical Chemistry C* **2008**, 112, (48), 18889-18894.
45. Yu, A.; Bekyarova, E.; Itkis, M. E.; Fakhrutdinov, D.; Webster, R.; Haddon, R. C. *Journal of the American Chemical Society* **2006**, 128, (30), 9902-9908.
46. Vichchulada, P.; Shim, J.; Lay, M. D. *The Journal of Physical Chemistry C* **2008**, 112, (49), 19186-19192.
47. Manivannan, S.; Jeong, I. O.; Ryu, J. H.; Lee, C. S.; Kim, K. S.; Jang, J.; Park, K. C. *Journal of Materials Science: Materials in Electronics* **2009**, 20, (3), 223-229.
48. O'Connell, M. J.; Boul, P.; Ericson, L. M.; Huffman, C.; Wang, Y.; Haroz, E.; Kuper, C.; Tour, J.; Ausman, K. D.; Smalley, R. E. *Chemical Physics Letters* **2001**, 342, (3-4), 265-271.
49. Tasis, D.; Tagmatarchis, N.; Bianco, A.; Prato, M. *Chemical reviews* **2006**, 106, (3), 1105-1136.
50. Lu, K. L.; Lago, R. M.; Chen, Y. K.; Green, M. L. H.; Harris, P. J. F.; Tsang, S. C. *Carbon* **1996**, 34, (6), 814-816.
51. Tan, Y.; Resasco, D. E. *The Journal of Physical Chemistry B* **2005**, 109, (30), 14454-14460.
52. Islam, M. F.; Rojas, E.; Bergey, D. M.; Johnson, A. T.; Yodh, A. G. *Nano Letters* **2003**, 3, (2), 269-273.
53. Strano, M. S.; Moore, V. C.; Miller, M. K.; Allen, M. J.; Haroz, E. H.; Kittrell, C.; Hauge, R. H.; Smalley, R. E. *Journal of Nanoscience and Nanotechnology* **2003**, 3, (1-1), 81-86.
54. Blake, R.; Gun'ko, Y. K.; Coleman, J.; Cadek, M.; Fonseca, A.; Nagy, J. B.; Blau, W. J. *Journal of the American Chemical Society* **2004**, 126, (33), 10226-10227.

55. Chen, J.; Hamon, M. A.; Hu, H.; Chen, Y.; Rao, A. M.; Eklund, P. C.; Haddon, R. C. *Science* **1998**, 282, (5386), 95-98.
56. Arnold, M. S.; Green, A. A.; Hulvat, J. F.; Stupp, S. I.; Hersam, M. C. *Nature nanotechnology* **2006**, 1, (1), 60-65.
57. Niyogi, S.; Densmore, C. G.; Doorn, S. K. *Journal of the American Chemical Society* **2009**, 131, (3), 1144-1153.
58. Aswal, D. K.; Lenfant, S.; Guerin, D.; Yakhmi, J. V.; Vuillaume, D. *Analytica Chimica Acta* **2006**, 568, (1-2), 84-108.
59. Bigelow, W. C.; Pickett, D. L.; Zisman, W. A. *Journal of Colloid Science* **1946**, 1, (6), 513-538.
60. Nuzzo, R. G.; Allara, D. L. *Journal of the American Chemical Society* **1983**, 105, (13), 4481-4483.
61. Maoz, R.; Sagiv, J. *Journal of Colloid and Interface Science* **1984**, 100, (2), 465-496.
62. Smith, R. K.; Lewis, P. A.; Weiss, P. S. *Progress in Surface Science* **2004**, 75, (1-2), 1-68.
63. Love, J. C.; Estroff, L. A.; Kriebel, J. K.; Nuzzo, R. G.; Whitesides, G. M. *Chemical Reviews* **2005**, 105, (4), 1103-1170.
64. Adhikari, P. D.; Song, W.; Cha, M.-J.; Park, C.-Y. *Thin Solid Films* **2013**, 545, (0), 50-55.
65. Liu, Z.; Shen, Z.; Zhu, T.; Hou, S.; Ying, L.; Shi, Z.; Gu, Z. *Langmuir* **2000**, 16, (8), 3569-3573.
66. Fujii, S.; Tanaka, T.; Suga, H.; Naitoh, Y.; Minari, T.; Tsukagoshi, K.; Kataura, H. *physica status solidi (b)* **2010**, 247, (11-12), 2750-2753.
67. Lin, W.; Xiu, Y.; Jiang, H.; Zhang, R.; Hildreth, O.; Moon, K.-S.; Wong, C. P. *Journal of the American Chemical Society* **2008**, 130, (30), 9636-9637.

68. Pernstich, K. P.; Haas, S.; Oberhoff, D.; Goldmann, C.; Gundlach, D. J.; Batlogg, B.; Rashid, A. N.; Schitter, G. *Journal of Applied Physics* **2004**, 96, (11), 6431-6438.
69. Chaki, N. K.; Vijayamohanan, K. *Biosensors and Bioelectronics* **2002**, 17, (1-2), 1-12.
70. Hu, L.; Hecht, D. S.; Grüner, G. *Nano Letters* **2004**, 4, (12), 2513-2517.
71. Balberg, I.; Binenbaum, N.; Anderson, C. H. *Physical Review Letters* **1983**, 51, (18), 1605-1608.
72. Zhang, Q.; Vichchulada, P.; Cauble, M.; Lay, M. *J Mater Sci* **2009**, 44, (5), 1206-1211.
73. Ryabenko, A. G.; Dorofeeva, T. V.; Zvereva, G. I. *Carbon* **2004**, 42, (8-9), 1523-1535.
74. Rance, G. A.; Marsh, D. H.; Nicholas, R. J.; Khlobystov, A. N. *Chemical Physics Letters* **2010**, 493, (1-3), 19-23.
75. Simpson, J. R.; Fagan, J. A.; Becker, M. L.; Hobbie, E. K.; Hight Walker, A. R. *Carbon* **2009**, 47, (14), 3238-3241.
76. Horcas, I.; Fernández, R.; Gómez-Rodríguez, J. M.; Colchero, J.; Gómez-Herrero, J.; Baro, A. M. *Review of Scientific Instruments* **2007**, 78, (1), 013705.
77. Hirano, A.; Tanaka, T.; Urabe, Y.; Kataura, H. *The Journal of Physical Chemistry C* **2012**, 116, (17), 9816-9823.
78. Yi, W.; Malkovskiy, A.; Chu, Q.; Sokolov, A. P.; Colon, M. L.; Meador, M.; Pang, Y. *The Journal of Physical Chemistry B* **2008**, 112, (39), 12263-12269.
79. Doorn, S. K.; Strano, M. S.; O'Connell, M. J.; Haroz, E. H.; Rialon, K. L.; Hauge, R. H.; Smalley, R. E. *The Journal of Physical Chemistry B* **2003**, 107, (25), 6063-6069.

CHAPTER 2

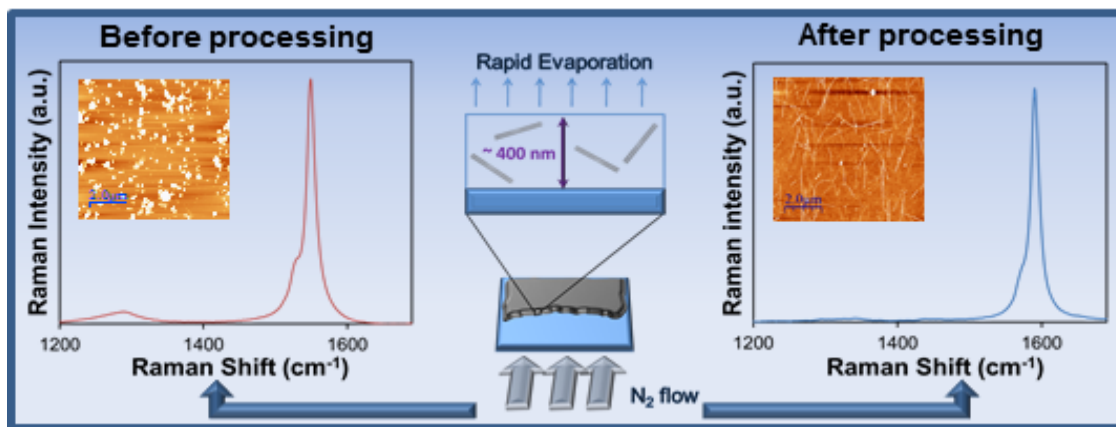
BULK PURIFICATION AND DEPOSITION METHODS FOR SELECTIVE ENRICHMENT OF HIGH ASPECT RATIO SINGLE WALLED CARBON NANOTUBES¹

¹N.Bhatt, P.Vichchulada, M.D.Lay, 2012, *Journal of American Chemical Society*, **134**, 9352-9361

Reprinted here with the permission of the publisher.

2.1 ABSTRACT

Aqueous batch processing methods for the concurrent purification of single-walled carbon nanotube (SWNT) soot and enrichment in high aspect ratio nanotubes are essential to their use in a wide variety of electronic, structural, and mechanical applications. This manuscript presents a new route to the bulk purification and enrichment of unbundled SWNTs having average lengths in excess of 2 μm . Iterative centrifugation cycles at low centripetal force not only removed amorphous C and catalyst nanoparticles, but also allowed the enhanced buoyancy of surfactant encapsulated, unbundled, high aspect ratio SWNTs to be used to isolate them in the supernatant. UV-Vis-NIR and Raman spectroscopy were used to verify the removal of residual impurities from as-produced (AP-grade) arc discharge soot and the simultaneous enrichment in unbundled, undamaged, high aspect ratio SWNTs. The laminar flow deposition process (LFD) used to form 2-D networks of SWNTs prevents bundle formation during network growth. Additionally, it further enhances the quality of deposits by taking advantage of the inverse relationship between the translational diffusion coefficient and length for suspended nanoparticles. This resulted in preferential deposition of pristine, unbundled, high aspect ratio SWNTs over residual impurities, as observed by Raman spectroscopy and atomic force microscopy (AFM).



2.2 INTRODUCTION

Single-walled carbon nanotubes (SWNTs) have attracted great attention because of their unique electronic and mechanical properties. They have the highest measured tensile strength, are flexible, lightweight, and exhibit low power consumption while retaining high on/off ratios in electronic materials.¹ These seamless tubes of graphene are typically microns long and one nanometer in diameter. However, unlike graphene, SWNTs exist as either semi conductive or metallic conductors due to quantum confinement effects resulting from their curvature. Therefore, there is particular interest in using SWNTs for electronic applications. In spite of their great potential, the widespread use of SWNTs in electronic materials remains stalled by issues with unbundling and purifying them in order to obtain much greater precision over their electronic properties. This is critical as regardless of the growth method, as-produced (AP) grade SWNT soot is a mixture of SWNTs (with bandgaps from 0 to ~ 1.8 eV), metal catalyst nanoparticles and amorphous carbon. Bulk processing methods for removing these impurities and unbundling SWNTs, without greatly increasing sidewall defects, is crucial to obtaining a fundamental understanding of the properties of individual SWNTs. Further, the fundamental electrical, optical, and electrochemical behavior of SWNT-based composites can be more reproducibly measured and understood if the suspensions from which they are deposited are well characterized.

Therefore, the development of scalable methods for incorporating SWNTs into a wide variety of structural and electron materials is strongly dependent on the creation of new liquid-processing techniques for purifying and separating nanotubes without damaging their enhanced physical attributes. However, significant issues remain with regard to forming suspensions of unbundled high aspect ratio SWNTs. These issues can be reduced to two broad challenge areas: 1) removing residual catalyst nanoparticles and amorphous C without damaging the SWNTs, and

2) forming suspensions of unbundled, high-aspect ratio SWNTs while maintaining control over the concentration and average length of the solvated nanotubes.

Addressing the first challenge area, the ability to form bulk quantities of suspensions composed of unbundled SWNTs having known average lengths, is particularly important for forming and characterizing 2-D SWNT networks that harness the enhanced electrical and physical properties of nanotubes.²⁻⁴ In fact, many researchers are investigating the formation of SWNT-network based transistors,⁵⁻⁷ sensors⁸⁻¹⁰ and field-emission sources.^{11,12} The electron mobility and on/off ratio of such materials is greatly hampered by residual impurities. Therefore, non-oxidizing purification methods will play a central role in SWNT-based electronics.

Methods of dealing with the second challenge area, forming suspensions of unbundled, high aspect ratio SWNTs, are also crucial to optimizing the performance of SWNT networks in electronic device structures. The electron mobility of SWNT networks decreases inversely with the number of SWNT-SWNT tunnel junctions. Therefore, maximizing the average length of SWNTs in a network will decrease the number of inter-SWNT tunnel junctions that must be bridged. This will allow the low resistance and near ballistic electronic transport observed for unbundled SWNTs to be exploited.¹³⁻¹⁵

The charge carrier mobility for SWNT networks¹⁶⁻¹⁸ has been reported to exceed two commonly used systems, amorphous Si¹⁹⁻²¹ and organic semiconductors.^{22, 23} A recent study has even demonstrated electron mobility approaching those observed for p-type crystalline Si.²⁴ This performance advantage, coupled with the mechanical flexibility and transparent nature of SWNT networks,²⁵⁻²⁷ as well as their ability to operate at low voltages, causes great interest for their use in portable electronic devices and displays. Furthermore, the tensile strength and heat conductance are greatly improved in polymer composites that contain cross-linked high aspect ratio

SWNTs.^{28,29} Therefore, bulk-processing methods for forming suspensions enriched in unbundled, undamaged, high aspect ratio SWNTs will play a central role in the development of a wide variety of electronic and structural materials.

Understanding bulk solution processing methods is crucial to the deposition of SWNT networks on heat-sensitive substrates used in flexible electronic materials, as direct growth of nanotubes (which requires temperatures in excess of 700 °C) is not possible. For these reasons, the recent literature is replete with reports of suspension purification and processing methods, which often begin with oxidative purification treatments.³⁰⁻³³ Yet, oxidation reduces the electrical conductivity of SWNTs through the introduction of sidewall defects.^{8,9} Following oxidation, other suspension processing methods include density gradient ultracentrifugation (DGU),^{34-36,37} and polymer wrapping.³⁸ While DGU has been shown to be useful for separating SWNTs based on diameter and type of conductivity, its major disadvantage is that it yields nanotubes with lengths only up to a few hundred nm, as it employs centripetal forces in excess of 100,000 G. Additionally, DGU and polymer wrapping involve the use of reagents that are difficult to remove, a requirement for electronic applications. In particular, DGU involves the use of several surfactants, as well as a density gradient medium, typically iodixanol. This compound binds strongly to SWNTs and requires a separate dialysis treatment for removal.

Therefore, while effective at reducing residual metal catalysts, the concurrent oxidation of SWNTs and the formation of highly carboxylated carbonaceous impurities which are difficult to remove are significant concerns.³³ This group has recently demonstrated that purification through iterative low G centrifugation cycles is effective at removing residual metal catalyst and carboxylated carbonaceous impurities, without increasing the density of defects observed for SWNTs.³⁹⁻⁴¹ This manuscript describes how this benign purification method can be used to

produces stable suspensions of SWNTs having lengths in excess of 2 μm . This group is currently investigating methods of further separating these high aspect ratio nanotubes by diameter and type of conductivity.

This report provides insight into the separation of unbundled, surfactant encapsulated, high-aspect ratio SWNTs from impurities under relatively low centripetal force (18,000 G), and demonstrates a great improvement in the quality of deposits that can be formed. Repeated centrifugation/decantation is shown to enrich suspensions in unbundled high aspect ratio SWNTs. The hydrophobic nature of SWNTs necessitates the use of an emulsifier to support SWNT dispersion. Various species, including surfactants, DNA, polymers, and lipids, can be used to this effect. Surfactants are commonly used if the ultimate goal involves formation of electronic materials, since they can be more easily removed after the nanotubes are deposited. Of the various surfactants available, sodium dodecyl sulfate (SDS) was chosen for these studies because it has the lowest binding energy with SWNTs of the average diameter ($\sim 1.55 \pm 0.1$ nm) observed for the arc discharge soot used in these studies.⁴² This is an important consideration, as the ultimate goal is to remove the surfactant after deposition of the SWNTs, in order to improve electronic performance and reproducibility.⁴³

Recently published work by this group concerned the use of chemical and heat treatments that are compatible with heat-sensitive substrates to improve the resistance and inter-device precision of networks that were cast from SDS suspensions.⁴⁴ When several highly resistive networks of similar SWNT densities were treated with mild oxidative and annealing treatments, a 13-fold reduction in resistance was accompanied by a 28-fold increase in inter-network precision. The effectiveness of this treatment for increasing conductivity by removing SDS was verified by Raman microscopy. Additionally, the increase in conductivity and precision was also ascribed to

the formation of “molecular anchors,” which served to decrease the tunnel barrier at junctions between SWNTs.

Although many commonly reported purification methods have the potential to address either of the two challenge areas listed earlier, the approach described in this manuscript concurrently addresses both challenges by achieving 1) purification of SWNT soot without damaging oxidative treatments, and 2) the formation of stable suspensions of unbundled, high aspect ratio SWNTs having controlled concentration and length. Raman spectroscopy and UV-Vis-NIR spectroscopy were used to confirm that impurities were removed by each purification cycle, while SWNTs remained suspended. Atomic force microscopy (AFM) demonstrated the effectiveness of this purification method for the formation of SWNT deposits in on Si/SiO_x wafer fragments.

The laminar flow deposition method developed by this group ensures that nanotube bundling does not occur during the deposition process.⁴⁵⁻⁴⁷ It has been shown to allow great control over the density and alignment of unbundled SWNTs deposited on self-assembled monolayer-modified surfaces.⁴⁷ This deposition method is a critical part of these studies, as the ability of the suspension processing method to remove SWNT bundles can only be ascertained by AFM if bundle formation is prohibited during the deposition process. This group’s deposition method is also an important new tool in SWNT network formation, as other common deposition methods, like layer-by-layer,⁴⁸ fluidic assembly,⁴⁹ and dip-coating⁵⁰ result in bundles of SWNTs.

2.3 Experimental Procedure

2.3.1 Formation and Purification of SWNT Suspensions.

To form the suspensions, 1 mg/mL AP grade arc discharge soot (Carbon Solutions, Inc) was dispersed in 1% SDS (J.T.Baker) solution via 30 min. of probe ultrasonication (Fisher Model

500) at a power density of 0.4 W/mL, which imparted 21 kJ of energy to the suspension. Previous work by Vichchulada et al. has demonstrated that these conditions are optimum for the production of suspensions of unbundled SWNTs while minimizing sonication-induced damage to the SWNTs.⁵¹ Next, SWNT suspensions were distributed into 1.5 mL centrifuge tubes and centrifuged (Beckman Microfuge) for either 45 or 90 min. at 18,000 G, as described in Figure 2.1a. After centrifugation, the supernatant was carefully removed in 0.2 mL aliquots, labeled A, B, C, D, and E. Spectroscopic and scanning probe data was obtained for each of these aliquots.

In order to determine the effect of multiple centrifugation cycles on the purity and enrichment in high aspect ratio SWNTs, the upper 50% of the supernatant was carefully collected after each of six 45 min. centrifugation cycles (Figure 2.1b). Then, the upper fractions were placed in new centrifuge tubes, and the process was repeated. This allowed observation of the effect of iterative processing steps on the purity and average length of SWNT suspensions and deposits.

2.3.2 Formation of SWNT Deposits via Laminar Flow Deposition (LFD)

Si/SiO_x wafers were cut into 1 x 1.5 cm fragments and cleaned with compressed CO₂. Prior to SWNT deposition, the substrates were modified with a self-assembled monolayer by a 45 min. immersion in a solution of 2.11 mg/mL 3-aminopropyl triethoxysilane (99%, Sigma Aldrich) in ethanol (99.5%, absolute 200 proof, ACROS). In order to ensure that only one monolayer of the silane remained, the substrates were washed with copious amounts of ethanol, and water. Then, they were dried in a stream of N₂ gas. Finally, they were cleaned with compressed CO₂, as this has been demonstrated to remove excess layers of polymerized silane.⁵²

After substrate preparation, two deposition cycles, each using 90 μL of SWNT suspension, were used to form the low-density SWNT deposits that would be used for AFM analysis. Each deposition cycle consisted of wetting the silane coated Si/SiO_x wafer with the SWNT suspension,

followed by quick drying in a stream of N₂ gas at a pressure of 60 psi (Figure 2.1c). The wafers were then rinsed with copious amounts of nanopure water (>18.1 MΩ) and then dried again under a stream of N₂ gas.

In this manner, bundle formation is prohibited during the drying process by greatly reducing the height of the suspension to a thin layer (~400 nm in thickness) that is characterized by viscous flow, prior to nanotube deposition, as described by Zhang et. al.⁴⁵ Because the translational diffusion of these isolated SWNTs is quite low, they are deposited on the surface in low densities during a brief evaporation phase. Therefore, this deposition method facilitates the deposition of individual SWNTs, as long as they are unbundled in the processed suspension.

2.3.3 Characterization of SWNT Suspensions and Deposits by UV-Vis-NIR Spectroscopy, AFM, and Raman Spectroscopy

UV-Vis-NIR spectroscopy (Cary, 5000) was performed using a quartz cell with a path length of 1 mm. An absorbance of 600 nm has been found to yield a linear relationship between SWNT concentration and absorbance.⁵³ This is likely due to the lower scattering efficiency of SWNTs at this wavelength and the fact that it falls between absorbance bands for semiconductive and metallic SWNTs. However, carbonaceous impurities have a maximum absorbance ~ 242 nm,⁵⁴ so comparison of the data obtained for these two wavelengths was used to quantitate the purity of the suspensions during processing.

AFM images were obtained via intermittent contact mode in air (Molecular Imaging, Pico Plus). Five areas of each sample were analyzed with AFM image analysis software (WSxM, v5.0)⁵⁵ to determine the effect of the separation process on the average height, and length of SWNTs, as well as the surface height and roughness. This provided information on the concentration of bundles and the degree of length separation obtained. Additionally, the change

in surface height and roughness was also evaluated in order to determine the density of residual impurities.

Raman spectroscopy (Thermo Scientific, DXR SmartRaman) was performed on suspensions in a sealed capillary tube and on SWNT deposits without any further modification. A charge-coupled device (CCD) detector was used to record spectra obtained using a 532 nm diode laser excitation source. Suspensions were analyzed with a 10 X objective and a source intensity of 10 mW at the sample, while for SWNT deposits, a 50 X objective with 1 mW intensity at the sample was employed.

2.4 Results and Discussion

2.4.1 Effect of Processing Time on the Purification of SWNT Soot

For both 45 and 90 min. processing times, the magnitude of the UV-Vis-NIR absorbance for each suspension increased in alphabetical order with each aliquot (Figure 2.2), indicating the presence of a density gradient in carbonaceous impurities. By comparison, the data for 45 min. has a higher absorbance for every layer, relative to its counterpart in the 90 min. data. Additionally, aliquots A for both samples had the lowest peak absorbance at ~ 242 nm, with values of 1.11 and 0.86 for 45 and 90 min., respectively. Aliquots B and C were relatively close to A in magnitude, but there is a significant increase in absorbance for D and E. As each aliquot represented 0.2 mL of suspension, this indicates that after both processing procedures, the upper 50% of the supernatant was significantly improved in purity.

Aliquot E consistently had the greatest absorbance for all samples, achieving a peak absorbance of 1.31 and 1.13 for 45 and 90 min., respectively. This greater absorbance indicates that 90 min. is more effective at isolating the amorphous carboxylated C impurities and SWNT bundles in the lower half of the centrifuge tube. Therefore, a large portion of the impurities in the

SWNT soot was sequestered in the lower 50% of the sample, culminating in a pellet at the bottom. The shoulder at ~275 nm, on the low-energy side of the peak, becomes more pronounced at longer centrifugation times. This is due to the high extinction coefficient for amorphous C impurities.^{56,57}

In the region of the spectra that corresponds to the second interband transitions (E_{22}) for semiconducting SWNTs, ~1010 nm, the absorbance decreased significantly after processing at either 45 or 90 min. (Figure 2.3). As the average absorbance observed for unprocessed suspensions was 2.14, it was normalized to the absorbance for aliquot E and offset by 0.1 absorbance units to allow visualization of the change in the size of the peak before and after processing. This significant reduction in absorbance between AP-grade and processed suspensions is expected, due to the significant reduction in residual carbonaceous impurities, which increase the baseline of the absorbance of the suspensions throughout the visible and NIR range and bundles of SWNTs.

The increased size of the semiconducting interband transition peak relative to the baseline is indicative of the enrichment of the suspension in unbundled SWNTs, as the absorbance due to these transitions is not quenched, as in bundled SWNTs. Also of note in the NIR spectra is the presence of small waves on the low-wavelength side of the band centered at 1010 nm. These peaks are indicative of electronic transitions in SWNTs of various chirality and diameters.⁵⁸ These peaks are better resolved in suspensions of short nanotubes.

Evidently, the viscosity of the aqueous solvent used in these studies was sufficient to stabilize the density gradients such that they could be observed in each aliquot, without the need for a density gradient in the solvent. This is consistent with a recent report of a NIR fluorescence videomicroscopy study that determined the translational diffusion coefficient for unbundled, surfactant encapsulated SWNTs may range from 0.3 to 6 $\mu\text{m}^2/\text{s}$, with high aspect ratio SWNTs at

the lower end of this range.⁵⁹ Short SWNTs, down to 130 nm, were observed to have the highest translational diffusion coefficients while those of $\sim 1 \mu\text{m}$ in length had the lowest coefficients.

The absorbance at 242 nm is sensitive to π electron-containing amorphous carbon impurities, as well as the plasmon resonances in the free-electron clouds of the nanotubes. The measured absorbance in this range is also augmented by scattering that occurs when short wavelength light interacts with suspensions of carbon nanotubes.⁵³ The absorbance at 600 nm is more sensitive to the SWNTs. This allows a qualitative estimate of the degree of purification, because a decrease in the magnitude of the ratio $A(242 \text{ nm}) / A(600 \text{ nm})$ indicates a decrease in the absorbance of carbonaceous impurities, relative to that for SWNTs (Figure 2.4). Across processing times, 90 min. was found to yield slightly lower ratios. This is likely due to the greater processing time facilitating the removal of more impurities. AFM analysis, discussed in a subsequent section, corroborates this assertion.

Raman spectroscopy is well suited for characterizing the relative purity of SWNT suspensions and deposits due to the high Raman scattering efficiency of both defect-free and disordered sp^2 hybridized carbon atoms. The graphite band (G-band), which occurs near 1590 cm^{-1} , is indicative of tangential phonons in the pristine nanotubes, while the disorder band (D-band), near 1370 cm^{-1} , is indicative of asymmetric stretching in amorphous sp^2 hybridized C (Figure 2.5 shows Raman data for suspensions and deposits after 90 min. processing). When the Raman spectra are normalized to the intensity of the G-band for each processing time, the ratio of the two intensities (I_G/I_D) is a measure of the relative enrichment of pristine SWNTs and removal of amorphous C impurities.

For both processing times, liquid Raman experiments exhibited a small trend toward lower I_G/I_D ratios for each aliquot (Figure 2.6). Yet, there was a pronounced difference between the I_G/I_D

ratios obtained for suspensions vs. deposits. The I_G/I_D ratio for suspensions increased by more than 100 % with increased processing time, the ratio for deposits formed from those suspensions increased by only 15 %. This indicates that the LFD process is another manner by which the impurities are removed.

2.4.2 Effect of Processing Time on the Enrichment in High Aspect Ratio SWNTs

AFM is indispensable in the study of purification and enrichment of SWNT soot as it allows a direct correlation between the suspension processing method and the qualities of the SWNT networks that can be formed. For both processing times, aliquot A was observed to have a higher density of SWNTs and globular impurities, with the density of impurities increasing in ascending order (Figure 2.7). For 45 min. processing times, the average length of SWNTs decreased from 1.45 ± 0.4 to 0.9 ± 0.2 μm between aliquots A and E. While for 90 min., the lengths decreased from 1.75 ± 0.4 to 0.85 ± 0.2 . This indicated that just one processing step was sufficient to begin the process of enriching the supernatant in high aspect ratio SWNTs, although significant impurities remained.

For both processing times, the suspended high aspect ratio SWNTs remained stable in the supernatant for periods that allowed removal of each aliquot. AFM analysis indicated average lengths between 1.2 and 2.0 μm . In order to determine the purity of each deposit, a histogram was plotted for the height, or z-range data for each AFM image. This allows quantitation of the average height, and thus level of impurities on the surface, since arc discharge nanotubes have an average height of 1.55 ± 0.1 nm, while impurities are generally much larger. There was a consistent trend toward a higher average height with ascending order for each aliquots, with the average height increasing from 7.98 to 34.87 nm for suspensions processed for 45 min., and from 10.48 to 13.05

nm for 90 min. Therefore, 45 min. periods resulted in better quality deposits formed from the upper levels of the supernatant.

Within each sample, the RMS surface roughness also increased in alphabetical order within each sample, while across processing times, the RMS roughness increased at a faster rate for the samples processed for the shorter period (Figure 2.8). The roughness values increased from 3.09 to 7.29 nm, and from 3.51 to 5.02 nm for 45 and 90 min., respectively. This indicates that the shorter processing period allows sufficient time for separation of impurities, but is less effective at pelletization of impurities. The consistent increase in the observance of impurities with each aliquot indicates the stability of the suspensions with regard to the impurities that were sequestered near the bottom of the centrifuge tube during processing. This represents a significant advance in the separation of SWNTs from impurities, and enrichment in high aspect ratio nanotubes, as this level of separation is achieved without requiring the addition of the density gradient media like iodixanol, commonly used in DGU. This reagent is much more difficult than SDS to remove after an SWNT deposit is formed, as described in recent reports.^{60, 61}

2.4.3 Effect of Iterative Processing on the Separation of High Aspect Ratio SWNTs

AFM analysis showed that processing periods of 45 min. yielded the highest density of high aspect ratio SWNTs, but also resulted in deposits that had significant residual impurities. Therefore, an iterative approach (Figure 2.1b) was used in order to determine the efficacy of this processing method for producing suspensions enriched in longer SWNTs, while also achieving a greater degree of purity in deposits. For these suspensions, the ratio $A(242 \text{ nm}) / A(600 \text{ nm})$ exhibited a slight increase with each processing step (Figure 2.9). This indicates that although both absorbance's decrease with each processing iteration, $A(600 \text{ nm})$ is decreasing at a faster rate relative to $A(242 \text{ nm})$, causing a slight increase in the ratio of the absorbance's from processing

iteration 1 to 6. This is consistent with previous work from this group that shows that most of the globular impurities are removed in the first processing step.⁴¹ Therefore, each successive processing step refines the suspension by removing small bundles of SWNTs, as well as residual carbonaceous impurities. Since $A(242\text{ nm})$ is sensitive to both impurities and the free-electron clouds in the SWNTs, the loss of these bundles causes $A(600\text{ nm})$ to decrease at a faster rate than $A(242\text{ nm})$, resulting in a slight increase in the ratio $A(242\text{ nm}) / A(600\text{ nm})$.

AFM images of unprocessed samples exhibited a high coverage of large globular impurities and large SWNT bundles (Figure 2.10). However, a dramatic improvement in the quality of the deposit can be seen after the first processing step, as most of the large impurities are removed as discussed previously. After the sixth iteration, the highest density of SWNTs, relative to impurities was observed. Semi conductive 2-D networks of SWNTs, for electronic materials applications, can be readily formed from suspensions of this quality by increasing the number of deposition cycles until the percolation threshold for semi conductive nanotubes is exceeded.

The average height was observed to decrease from 40.00 to 1.31 nm (Table 1). This final height, which is consistent with the height of one SWNT, indicates a significant improvement over previous reports of the deposition of SWNTs. With each processing step, there was also a steady decrease in the average height and RMS roughness values, indicating that the few impurities that remained were significantly smaller than in the unprocessed sample. Importantly, there was a concurrent increase in the average length of SWNTs from 1.18 to 2.07 μm , indicating that each iteration further enriched the supernatant in high aspect ratio SWNTs, while removing shorter nanotube fragments with other impurities.

Of great significance is the fact that the average density of SWNTs in each deposit increased from 0.31 to 0.79 SWNTs/ μm^2 , further indicative of the continued enrichment of high

aspect SWNTs in the supernatant with each processing step. This can be explained by the increased buoyancy of longer SWNTs in these aqueous suspensions. Nair et al. observed that the buoyancy of a surfactant-encapsulated SWNT increases with the density of surfactant molecules adsorbed along the nanotubes length for various surfactants and chiralities.⁶² Further, recent work has indicated that SDS molecules orient perpendicular to the hydrophobic sidewalls of suspended SWNTs. This increases the volume while decreasing the density of the SDS/SWNT construct.⁶³ Therefore, in this work, these unbundled, high aspect ratio SWNTs provide more area for the adsorption of SDS, increasing their relative buoyancy. Then, the low centripetal forces used in these studies not only removed low aspect ratio impurities, but also allowed the enhanced buoyancy of unbundled high aspect ratio surfactant-encapsulated SWNTs to isolate them in the supernatant.

2.4.4 The LFD Method Results in Further Purified Deposits

The I_G/I_D ratios calculated from Raman spectra of suspensions and deposits indicated an increase in the quality of the deposit relative to the suspension, as determined from the increased signal for pristine sp^2 -hybridized C, relative to defect-containing allotropes (Figure 2.11). This increase in I_G/I_D ratio with increasing processing iterations is due to the enrichment of the suspensions in high aspect ratio SWNTs with pristine sidewalls, as well as the removal of amorphous carbon. For suspensions, the I_G/I_D ratios increased by roughly a factor of three over the course of the first two processing iterations. However, there was a factor of four increase for deposits over this same range, indicating that the LFD network formation step is an additional purification step in the formation of thin-films, providing the suspension has been purified of the more dense particulates. The formation of deposits of high aspect ratio SWNTs is further facilitated by the greater translational diffusion coefficient for shorter SWNTs making it more

likely that they remain in suspension during the deposition process. Therefore, the increase in the ratio for deposits relative to that observed for suspensions is also due to the decreased presence of short SWNTs that likely have oxidized ends.

2.5 Conclusions

Enrichment of high aspect ratio SWNTs was obtained via a readily scalable batch purification method. The sedimentation method of centrifugation that was used in these studies differs from density gradient ultracentrifugation in that the addition of solutes to form zones of varying gradients in the solvent are not needed. This allows the purification and enrichment process to occur without the addition of additional reagents, many of which are difficult to remove in subsequent steps. The buoyancy of surfactant-encapsulated SWNTs increases with length. Then, the low centripetal forces used in these studies not only removed low aspect ratio SWNTs and impurities, but also allowed the enhanced buoyancy of unbundled high aspect ratio surfactant-encapsulated SWNTs to be used to isolate them in the supernatant. For all processing conditions, an increase in the purity deposits, relative to the suspensions, was observed via Raman spectroscopy. This indicates that the reduced translational diffusion coefficient of high aspect ratio SWNTs promotes their deposition over residual low aspect ratio impurities and nanotubes.

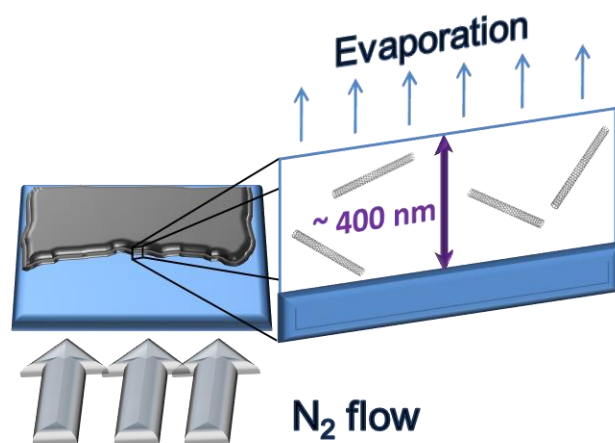
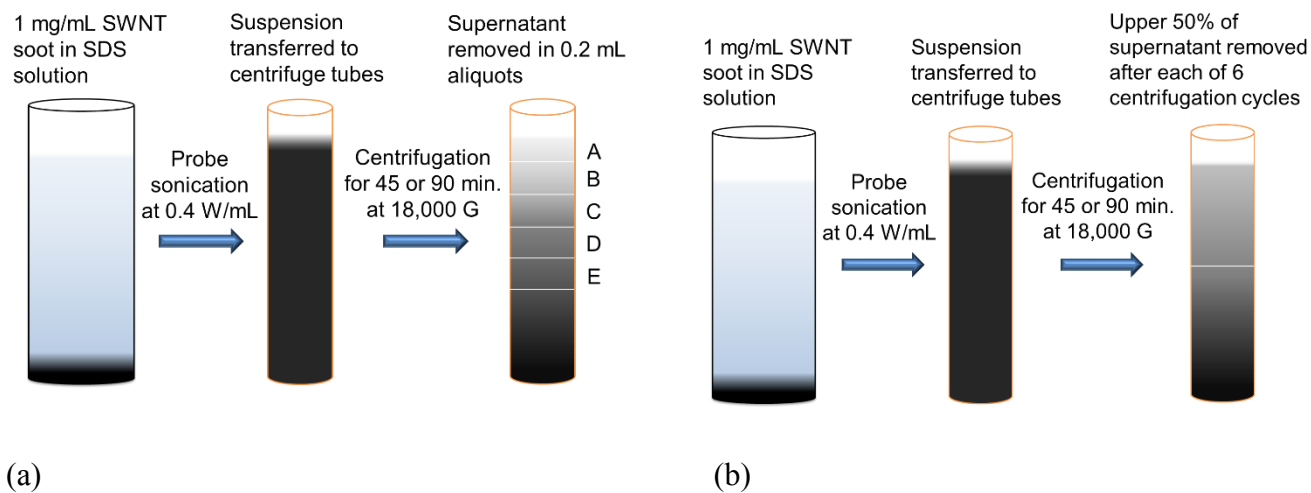
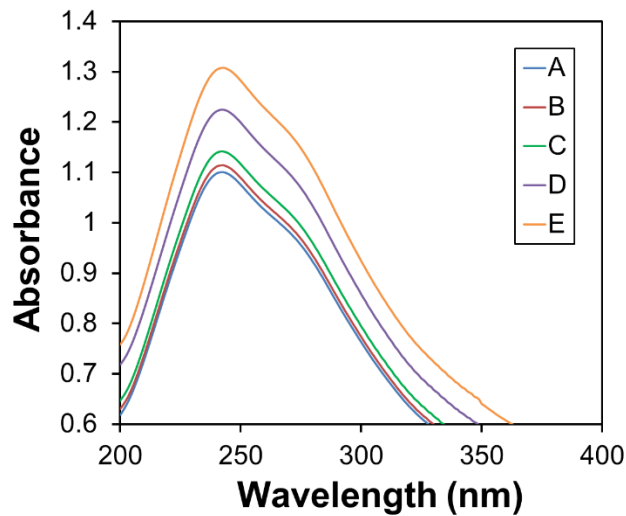
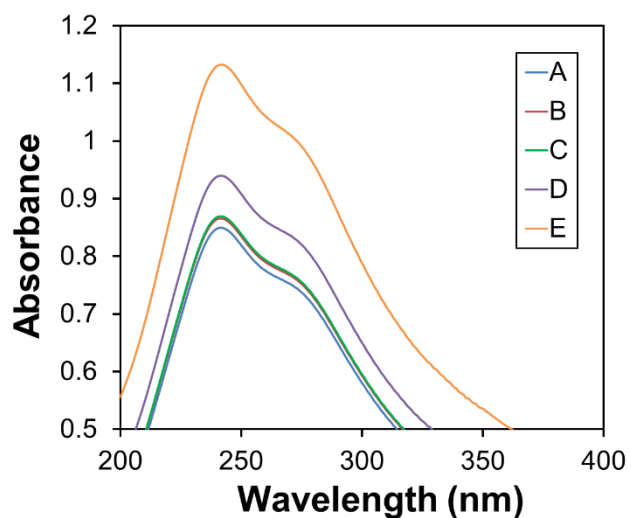


Figure 2.1. Schematic for the two experimental approaches employed (not to scale). Probe sonication at a power density of 0.4 W/mL was used to form suspensions of AP-grade SWNT. Then, the suspensions were either: a) treated with centrifugation at 18,000 G for 45 or 90 min., followed by careful removal of the supernatant in 0.20 mL aliquots, or; b) the upper 50% of the supernatant was carefully removed after each of six 45 min. centrifugation cycles; c) since the importance of shear forces is supplanted by viscous forces as the suspension thins, low densities of unbundled SWNTs are isolated and deposited via rapid evaporation, without the possibility of

bundle formation. This allows the degree of SWNT bundling in the processed suspension to be assessed.

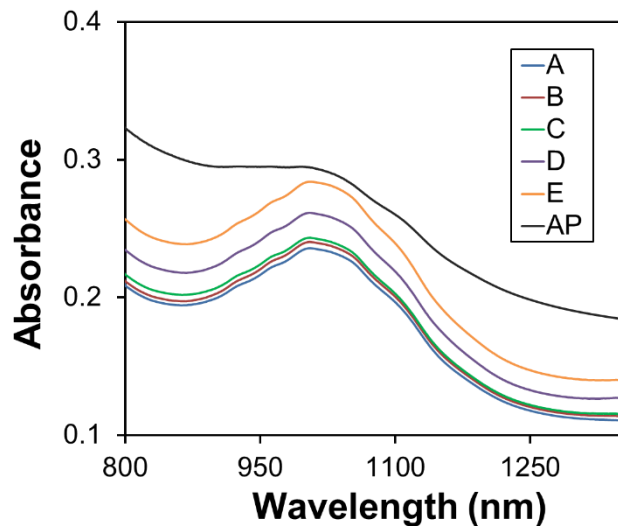


(a)

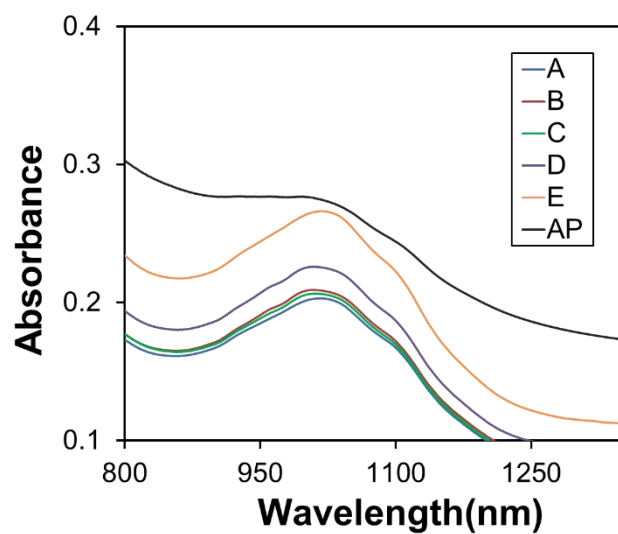


(b)

Figure 2.2. The absorbance in the UV region of the spectra for aliquots A-E increased from the top to the bottom for both processing times; a) after one 45 min. step, the shoulder on the low energy side of the band at 242 nm is less pronounced than; b) after processing at 90 min.



(a)



(b)

Figure 2.3. For NIR spectra of the E₂₂ transitions for semiconducting SWNTs, the unprocessed suspension was normalized to the peak ~1010 for sample E and then offset by 0.1 absorbance units for clarity. a) After 45 min. of processing, a greater absorbance, and presence of fine structure, was observed on the high-energy side of the band, while; b) for 90 min., the absorbance was lower and a greater difference in the magnitude of the absorbance was observed between aliquots

corresponding to the line between the upper and lower 50 % of the suspension (between aliquots labeled D and E).

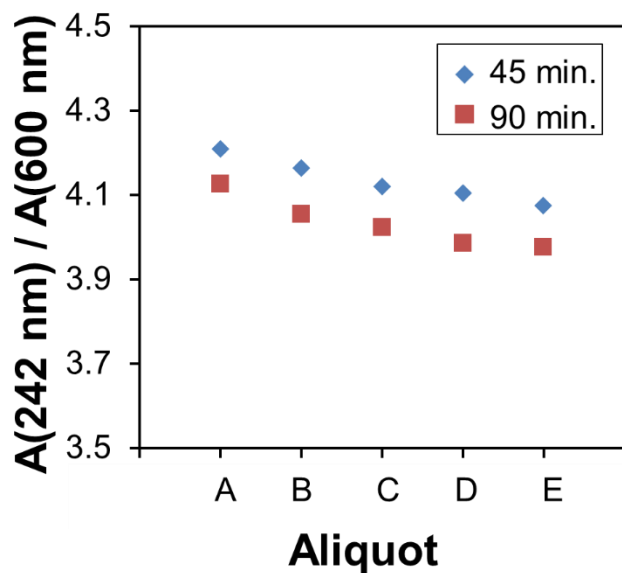
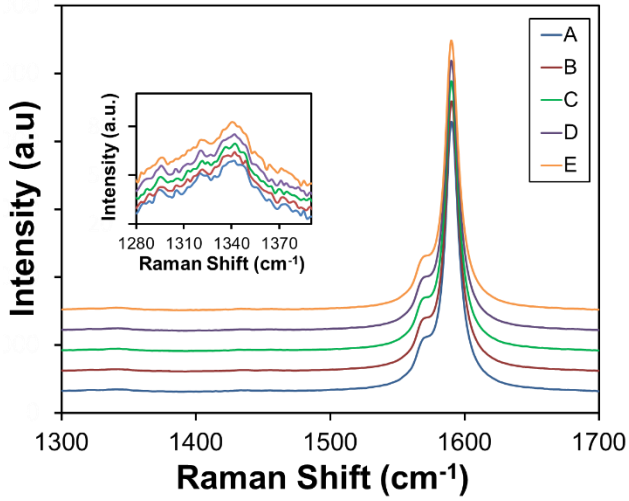
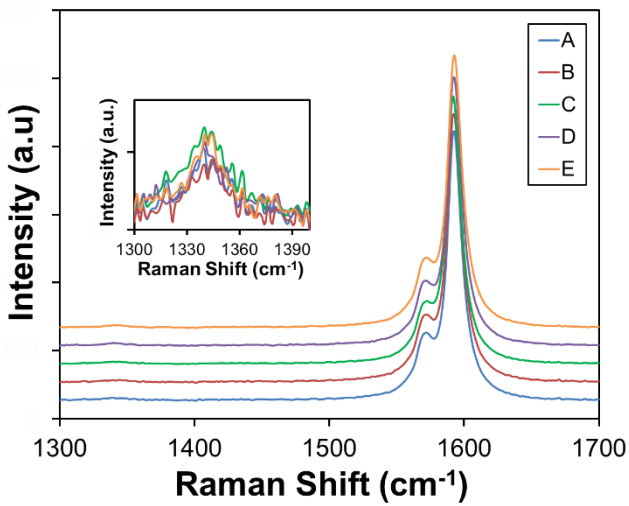


Figure 2.4. Due to the high extinction coefficient of impurities at 242 nm, relative to that of SWNTs at 600 nm, the ratio of the absorbance at these two wavelengths is indicative of changes in the purity and concentration of SWNT after each processing step. The slighter lower ratios for 90 min. processing periods indicate a slight increase in the ability to remove impurities.

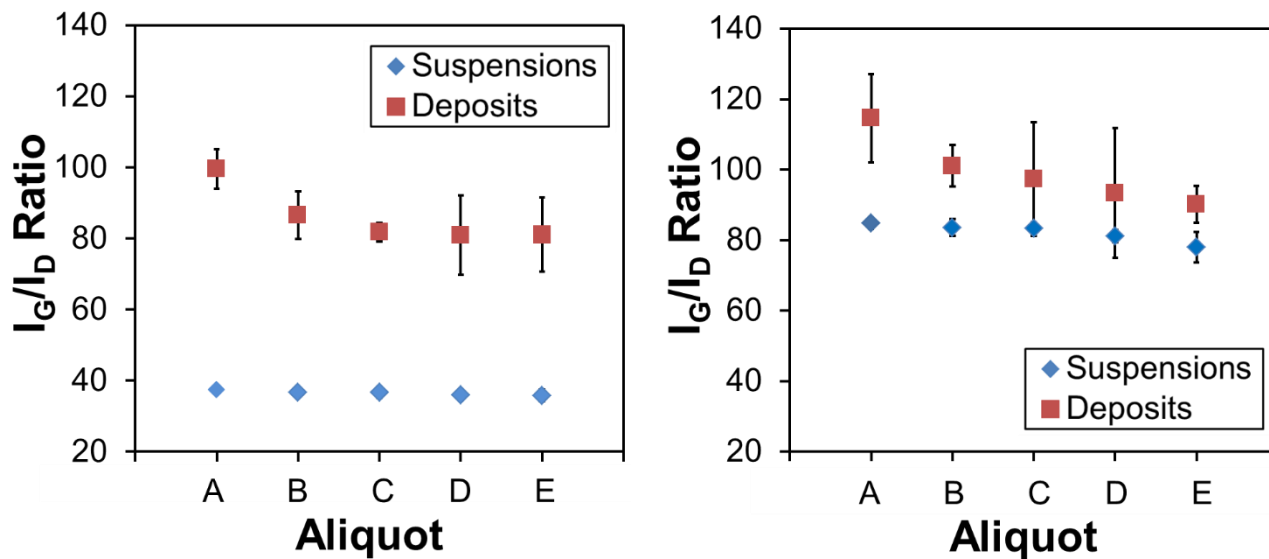


(a)



(b)

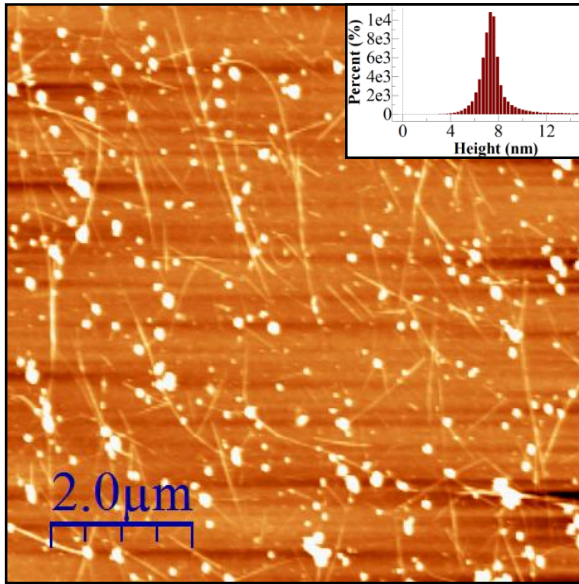
Figure 2.5. Representative Raman spectra obtained after 90 min. processing periods for: a) SWNT suspensions and b) deposits. The insets show the D-band regions.



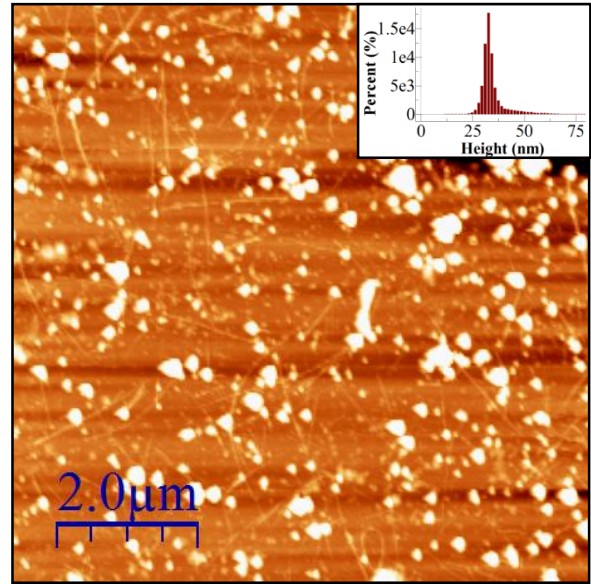
(a)

(b)

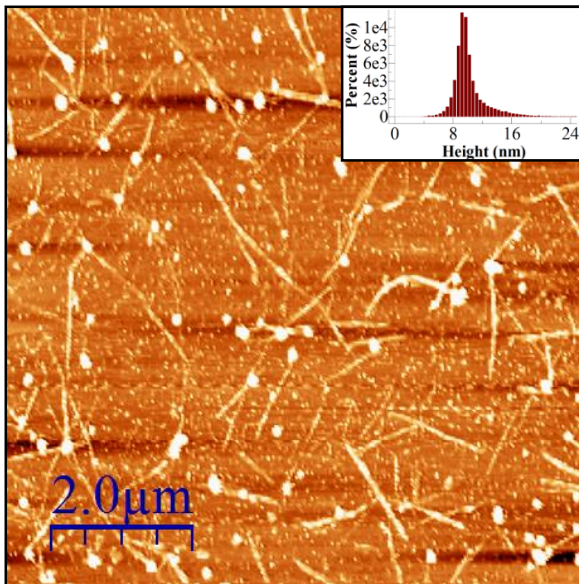
Figure 2.6. The average I_G/I_D ratios observed for SWNT suspensions and deposits formed from each aliquot showed an overall decrease in magnitude with ascending order. A greater difference in the ratios for suspensions and deposits was observed for a) 45 min. than b) 90 min., indicating that the LFD method used to form the deposits preferentially deposits high aspect ratio SWNTs over residual impurities in the suspension processed for 45 min.



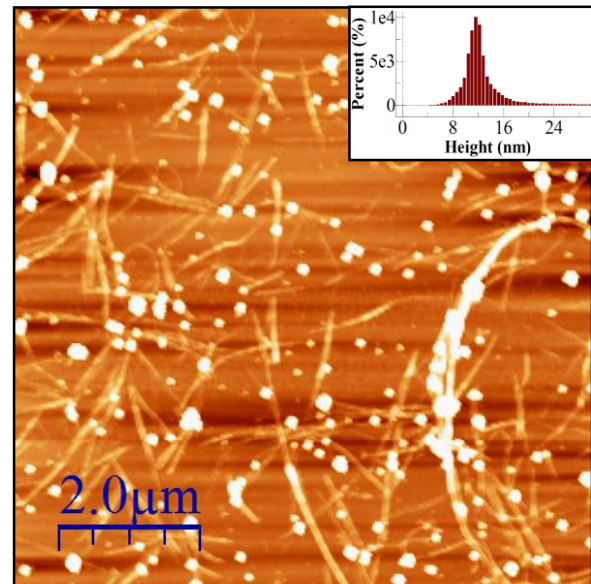
(a)



(b)



(c)



(d)

Figure 2.7. AFM images ($8 \times 8 \mu\text{m}$) for SWNT deposits on Si/SO_x wafer fragments showed that; a,b) 45 min. processing times lead to a greater density of SWNTs and impurities between aliquots A and E, respectively than; c,d) 90 min. periods for aliquots A and E, respectively.

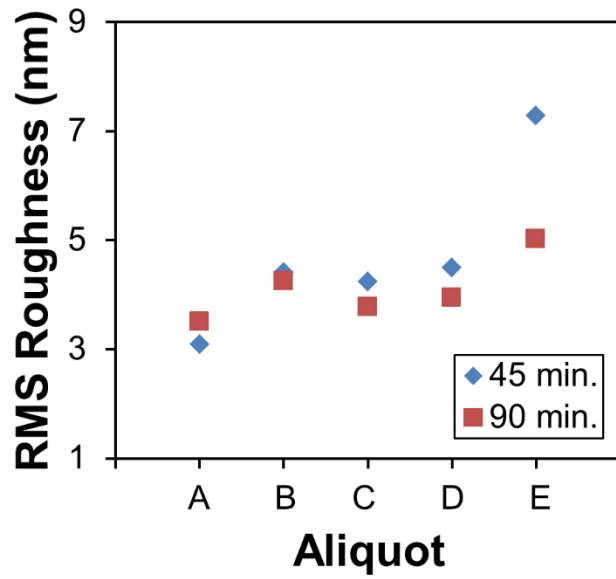


Figure 2.8. RMS roughness values for 45 and 90 min. processing times were in close agreement for the first few aliquots. However, at lower levels of the suspensions, the shorter time for separation and pelletization of impurities resulted in increased surface roughness.

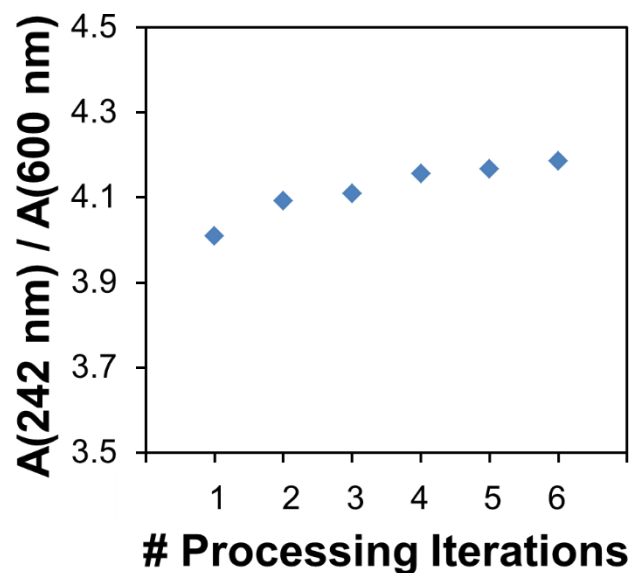
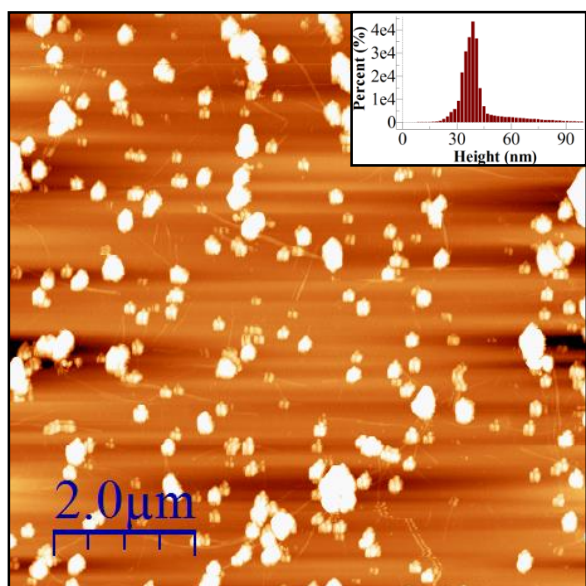
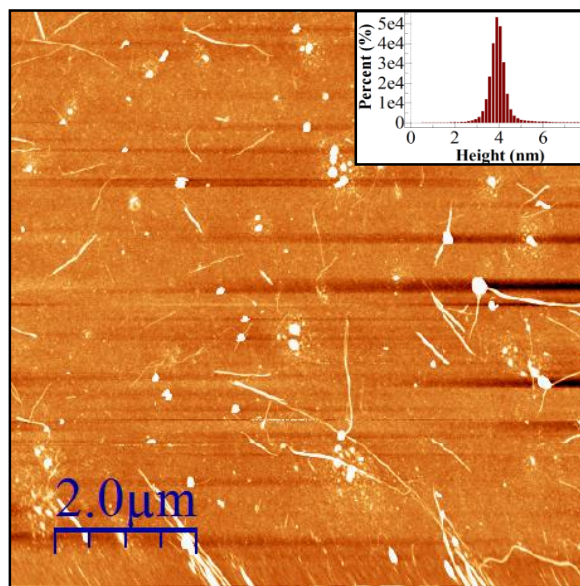


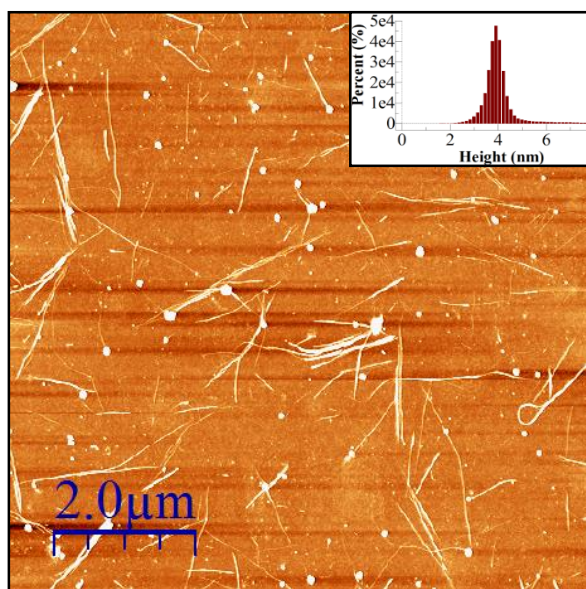
Figure 2.9. The ratio of $A(242 \text{ nm}) / A(600 \text{ nm})$ was highest for an AP suspension of 0.1 mg/mL SWNT soot. A sudden drop in the ratio after the first processing step indicated that much of the carbonaceous impurities were removed in the first processing step. Then, the increase in this ratio with each processing step is indicative of the enrichment in unbundled SWNTs.



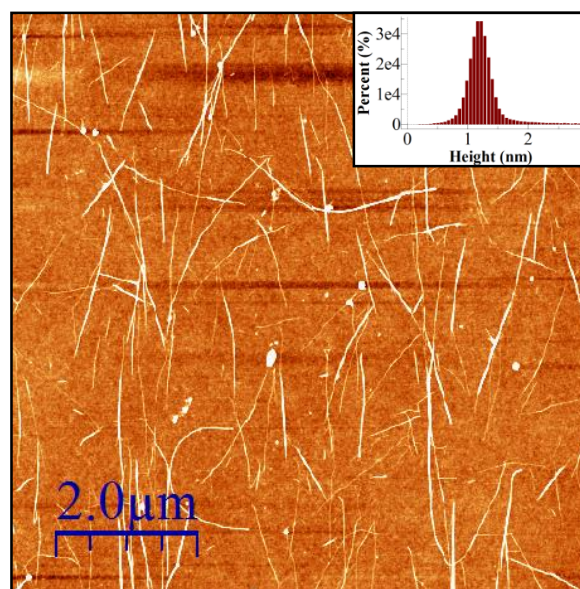
(a)



(b)



(c)



(d)

Figure 2.10. Representative AFM images ($8 \times 8 \mu\text{m}$) for deposits formed from suspensions at various stages of processing; a) an unprocessed suspension resulted in a deposit with average height of 40.00 nm; b) the average height decreased to 4.89 nm after the first processing iteration;

c) after three steps, the average height was 3.38 nm; d) six stages resulted in average height of 1.31 nm, indicating significant removal of impurities and unbundling of SWNTs.

Table 2.1. AFM analysis of the effect of iterative processing steps on low-density SWNT deposits.

# SWNTs/ μm^2	-	0.31	0.42	0.48	0.54	0.59	0.79
Average Length (μm)	-	1.18	1.31	1.55	1.65	1.7	2.07
% Standard Deviation	-	10	17	12	15	8	11
Average Surface Height (nm)	42.31	4.11	4.67	4.16	3.18	3.48	1.31
RMS Surface Roughness (nm)	14.93	1.65	1.89	1.69	1.39	1.31	0.74

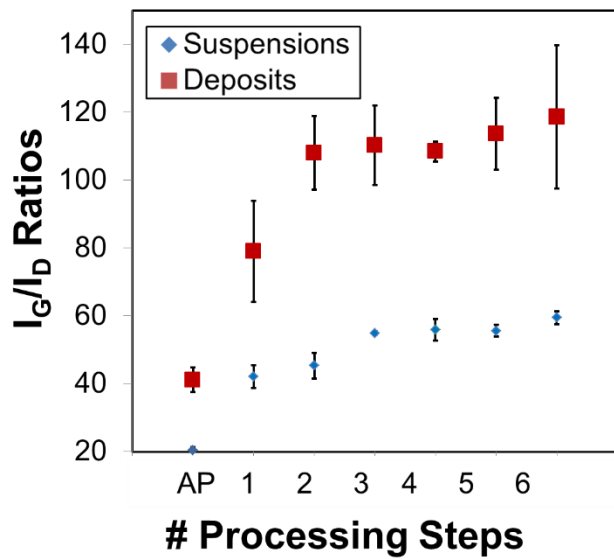


Figure 2.11. The evolution of Raman I_G/I_D ratios for suspensions and deposits of SWNTs over six processing iterations shows that the deposition process plays an important role in separating pristine SWNTs from impurities.

2.6 REFERENCES

1. Ruoff, R. S.; Yu, M.-F.; Rohrs, H., Nanomanipulation and Characterization of Individual Carbon Nanotubes Recent Advances in Experimental Mechanics. Gdoutos, E. E., Ed. Springer Netherlands: 2004; pp 65-74.
2. Bocharova, V.; Kiriy, A.; Oertel, U.; Stamm, M.; Stoffelbach, F.; Jerome, R.; Detrembleur, C. *J. Phys. Chem. B* **2006**, 110, (30), 14640-14644.
3. Hu, L.; Hecht, D. S.; Grüner, G. *Nano Letters* **2004**, 4, (12), 2513-2517.
4. Durkop, T.; Getty, S. A.; Cobas, E.; Fuhrer, M. S. *Nano Lett.* **2004**, 4, (1), 35-39.
5. Nakamura, S.; Ohishi, M.; Shiraishi, M.; Takenobu, T.; Iwasa, Y. *Appl. Phys. Lett.* **2006**, 89, (1), 013112.
6. Bradley, K.; Gabriel, J. C. P.; Gruner, G. *Nano Lett.* **2003**, 3, (10), 1353-1355.
7. Wildoer, J. W. G.; Venema, L. C.; Rinzler, A. G.; Smalley, R. E.; Dekker, C. *Nature* **1998**, 391, (6662), 59-62.
8. Weber, J.; Kumar, A.; Kumar, A.; Bhansali, S. *Sens. Actuator B-Chem.* **2006**, 117, (1), 308-313.
9. Kwon, J.-H.; Lee, K.-S.; Lee, Y.-H.; Ju, B.-K. *Electrochem. Solid-State Lett.* **2006**, 9, (9), H85-H87.
10. Pengfei, Q. F.; Vermesh, O.; Grecu, M.; Javey, A.; Wang, O.; Dai, H. J.; Peng, S.; Cho, K. *J. Nano Lett.* **2003**, 3, (3), 347-351.
11. Patra, S. K.; Rao, G. M. *J. Appl. Phys.* **2006**, 100, (2), 024319.
12. Wang, M. S.; Peng, L. M.; Wang, J. Y.; Jin, C. H.; Chen, Q. *J. Phys. Chem. B* **2006**, 110, (19), 9397-9402.

13. Newson, R. W.; Green, A. A.; Hersam, M. C.; van Driel, H. M. *Phys. Rev. B* **2011**, 83, (11), 115421.
14. Li, E. Y.; Marzari, N. *Acs Nano* **2011**, 5, (12), 9726-9736.
15. Javey, A.; Guo, J.; Wang, Q.; Lundstrom, M.; Dai, H. J. *Nature* **2003**, 424, (6949), 654-657.
16. Zhao, J.; Lin, C.; Zhang, W.; Xu, Y.; Lee, C. W.; Chan-Park, M. B.; Chen, P.; Li, L.-J. *J. Phys. Chem. C* **2011**, 115, (14), 6975-6979.
17. Sarker, B. K.; Shekhar, S.; Khondaker, S. I. *Acs Nano* **2011**, 5, (8), 6297-6305.
18. Engel, M.; Small, J. P.; Steiner, M.; Freitag, M.; Green, A. A.; Hersam, M. C.; Avouris, P. *Acs Nano* **2008**, 2, (12), 2445-2452.
19. Cheon, J. H.; Bae, J. H.; Jang, J. *Solid-State Electron.* **2008**, 52, (3), 473-477.
20. Gleskova, H.; Hsu, P. I.; Xi, Z.; Sturm, J. C.; Suo, Z.; Wagner, S. *J. Non-Cryst. Solids* **2004**, 338, 732-735.
21. Schmidt, J. A.; Hundhausen, M.; Ley, L. *Phys. Rev. B* **2001**, 64, (10).
22. Sato, S.; Seki, S.; Honsho, Y.; Wang, L.; Nikawa, H.; Luo, G.; Lu, J.; Haranaka, M.; Tsuchiya, T.; Nagase, S.; Akasaka, T. *J. Am. Chem. Soc.* **2011**, 133, (8), 2766-2771.
23. Heremans, P.; Cheyns, D.; Rand, B. P. *Acc. Chem. Res.* **2009**, 42, (11), 1740-1747.
24. Rouhi, N.; Jain, D.; Burke, P. J. *Acs Nano* **2011**, 5, (11), 8471-8487.
25. Jeong, H. J.; Jeong, H. D.; Kim, H. Y.; Kim, J. S.; Jeong, S. Y.; Han, J. T.; Bang, D. S.; Lee, G. W. *Adv. Funct. Mater.* **2011**, 21, (8), 1526-1532.
26. Kim, S.; Park, J.; Ju, S.; Mohammadi, S. *Acs Nano* **2010**, 4, (6), 2994-2998.
27. Jiao, L. Y.; Xian, X. J.; Wu, Z. Y.; Zhang, J.; Liu, Z. F. *Nano Lett.* **2009**, 9, (1), 205-209.

28. Gonzalez-Dominguez, J. M.; Gonzalez, M.; Anson-Casaos, A.; Diez-Pascual, A. M.; Gomez, M. A.; Martinez, M. T. *J. Phys. Chem. C* **2011**, 115, (15), 7238-7248.
29. Shim, B. S.; Zhu, J.; Jan, E.; Critchley, K.; Ho, S.; Podsiadlo, P.; Sun, K.; Kotov, N. A. *Acs Nano* **2009**, 3, (7), 1711-1722.
30. Porro, S.; Musso, S.; Vinante, M.; Vanzetti, L.; Anderle, M.; Trotta, F.; Tagliaferro, A. *Physica E* **2007**, 37, (1-2), 58-61.
31. Holzinger, M.; Hirsch, A.; Bernier, P.; Duesberg, G. S.; Burghard, M. *Appl. Phys. A* **2000**, 70, (5), 599-602.
32. Li, J. X.; Chajara, K.; Lindgren, J.; Grennberg, H. *J. Nanosci. Nanotechnol.* **2007**, 7, (4-5), 1525-1529.
33. Worsley, K. A.; Kalinina, I.; Bekyarova, E.; Haddon, R. C. *J. Am. Chem. Soc.* **2009**, 131, (50), 18153-18158.
34. Hersam, M. C. *Nat. Nano.* **2008**, 3, (7), 387-394.
35. Tabakman, S. M.; Welsher, K.; Hong, G.; Dai, H. *J. Phys. Chem. C* **2010**, 114, (46), 19569-19575.
36. Carvalho, E. J. F.; dos Santos, M. C. *Acs Nano* **2010**, 4, (2), 765-770.
37. Ghosh, S.; Bachilo, S. M.; Weisman, R. B. *Nat Nano* **2010**, 5, (6), 443-450.
38. Yi, W.; Malkovskiy, A.; Chu, Q.; Sokolov, A. P.; Colon, M. L.; Meador, M.; Pang, Y. *J. Phys. Chem. B* **2008**, 112, (39), 12263-12269.
39. Vichchulada, P.; Shim, J.; Lay, M. D. *J. Phys. Chem. C* **2008**, 112, (49), 19186-19192.
40. Vairavapandian, D.; Vichchulada, P.; Lay, M. D. *Anal. Chim. Acta* **2008**, 626, (2), 119-129.

41. Shim, J.; Vichchulada, P.; Zhang, Q.; Lay, M. D. *J. Phys. Chem. C* **2010**, 114, (1), 652-657.
42. Carvalho, E. J. F.; dos Santos, M. C. *ACS Nano* **2010**, 4, (2), 765-770.
43. Valcarcel, M.; Cardenas, S.; Simonet, B. M. *Anal. Chem.* **2007**, 79, (13), 4788-4797.
44. Zhang, Q.; Vichchulada, P.; Shivareddy, S. B.; Lay, M. D. *J. Mat. Sci.* **2012**, 47, 6812-6822.
45. Zhang, Q.; Vichchulada, P.; Lay, M. D. *J. Phys. Chem. C* **2010**, 114, (39), 16292-16297.
46. Vichchulada, P.; Zhang, Q.; Duncan, A.; Lay, M. D. *ACS Applied Materials & Interfaces* **2010**, 2, (2), 467-473.
47. Zhang, Q.; Vichchulada, P.; Cauble, M. A.; Lay, M. D. *J. Mater. Sci.* **2009**, 44, (5), 1206-1211.
48. Zhu, J.; Shim, B. S.; Di Prima, M.; Kotov, N. A. *J. Am. Chem. Soc.* **2011**, 133, (19), 7450-7460.
49. Jaber-Ansari, L.; Hahm, M. G.; Somu, S.; Sanz, Y. E.; Busnaina, A.; Jung, Y. J. *J. Am. Chem. Soc.* **2009**, 131, (2), 804-808.
50. Jang, E. Y.; Kang, T. J.; Im, H. W.; Kim, D. W.; Kim, Y. H. *Small* **2008**, 4, (12), 2255-2261.
51. Vichchulada, P.; Cauble, M. A.; Abdi, E. A.; Obi, E. I.; Zhang, Q.; Lay, M. D. *J. Phys. Chem. C* **2010**, 114, (29), 12490-12495.
52. Chow, B. Y.; Mosley, D. W.; Jacobson, J. M. *Langmuir* **2005**, 21, (11), 4782-4785.
53. Priya, B. R.; Byrne, H. J. *J. Phys. Chem. C* **2008**, 112, 332-337.
54. Rance, G. A.; Marsh, D. H.; Nicholas, R. J.; Khlobystov, A. N. *Chem. Phys. Lett.* **2010**, 493, (1-3), 19-23.

55. Horcas, I.; Fernandez, R.; Gomez-Rodriguez, J. M.; Colchero, J.; Gomez-Herrero, J.; Baro, A. M. *Rev. Sci. Instrum.* **2007**, *78*, (1).
56. Ryabenko, A. G.; Dorofeeva, T. V.; Zvereva, G. I. *Carbon* **2004**, *42*, (8–9), 1523-1535.
57. Hare, J. P.; Kroto, H. W.; Taylor, R. *Chem. Phys. Lett.* **1991**, *177*, (4-5), 394-398.
58. Bachilo, S. M.; Strano, M. S.; Kittrell, C.; Hauge, R. H.; Smalley, R. E.; Weisman, R. B. *Science* **2002**, *298*, (5602), 2361-6.
59. Tsyboulski, D. A.; Bachilo, S. M.; Kolomeisky, A. B.; Weisman, R. B. *Acs Nano* **2008**, *2*, (9), 1770-1776.
60. Arnold, M. S.; Green, A. A.; Hulvat, J. F.; Stupp, S. I.; Hersam, M. C. *Nature Nanotechnology* **2006**, *1*, (1), 60-65.
61. Kavan, L.; Frank, O.; Green, A. A.; Hersam, M. C.; Koltai, J. n.; Zólyomi, V.; Kürti, J.; Dunsch, L. *J. Phys. Chem. C* **2008**, *112*, (36), 14179-14187.
62. Nair, N.; Kim, W.-J.; Braatz, R. D.; Strano, M. S. *Langmuir* **2008**, *24*, (5), 1790-1795.
63. Duque, J. G.; Densmore, C. G.; Doorn, S. K. *J. Am. Chem. Soc.* **2010**, *132*, (45), 16165-16175.

CHAPTER 3

EFFECT OF SUCROSE GRADIENT ON THE LENGTH, DENSITY AND PURITY OF SINGLE-WALLED CARBON NANOTUBES

Bhatt.N.P; Vichchualada; Lay.M.D. To be submitted to *Journal of Physical Chemistry*

3.1 ABSTRACT

Separating single-walled carbon nanotubes from carbonaceous impurities by density gradient centrifugation using sucrose gradient has been investigated. The manuscript presents a route to single step purification of SWNTs with varied concentrations by using sucrose gradient and producing greater yield of the high aspect ratio nanotubes. The purpose of the study is to see the effect of density gradient on the length, purity and the density of SWNTs using spectroscopic techniques. UV-vis and NIR spectroscopy was used to verify the separation of the carbon nanotubes from different sucrose densities. Across all different SWNT concentrations, the absorbance increased from 5% (w/v) to the bottom layer indicating effective separation of nanotubes within the sucrose densities. The unbundling was confirmed with M_{11} and S_{22} electronic transitions in NIR spectroscopy. The effect of viscosity in SDS is seen especially at higher sucrose concentration and lower SWNT concentration. Raman spectroscopy was used to confirm the separation of densities by measuring the I_G/I_D ratios. Lower ratios were observed from the top layer going towards the bottom of the centrifuge tube, indicating effective separation between the sucrose layers. Bundling in the suspension contributed to red shifts in Raman spectroscopy. Atomic Force Microscopy (AFM) was used to show the length, height and the roughness of each sucrose gradient. The density of SWNTs from AFM analysis concluded that, lower the SWNT concentration, lower the density of the network. The density increased with the increase in the sucrose layer, which can be explained by the theory of centripetal forces.

3.2 INTRODUCTION

Single-walled carbon nanotubes are emerging as potential candidates for wide range of applications due to their structural, mechanical, and electronic properties and particularly in electronic devices like thin-films, field emission sources¹ and sensors.^{2, 3} However, major hurdle must be overcome before many of these applications can be used, most importantly purification of as-produced carbon nanotube soot and also their tendency to aggregate into bundles. The carbon nanotubes can be synthesized using various techniques: arc discharge,^{4, 5} laser ablation,^{6, 7} and chemical vapor deposition.⁸ But regardless of the growth method, as produced (AP) SWNT soot consists of (30-70% by weight) impurities such as metal catalysts nanoparticles, amorphous carbon, and fullerenes. These impurities have deleterious effect on the performance of different electronic device such as transistors, sensors etc. So developing a purification technique without damaging the SWNTs is crucial in obtaining a fundamental understanding of properties of individual SWNTs.

In the recent years, several techniques have been developed for sorting SWNTs including gel electrophoresis,⁹ ultracentrifugation¹⁰, polymer wrapping,¹¹ DNA wrapping,¹²⁻¹⁴ and amine extraction.^{15, 16} Density-gradient centrifugation is an established method which is used to separate materials based on buoyant density. In this method, SWNTs move towards the isopycnic point forming a density gradient in the centrifuge tube. It also has been useful for separating SWNTs based on diameter and type of conductivity. Most DGU methods use high centripetal forces in excess of 100,000g that yields shorter nanotubes with length in nanometers.

Additionally, DGU and polymer wrapping involves reagents which are difficult to remove. DGU typically involves use of iodixanol as a gradient medium. This compound binds strongly to SWNTs and requires a separate dialysis treatment. Therefore this compound has other problems

which might interfere with the characteristics of the SWNTs during the separation process. Firstly, iodixanol has iodine atoms, so it will work as an electron acceptor for the SWNTs and will increase the conductivity of the semiconducting SWNTs and will degrade their characteristics.¹⁷ Secondly, it is a large molecule with the molecular weight of 1550 g/mol so it is difficult to remove it from the solution; an important consideration for electrical applications.¹⁷

Polymer wrapping can be used for the separation of metallic and semiconducting nanotubes. Polymers given an appropriate structure can wrap around the nanotubes. Among the widely used polymers for this purpose, polyvinylpyrrolidone (PVP) has been identified as one the best for wrapping functionalization of the tubes and already used to disperse or stabilize SWNTs in aqueous solutions.¹⁸ Recently, PVP has been used to stabilize debundled SWNTs in N-methyl-2-pyrrolidone (NMP).^{18, 19} However no studies about the stability of the dispersion have been reported. Using organic media in SWNT suspension can be challenging to remove, which is a requirement for electrical applications. It might require an additional treatment similar to the one mentioned for iodixanol. So the technique discussed in this paper does not include use of any reagents nor a polymer and hence it purifies SWNTs without any oxidative treatments or damage to them.

Hirano and group developed a technique to separate SWNTs using agarose gel column.²⁰ Agarose gel acts as an absorbent for semiconducting nanotubes and allows them to be separated by conductivity. This can be achieved by freeze squeeze technique²¹. Use of Agarose gel columns is relatively simple and cost effective, so it can be useful for metal/semiconductor separation. Although these separation methods are effective in obtaining the two types of nanotubes, purity of SWNT can be a hurdle because of presence of impurities in the column containing allyl-dextran-

based gel^{20,20}. So preparing a gradient for purifying nanotubes that do not require any use of additional reagents is of utmost importance.

The advantage of using sucrose over iodixanol for forming the density gradient is that sucrose does not act as an electron acceptor since it does not have any reactive atoms or aromatic groups.¹⁷ Because of this, the sucrose molecules will not increase the conductivity of semiconducting SWNTs and will not degrade their semiconducting characteristics. Comparing iodixanol with sucrose, iodixanol is a large molecule, thus it takes time to remove from the SWNT samples. This might interfere with the optical and electrical properties of SWNTs. Also sucrose being a smaller molecule and soluble with SDS gets removed easily by centrifuge filter. Sucrose has eight hydroxyl groups which help in enhancement of the solubility.²² This serves an important purpose in electrical applications as no additional reagents are required to remove unlike in iodixanol. Another factor that can influence the separation capability is the viscosity of sucrose as compared to iodixanol.

In the case of SWNT-SDS dispersion, SDS molecules tend to assemble into cylindrical aggregates on SWNT surface. It would be interesting to see how the SDS-sucrose molecules interact with each other as sucrose being a neutral molecule along with negatively charged SDS molecule. This approach will help understand how the surfactant (SDS) behaves when each layer of sucrose is surrounded by SDS and also to see whether this method produces higher yield than the ones discussed in literature. In this study, we present a method to purify SWNTs using sucrose as a gradient by using fixed angle rotor at low g (10,000g) centrifugation cycle without any coexisting impurities in the tube. UV-Vis-NIR were used to confirm the separation achieved while centrifuging and AFM demonstrates the effectiveness of the separation technique by making SWNT deposits on the Si/SiO₂ wafers.

3.3 EXPERIMENTAL PROCEDURE

3.3.1 Formation of SWNT Suspensions

To form the suspensions, 1 mg/mL and 0.5mg/mL and 0.1 mg/mL AP grade arc discharge soot (Carbon Solutions, Inc) was dispersed in 1% SDS (Sodium dodecyl sulfate) (J.T.Baker) solution via 30 min. of probe ultrasonication (Fisher Model 500) at a power density of 0.4 W/mL. Next, a sucrose density gradient in a 15 mL falcon tube was prepared by sequentially layering 0.5 mL each of the 25 % (w/v), 20 % (w/v), 15 % (w/v), 10 % (w/v) and 5 % (w/v) sucrose solutions from bottom to top and the SWNT suspensions were carefully added on the top of the sucrose gradient solution as shown in Figure 1. Then 5 mL of SWNT suspension was carefully added to the density gradient and the tubes were loaded in a fixed angled rotor (Rotor JA-10, Avanti-JE) and centrifuged at 10,000G for 60 min. After centrifugation, the solution was carefully removed in 1 mL aliquots and analyzed via scanning probe and spectroscopic methods.

To see the effect of SDS on sucrose solutions with SWNTs, the sucrose solutions were made with SDS as a solvent instead of water. After that similar steps were followed as shown in Figure 3.1. The effect of different sucrose concentrations ranging from 10% (w/v) to 50 % (w/v) and 15% (w/v) to 75% (w/v) on separation of SWNTs was also observed using the same procedure.

3.3.2 Formation of SWNT deposits via Laminar Flow Deposition (LFD)

The process of Laminar flow deposition has been explained in previous work.²³ Briefly, the Si/SiO₂ wafers were cleaned with compressed CO₂. Prior to SWNT deposition, the substrates were modified with different self-assembled monolayers for 45 min, firstly immersing the substrates in a solution of 3-aminopropyl triethoxysilane (99%, Sigma Aldrich) and ethanol (99.5%, absolute 200 proof, ACROS). In order to ensure that only one monolayer of the silane

remained, substrates were washed with ethanol, water, and then dried in a stream of N₂ gas. Then, they were cleaned with compressed CO₂.

After substrate preparation, three deposition cycles (1 mg/mL and 0.5 mg/mL concentrations), each using 70 μL of SWNT suspension, were used to form the low-density SWNT deposits that would be used for AFM analysis and Raman spectroscopy. For 0.1mg/mL concentration, eight depositions cycles were used because of the very low concentration of SWNT/SDS suspension. Each deposition cycle consisted of wetting the silane coated Si/SiO₂ wafer with the SWNT suspension, followed by quick drying in a stream of N₂ gas at a pressure of 60 psi. The wafers were then rinsed with nanopure water (>18.1 MΩ) and then dried again under a stream of N₂ gas.

3.3.2 Characterization of SWNT Suspensions by UV-Vis-NIR Spectroscopy and Raman Spectroscopy

UV-Vis-NIR spectroscopy (Cary, 5000) was performed using a quartz cell with a path length of 1 mm. AFM images were obtained via intermittent contact mode in air (Molecular Imaging, Pico Plus). Raman spectroscopy (Thermo Scientific, DXR SmartRaman) was performed on suspensions in a sealed capillary tube and on SWNT deposits without any further modification. A CCD detector was used to record spectra obtained using a 532 nm diode laser excitation source. Suspensions were analyzed with a 10 X objective and a source intensity of 10 mW at the sample, while for SWNT deposits, a 50 X objective with 10 mW intensity at the sample was used for 0.1mg/mL and 7mW for 1 mg/mL and 0.5 mg/mL.

3.3.3 Characteristics of SWNT Deposits by AFM

AFM image analysis software (WSxM, v.5.0)²⁴ was used to determine the effect of the separation process of SWNT suspension. The low- density SWNT deposits were used to analyze the average length, height and RMS roughness on the SWNT substrate.

3.4 RESULTS AND DISCUSSION

3.4.1 Effect of different SWNT concentrations on density gradient separation

For different initial SWNT concentrations (1mg/mL, 0.5mg/mL and 0.1mg/mL), UV-vis and NIR absorbance (Figure 3.2a, 3.2b, 3.3a, 3.3b and 3.4a, 3.4b) for each fraction increased from lowest to highest (5% to 25%), indicating the presence of sucrose density gradient. The absorbance at 5% is lowest at 242nm with values 0.96, 0.50, and 0.19 for 1mg/mL, 0.5mg/mL, and 0.1mg/mL SWNT concentrations respectively. For 1mg/mL SWNT concentration, the fractions 5% to 25 % showed equal separation, but there was a significant increase from 25% to the bottom layer. This indicates that the nanotubes are isolating at the bottom of the centrifuge tube. Whereas for 0.5mg/mL SWNT concentration, the top fractions 5%, 10% and 15% were relatively close to each other and the bottom three fractions showed larger increase in absorbance NIR spectra showed the semiconducting SWNTs around 1010nm and the absorbance decreased from 1mg/mL to 0.5mg/mL SWNT concentration. This might be because of the lower initial concentration of the SWNTs used in the separation process.

As mentioned earlier, the absorbance increased from 5% to 25% for all the three SWNT concentrations. For 0.1mg/mL SWNT concentration, the absorbance of 0.1 mg/mL SWNT concentration is lower than the 1 mg/mL. At 0.1mg/mL SWNT concentration, 5% to 20% showed separation but the peaks are relatively closer and a minimum increase from 25% to the bottom layer was observed. This might be due to the bundle formation in the suspension because of the

diluted SWNT concentration. In addition to the quantitative information obtained by UV-vis spectroscopy, NIR spectroscopy provides qualitative information on the efficiency of the unbundling of nanotubes. Features around 1010 nm and 490nm, due to electronic transitions for semiconducting S₂₂ and metallic M₁₁ nanotubes (Figure 3.5) transitions showed sharp peaks for the 1mg/mL SWNT concentrations compared to the 0.5mg/mL and 0.1mg/mL. This indicates that the nanotubes are individually dispersed vs. probable bundle formation at the lower SWNT concentrations. These features consist of several van Hove transitions of nanotubes of different diameters. Usually these peaks are not individually resolved. Therefore, the locations of these unresolved prominent features in the absorption spectrum to some extent depend on the nanotube diameter distribution in sample.²⁵

3.4.2 Effect of surfactant (SDS) vs. water on sucrose gradient in the SWNT suspension

The absorbance of sucrose layers 5% to 25% (Figure 3.6) and 15% to 75% (Figure 3.7) made with SDS and water is around the same, which indicates that separation of the SWNTs have been achieved equally. But as the density gradient of the sucrose increases, the absorbance increases simultaneously. Individual SWNTs are obtained rather than bundled while using sucrose solution with water as compared to the SDS and this can be confirmed via AFM analysis as well. This might be due to the fact that sucrose is more viscous in SDS than water and exponentially increases at higher concentrations^{26, 27}, which holds the nanotubes close to each other in bundled form. The higher the sucrose density, the more bundled SWNT is observed. This might be due to the viscosity of sucrose in SDS which restricts nanotubes from travelling in the tube unbundled leading to agglomeration. Viscosity can affect the separation capability and this can be compensated by using a high speed rotor.¹⁷ The NIR region showing S₂₂ electronic transitions for the semiconducting nanotubes is better resolved in sucrose solutions with water as compared to

the SDS due to the viscosity of sucrose in SDS. Similar trends are seen for 0.5mg/mL and 0.1mg/mL SWNT concentration with different sucrose densities ranging from 10% to 75% (w/v) (not shown here). But the absorbance is lower as compared to 1mg/mL since the initial concentration of SWNTs in the solution is reduced by 50% for 0.5mg/mL and even higher for 0.1mg/mL.

At 0.1mg/mL, as the sucrose density increases, the S₂₂ peaks start to overlap in the NIR region and separation is not achieved efficiently. This might be because the SWNT suspension does not reach to the bottom of the tube and also due to the interference of the sucrose density (due to the thickness of sucrose at higher densities) in the SWNT suspension leading to overlapping of the peaks. The concentration of SWNTs after one processing step is calculated by the extinction coefficient for the SWNTs which is the slope of the Beer's law plot constructed for diluted suspension.²⁸ The absorbance at 600 nm was chosen since it lies between the semiconducting and metallic band and also due to the lower scattering efficiency of SWNTs at this wavelength.²⁹ The SWNT concentration increases (Figure 3.8 and 3.9) with the increase in the sucrose layers. This is due to more impurities isolated at the bottom of the tube due to increase in the sucrose density and density of SWNTs above the critical density. The SWNT concentrations on the top layers of sucrose densities 5%, 10% 15% for 5-25% and 15%, 30% for 15-75% have similar concentration values. This indicates that the upper 50% supernatant is relatively improved in purity and is similar to the previous work from this group. So this level of purity can be achieved using sucrose gradient with just one processing step.

3.4.3 Characterization of SWNT in sucrose by Raman Spectroscopy

Raman spectroscopy is used to characterize molecular morphology of the carbon nanotubes. Every band in the Raman spectrum corresponds to the vibrational frequency of a bond,

consisting of sp^2 and sp^3 hybridized carbon atoms. The graphite band (G-band) which occurs near 1590 cm^{-1} is a characteristic feature of graphite layers and corresponds to tangential vibration of carbon atoms. This is also directly proportional to the purity of as grown nanotubes produced by any of the techniques like CVD, arc discharge or laser ablation.^{30,31} The disorder band (D-band), near 1370 cm^{-1} is sign of the presence of disordered sp^2 carbon atoms, caused by impurities in carbon lattice. The comparison of ratios (I_G/I_D) of these two peaks is a measure of quality of purified SWNTs and removal of impurities. In addition, the radial breathing mode (RBM) near 150 and 350 cm^{-1} measures the diameter and expansion and contraction of the SWNTs.²⁸

For all the SWNT concentrations, Raman spectrum showed lower I_G/I_D ratios for each fraction from 5% (w/v) to 25% (w/v) indicating a density gradient. This is likely due to the fact that the nanotubes for high density sucrose gradient sequester to the bottom of the centrifuge tube. This resulted in impurities settling down the centrifuge tube, producing lower ratios. The ratios for the deposition were much higher than the suspension due to the laminar flow deposition which acts as an additional purification step explained in the previous works from the group²³. The I_G/I_D ratios for the 1 mg/mL (Table 3.1) and 0.5mg/mL (Table 3.2) is twice compared 0.1 mg/mL (Table 3.3) SWNT concentrations. This is because of the higher concentration of the SWNTs in one solution compared to the other. More deposits (8 depositions cycles) were made with 0.1mg/mL suspension, because of lower concentration of SWNTs in the suspension.

The spectra have been normalized to the G band to see the effects near the RBM region. In Figure 3.10a, the shoulder at 25% on the high energy side of the peak, is more pronounced at the higher (1mg/mL SWNT suspension) than compared to 0.5mg/mL (Figure 3.10b) and 0.1mg/mL (Figure 3.10c) SWNT suspensions. For 0.5mg/mL SWNT suspension (Figure 3.10b), there is a slight shift of the peaks to the higher energy side and lower energy side of the spectra and for

0.1mg/mL, the shoulder at 10% is more pronounced as compared to the other concentrations and different sucrose layers. Bundling of the SWNTs can affect both the shifting and broadening of transition energies.^{32, 33} The red shift in the RBM region can be contributed to the bundling of nanotubes vs. the individual ones in the suspension. Figure 3.11 shows the peak shifts of SWNT deposits between different SWNT concentrations. A more pronounced peak shift to the lower energy side of the spectrum is observed for 0.1mg/mL in different sucrose layers (Figure 3.11). A similar trend is observed between the SWNT deposits at different concentration. But along with the peak shift, a decrease in Raman intensity is also observed. The greater peak shift at 0.1mg/mL SWNT concentration corroborates this assertion mentioned previously. Bundling in the suspension broadens the electronic transitions leading to peak shifts in the spectra.^{32, 33} This proves that at lower SWNT concentration with SDS, SWNTs are produced in bundled form due to the higher viscosity of SDS in sucrose. This is observed by the peak shift in the RBM region.

Similar trend in the I_G/I_D ratios for suspensions and deposits has been observed for different SWNT concentrations with sucrose solutions with SDS and water and at higher sucrose densities ranging from 5% to 75%. The difference in the ratios for the suspensions and deposits is the similar to ones observed before for all SWNT concentrations (1mg/mL, 0.5mg/mL and 0.1mg/mL) not shown here. The only exception is that the data for 0.1mg/mL suspension is not obtained for higher sucrose densities since the solution is very dilute and it's challenging to get a Raman signal. With such low concentration of SWNT, it prevents the nanotubes to go through the higher viscous layers in the gradient, so the data obtained would not be reliable and reproducible and hence not included.

3.4.4 Effect of different SWNT concentrations on the separation of the nanotubes using sucrose gradient

AFM analysis showed that 1 mg/mL SWNT concentration yielded the highest density of high aspect ratio SWNTs (Figure 3.12) as compared to 0.5mg/mL (Figure 3.13) and 0.1mg/mL (Figure 3.14) SWNT concentrations. The average height for all the three concentrations (Table 3.4a, 3.4b, 3.4c) was observed to increase from 5% to the bottom layer, representing sucrose density gradient in the tube. The length of the nanotubes decreases from 5% to 25% and bottom layer. This indicates that all the nanotubes assemble towards the bottom as the sucrose density gradient is higher. This also indicates that there are less number of tubes and more pellets towards the bottom of the centrifuge tube. With each increasing sucrose concentration the roughness also increased, while across concentrations the RMS roughness increased from 0.98 to 3.17 for 1 mg/mL SWNT concentration, 1.59 to 2.57 for 0.5mg/mL and 1.40 to 2.52 for 0.1mg/mL.

AFM images showed longer nanotubes towards the top (5%) and as the concentration of the sucrose increased, fewer tubes and more globular impurities are observed across all the SWNT concentrations. But the average density of the nanotubes for 0.1 mg/mL is half for all the sucrose layers compared to the 1 mg/mL concentration. The average density of SWNTs at 0.5mg/mL SWNT concentration fall in between 1mg/mL and 0.1mg/mL. This indicates the buoyancy effect³⁴ where the longer nanotubes stay in the suspension isolating the shorter one towards the bottom of the tube. Initial concentration has a direct effect on the density and the length of the SWNT on the substrate. Higher the SWNT concentration, higher the average density of SWNT on sucrose layers and vice versa. The average length of the nanotubes decreased across concentrations, wherein the longer nanotubes were observed at the higher SWNT concentration and the length decreased from 0.5mg/mL to 0.1mg/mL. This might be due to the difference in starting SWNT concentration.

AFM analysis showed that the average height of all different density gradients increased from top layer (5%, 10%, and 15%) to the bottom layer regardless of the sucrose solutions made

in water or SDS. This indicates that the nanotubes isolate towards to the bottom of the centrifuge tube showing a density gradient. The RMS roughness also followed a similar trend. But the average density of the nanotubes decreased going towards the bottom of the tube since more globular impurities, pellets and fewer tubes are formed. Long, pristine, unbundled SWNTs are formed with just one processing step using the sucrose density.

Comparing different sucrose density gradients from 5% all the way to 75%, it shows that the sucrose solutions made with SDS have a higher average height than ones made with water. The viscosity of sucrose in SDS, yeild long bundled SWNTs. The average density is also higher which can be confirmed by the AFM images. AFM images show bundled nanotubes of the sucrose solutions made with SDS vs. individual nanotubes (Figure 3.15 and 3.16) with sucrose solutions made with water. The density of the nanotubes decrease from the lowest density gradient to the highest (top to bottom). This is because the nanotubes can travel easily through the lower gradients and the impurities are sequestered towards the bottom with fewer nanotubes. If surfactant molecules (SDS) are in excess, they form free micelles. If the size of the micelles is higher than the distance between the tubes, it will be difficult for the micelles to penetrate between the tubes creating bundles. As reported in the literature,³⁵ unbundling of SWNTs in aqueous solution is due to the hydrophobic/hydrophilic interactions, in which the hydrophobic tail of the surfactant molecule adsorbs on the surface and hydrophilic head associates water for dissolution. This allows for encapsulation of surfactant molecules forming either cylindrical or hemispherical micelles around the hydrophobic SWNTs.

The separation of SWNTs from sucrose can be explained by the theory of centripetal forces. Under the centripetal force of an ultracentrifuge, the species sediment toward their respective isopycnic points (i.e. the position where their density matches that of the gradient). The

centripetal force is where an object moves in a circular path at constant velocity and same rotational speed, where the force is directed towards the center. The rotor used in the experiment is set spinning. The SWNT suspension inside the centrifuge tube is set against the wall of the rotor to spin and as the speed increases, the denser SWNTs goes to the bottom of the centrifuge tube. This forms a pellet at the bottom leaving the lighter ones on the top. The pellet formation is directly related to the centrifugal angular velocity, density and viscosity of the solution.³⁶ Since the sucrose layers are filled from increasing order from 25% towards the bottom to the 5% on the top, the SWNT suspension will be lower in density at 5% as compared to 25% . Since it is a one step process in purifying the SWNTs, the yield in the end is around 80% for each layer. This indicates that this one step purification of SWNT using sucrose can produce greater yield and similar level of purification than compared to multiple cycles of centrifugation discussed in recent works. So use of gradient acts an additional purification step for SWNTs in suspension.

3.5 CONCLUSIONS

The separation method using sucrose gradient centrifugation in this study differ from the density gradient centrifugation, which allowed the separation process without any involvement of the reagents which can be difficult to remove. The separation by using sucrose with different SWNT concentration was achieved successfully and was confirmed by UV-vis and NIR spectroscopy. Viscosity of SDS in sucrose at higher sucrose concentration and lower SWNT concentration can lead to bundling of SWNTs in the suspension. Bundling effect caused the electronic transitions to broaden leading to red shifts in the spectra. The use of 10,000g centripetal force obtained high aspect ratio SWNTs for all the SWNT concentrations. The one step process allowed a higher yield of SWNT suspension after centrifugation, which is time and cost effective. Besides the higher yield, sucrose also produced pristine SWNTs with just one processing step. So

sucrose gradient can be used as a purification tool in the process. This technique can potentially improve and enlarge applications of SWNTs in many fields.

3.6 REFERENCES

1. Patra, S.; Mohan Rao, G. *Journal of Applied Physics* **2006**, 100, (2), 024319-024319-5.
2. Weber, J.; Kumar, A.; Kumar, A.; Bhansali, S. *Sensors and Actuators B: Chemical* **2006**, 117, (1), 308-313.
3. Kwon, J.-H.; Lee, K.-S.; Lee, Y.-H.; Ju, B.-K. *Electrochemical and solid-state letters* **2006**, 9, (9), H85-H87.
4. Kim, H. H.; Kim, H. J. *Materials Science and Engineering: B* **2006**, 133, (1-3), 241-244.
5. Iijima, S.; Ichihashi, T. **1993**.
6. Arepalli, S. *Journal of Nanoscience and Nanotechnology* **2004**, 4, (4), 317-325.
7. Guo, T.; Nikolaev, P.; Thess, A.; Colbert, D.; Smalley, R. *Chemical physics letters* **1995**, 243, (1), 49-54.
8. Su, M.; Zheng, B.; Liu, J. *Chemical Physics Letters* **2000**, 322, (5), 321-326.
9. Moshhammer, K.; Hennrich, F.; Kappes, M. *Nano Res.* **2009**, 2, (8), 599-606.
10. Hersam, M. C. *Nature Nanotechnology* **2008**, 3, (7), 387-394.
11. Chen, F.; Wang, B.; Chen, Y.; Li, L.-J. *Nano Letters* **2007**, 7, (10), 3013-3017.
12. Star, A.; Tu, E.; Niemann, J.; Gabriel, J.-C. P.; Joiner, C. S.; Valcke, C. *Proceedings of the National Academy of Sciences of the United States of America* **2006**, 103, (4), 921-926.
13. Zheng, M.; Jagota, A.; Strano, M. S.; Santos, A. P.; Barone, P.; Chou, S. G.; Diner, B. A.; Dresselhaus, M. S.; Mclean, R. S.; Onoa, G. B.; Samsonidze, G. G.; Semke, E. D.; Usrey, M.; Walls, D. J. *Science* **2003**, 302, (5650), 1545-1548.
14. Tu, X.; Manohar, S.; Jagota, A.; Zheng, M. *Nature* **2009**, 460, (7252), 250-253.
15. Maeda, Y.; Kimura, S.-i.; Kanda, M.; Hirashima, Y.; Hasegawa, T.; Wakahara, T.; Lian, Y.; Nakahodo, T.; Tsuchiya, T.; Akasaka, T.; Lu, J.; Zhang, X.; Yu, Y.; Nagase, S.; Kazaoui, S.;

- Minami, N.; Shimizu, T.; Tokumoto, H.; Saito, R. *Journal of the American Chemical Society* **2005**, 127, (29), 10287-10290.
16. Maeda, Y.; Kanda, M.; Hashimoto, M.; Hasegawa, T.; Kimura, S.-i.; Lian, Y.; Wakahara, T.; Akasaka, T.; Kazaoui, S.; Minami, N.; Okazaki, T.; Hayamizu, Y.; Hata, K.; Lu, J.; Nagase, S. *Journal of the American Chemical Society* **2006**, 128, (37), 12239-12242.
17. Yanagi, K.; Iitsuka, T.; Fujii, S.; Kataura, H. *The Journal of Physical Chemistry C* **2008**, 112, (48), 18889-18894.
18. Manivannan, S.; Jeong, I.; Ryu, J.; Lee, C.; Kim, K.; Jang, J.; Park, K. *J Mater Sci: Mater Electron* **2009**, 20, (3), 223-229.
19. Hasan, T.; Scardaci, V.; Tan, P.; Rozhin, A. G.; Milne, W. I.; Ferrari, A. C. *The Journal of Physical Chemistry C* **2007**, 111, (34), 12594-12602.
20. Hirano, A.; Tanaka, T.; Urabe, Y.; Kataura, H. *The Journal of Physical Chemistry C* **2012**, 116, (17), 9816-9823.
21. Łukaszczyk, P.; Borowiak-Paleń, E.; Rummeli, M. H.; Kaleńczuk, R. *J. Materials Research Bulletin* **2011**, 46, (10), 1535-1539.
22. Kuznetsov, O. V.; Pulikkathara, M. X.; Lobo, R. F. M.; Khabasheskua, V. N. *Russ Chem Bull* **2010**, 59, (8), 1495-1505.
23. Bhatt, N. P.; Vichchulada, P.; Lay, M. D. *Journal of the American Chemical Society* **2012**, 134, (22), 9352-9361.
24. Horcas, I.; Fernandez, R.; Gomez-Rodriguez, J. M.; Colchero, J.; Gomez-Herrero, J.; Baro, A. M. *Review of Scientific Instruments* **2007**, 78, (1).
25. Ryabenko, A. G.; Dorofeeva, T. V.; Zvereva, G. I. *Carbon* **2004**, 42, (8-9), 1523-1535.

26. Bonaccorso, F.; Hasan, T.; Tan, P.; Sciascia, C.; Privitera, G.; Di Marco, G.; Gucciardi, P.; Ferrari, A. *The Journal of Physical Chemistry C* **2010**, 114, (41), 17267-17285.
27. Coombs, D. H.; Watts, N. R. M. *Analytical Biochemistry* **1985**, 148, (1), 254-259.
28. Vichchulada, P.; Cauble, M. A.; Abdi, E. A.; Obi, E. I.; Zhang, Q.; Lay, M. D. *The Journal of Physical Chemistry C* **2010**, 114, (29), 12490-12495.
29. Priya, B.; Byrne, H. *The Journal of Physical Chemistry C* **2008**, 112, (2), 332-337.
30. Itkis, M. E.; Perea, D. E.; Jung, R.; Niyogi, S.; Haddon, R. C. *Journal of the American Chemical Society* **2005**, 127, (10), 3439-3448.
31. Miyata, Y.; Mizuno, K.; Kataura, H. *Journal of Nanomaterials* **2011**, 2011, 18.
32. Fantini, C.; Jorio, A.; Souza, M.; Strano, M.; Dresselhaus, M.; Pimenta, M. *Physical review letters* **2004**, 93, (14), 147406.
33. O'Connell, M. J.; Sivaram, S.; Doorn, S. K. *Physical Review B* **2004**, 69, (23), 235415.
34. Nair, N.; Kim, W.-J.; Braatz, R. D.; Strano, M. S. *Langmuir* **2008**, 24, (5), 1790-1795.
35. Tan, Y.; Resasco, D. E. *The Journal of Physical Chemistry B* **2005**, 109, (30), 14454-14460.
36. Yu, H.; Qu, Y.; Dong, Z.; Li, W. J.; Wang, Y.; Ren, W.; Cui, Z. In *Separation of mixed SWNTs and MWNTs by centrifugal force-an experimental study*, Nanotechnology, 2007. IEEE-NANO 2007. 7th IEEE Conference on, 2007; IEEE: pp 1212-1216.

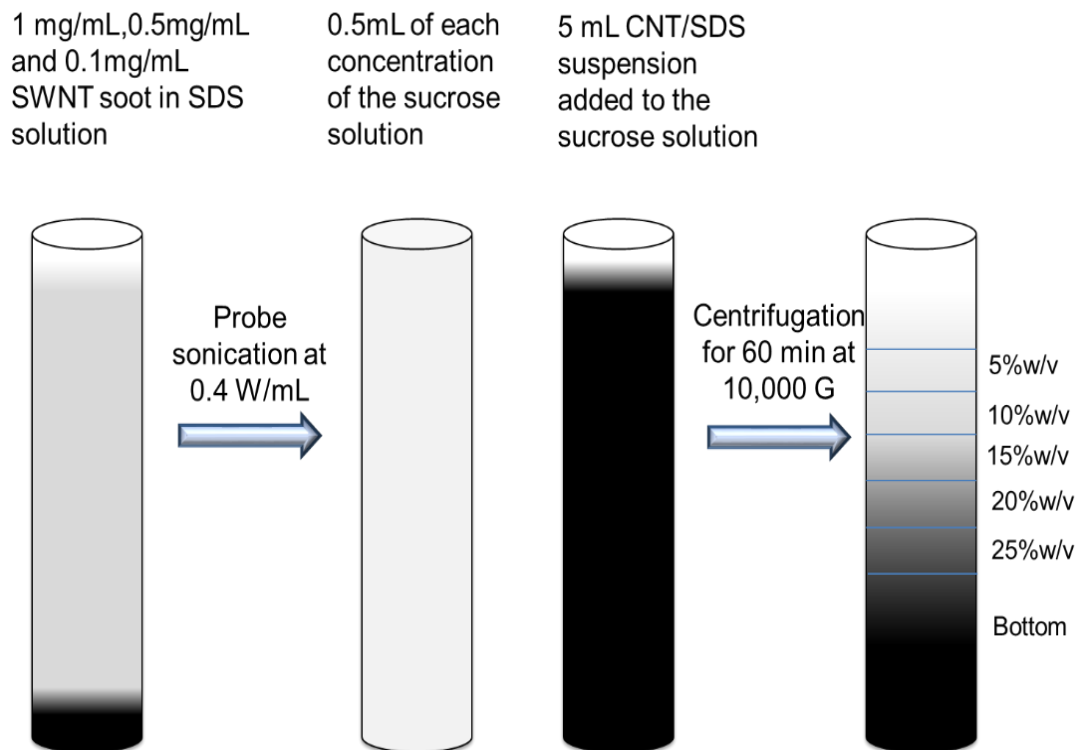
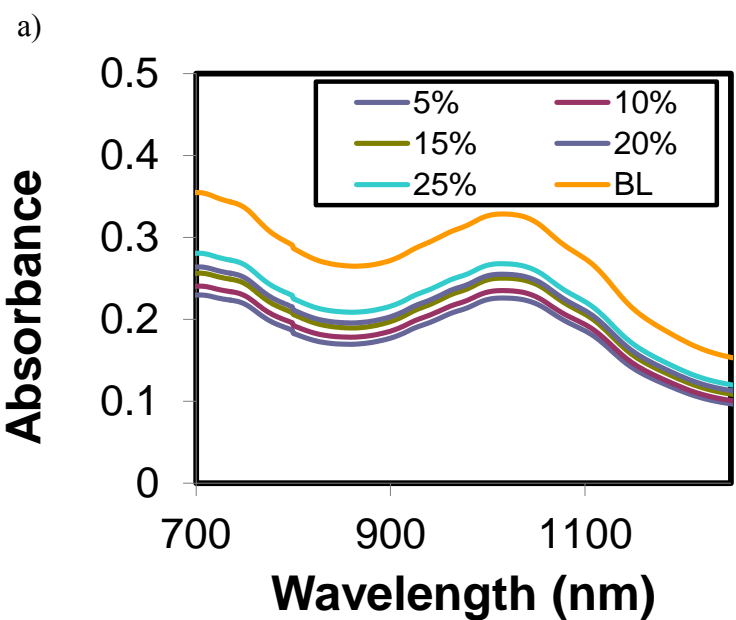
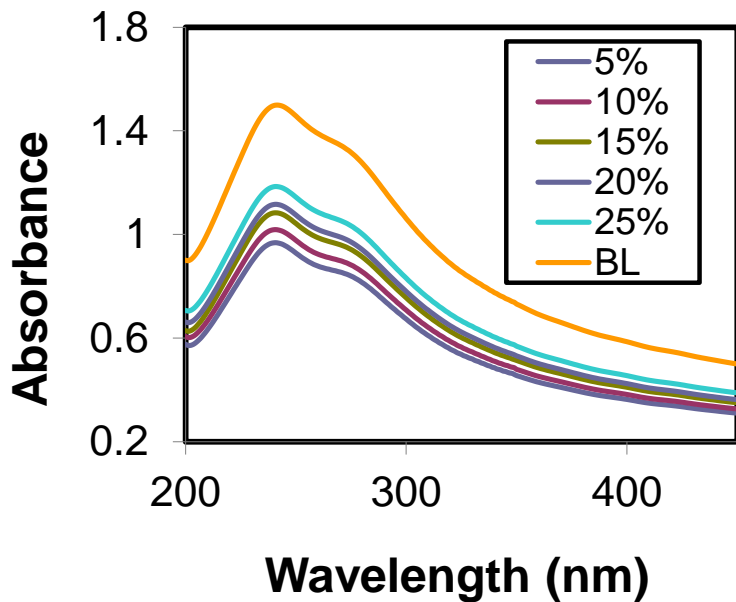
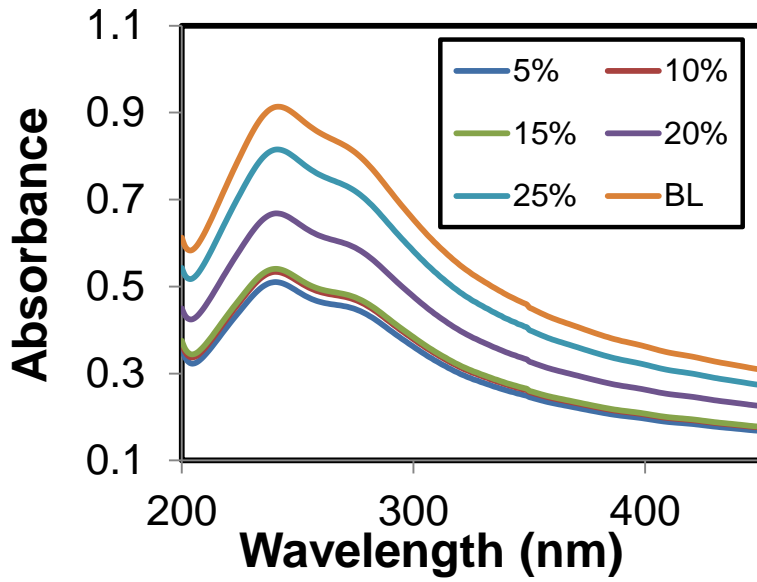


Figure 3.1: Schematic for the experimental approach used in the report, wherein the SWNT suspension is sonicated for 30 min at the power density of 0.4W/mL. After one cycle of centrifugation at 10,000G for 60min, fractions of the different sucrose layers were carefully removed.

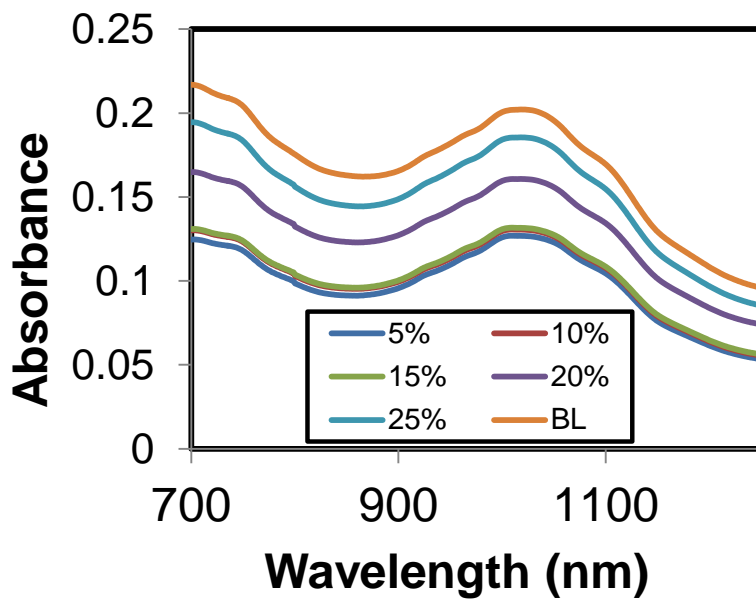


b)

Figure 3.2: a) Absorbance in the UV region of the spectrum increased from 5% to 25% for 1mg/mL SWNT concentration indicating a direct correlation between SWNT concentration and sucrose layers; b) NIR spectra for semiconducting SWNTs showing around 1010nm.



a)



b)

Figure 3.3: a) Absorbance in the UV region of the spectrum increased from 5% to 25% for 0.5mg/mL SWNT concentration indicating a direct correlation between SWNT concentration and sucrose layers; b) NIR spectra for semiconducting SWNTs showing around 1010nm.

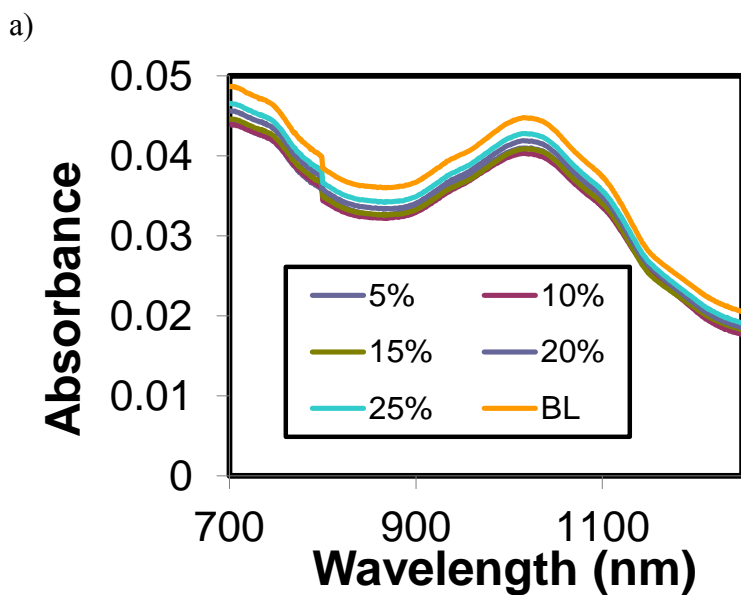
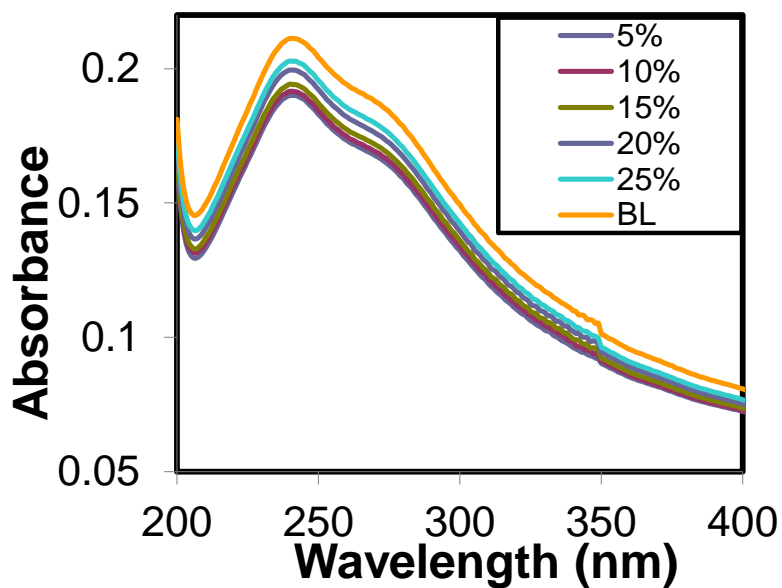
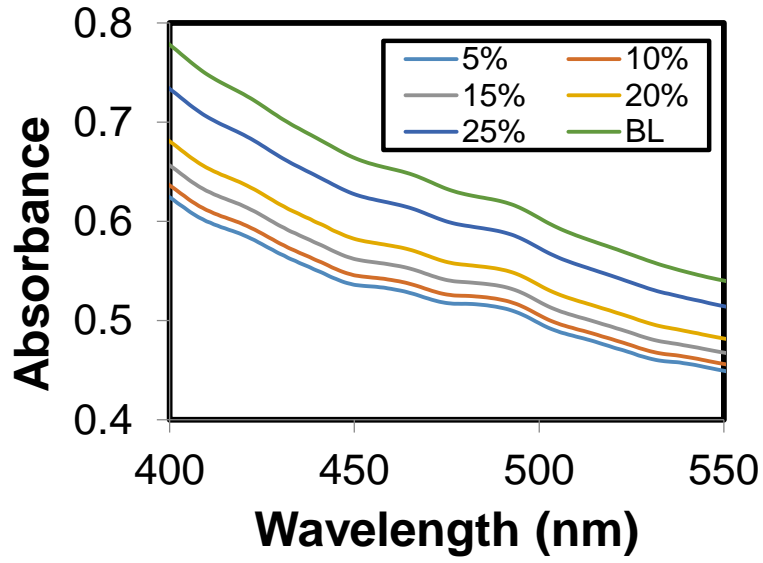
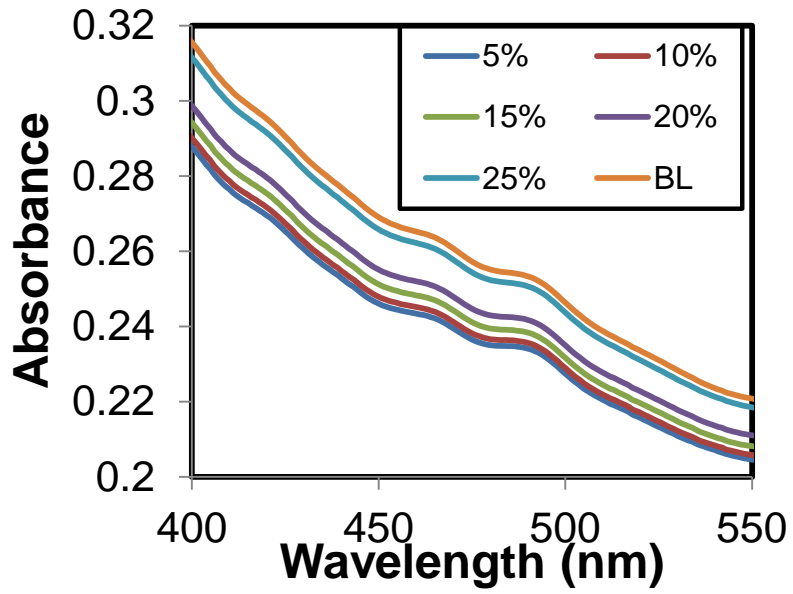


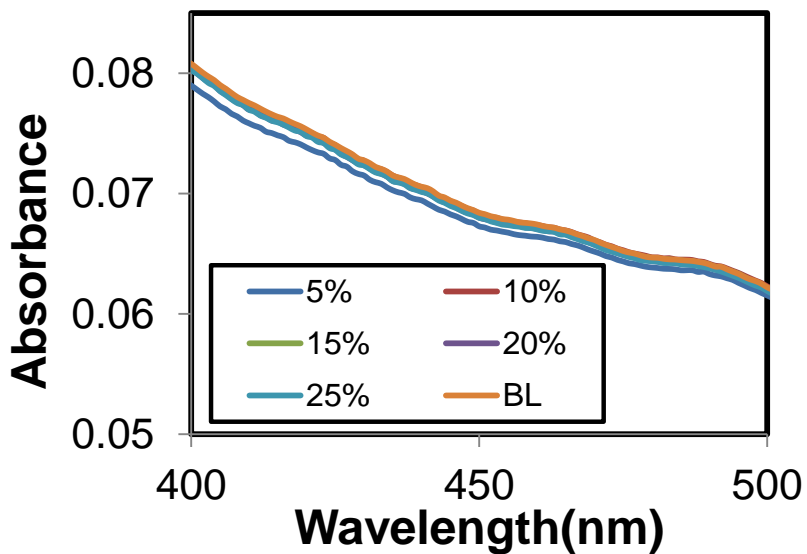
Figure 3.4a: Absorbance in the UV region of the spectrum increased from 5% to 25% for 0.1mg/mL SWNT concentration; b) NIR spectra for semiconducting SWNTs showing around 1010nm.



a)

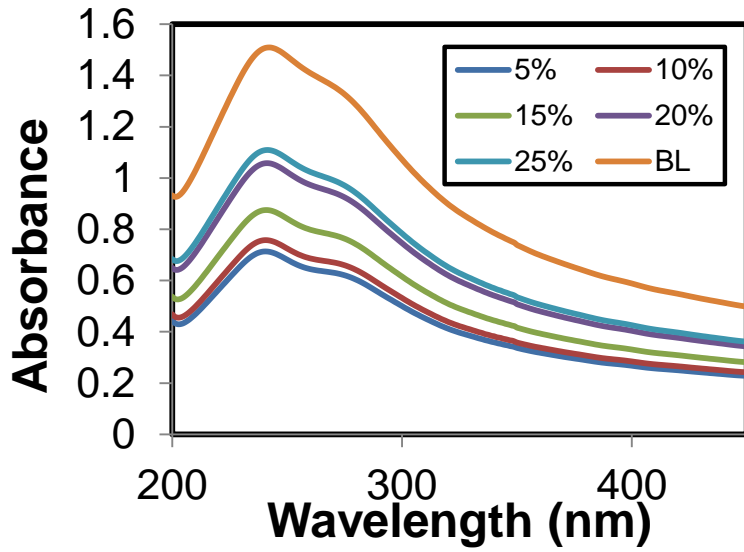


b)

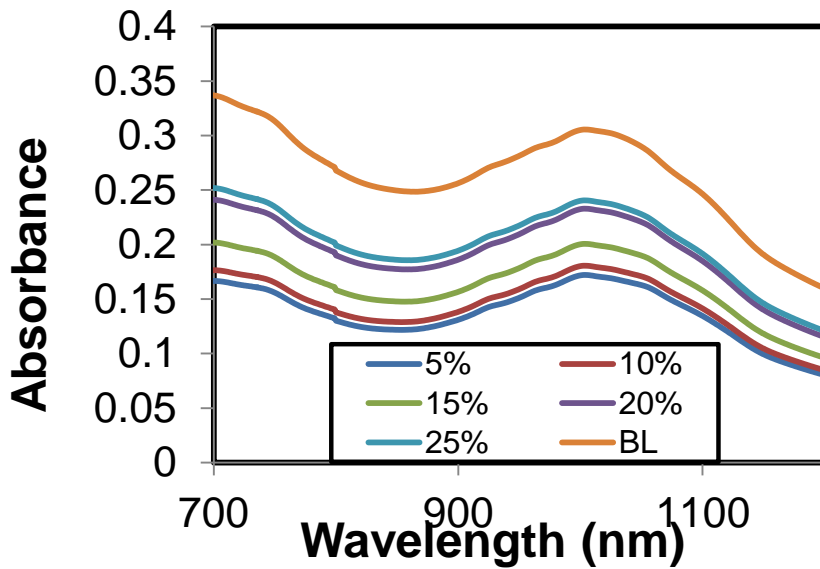


c)

Figure 3.5: NIR spectra of sucrose layers at different SWNT concentrations showing features due to M_{11} transitions normalized around 1010nm to the Bottom layer; a) M_{11} transition for 1mg/mL SWNT concentration shows the peaks are well resolved and dispersed as compared to; b) 0.5mg/mL and c) 0.1mg/mL SWNT concentration.

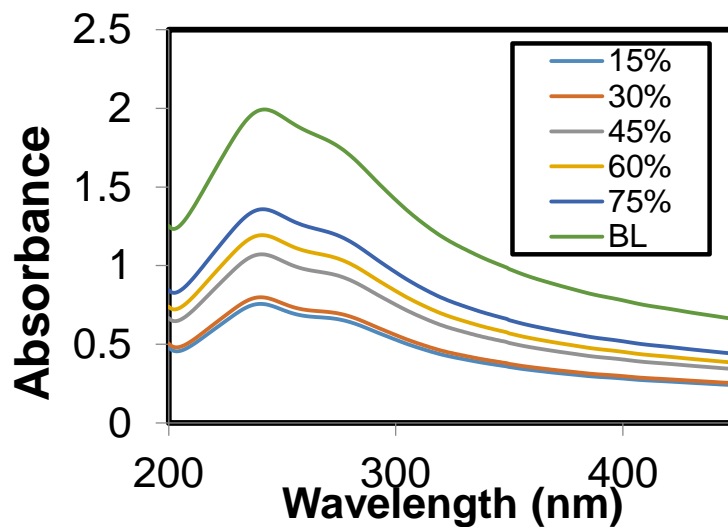


a)

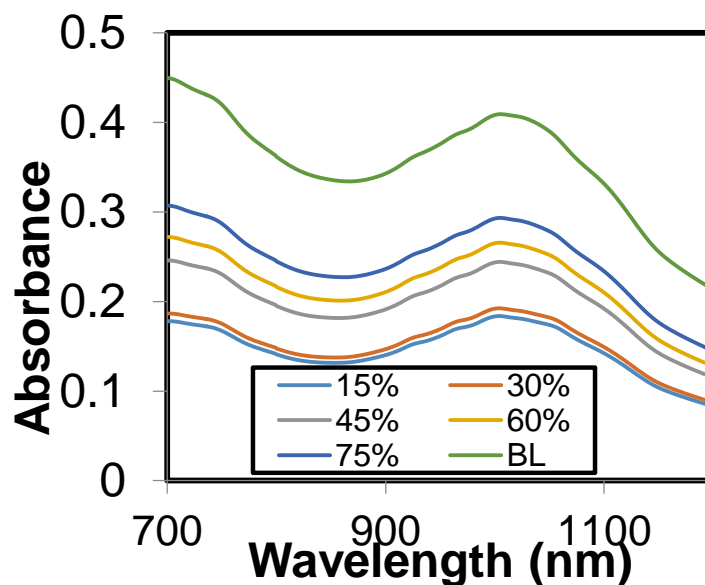


b)

Figure 3.6: Representative UV-vis NIR images for sucrose concentration with SDS; a) UV-vis image of 1mg/mL SWNT concentration showing increase in absorbance from 5% to 25%; b) NIR showing S_{22} transitions around 1010nm.

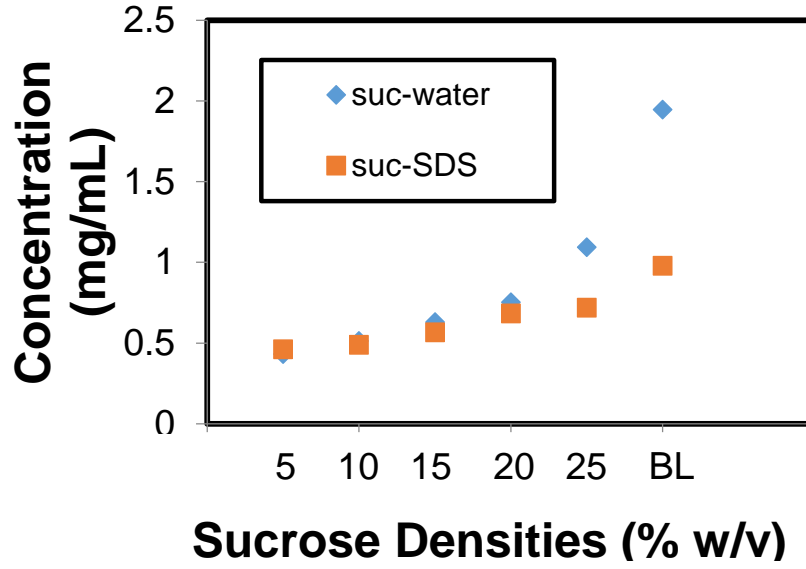


a)

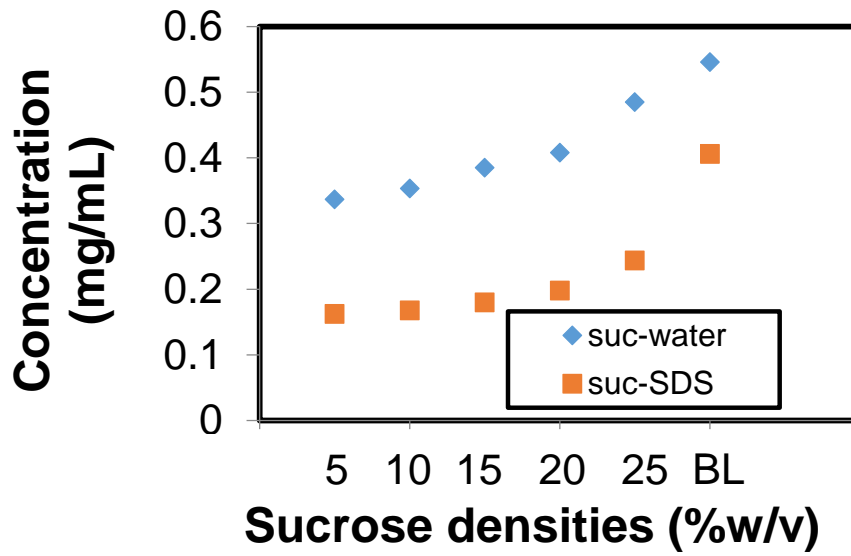


b)

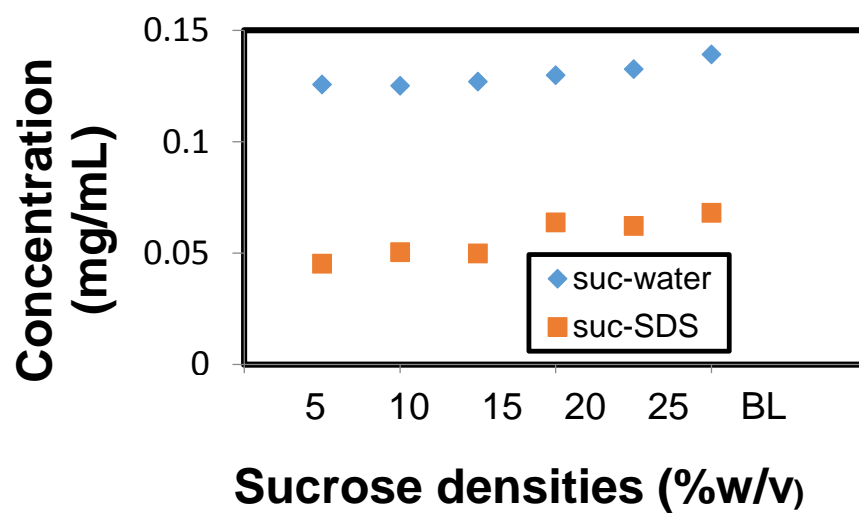
Figure 3.7: Representative UV-vis NIR images for sucrose concentration with SDS at 1mg/mL; a) sucrose concentrations showing increase in absorbance from 15% to 75%; b) NIR shows S_{22} transitions around 1010nm. The peaks are more resolved and the separation of the SWNT is achieved better in sucrose solution with water compared to the SDS.



a)

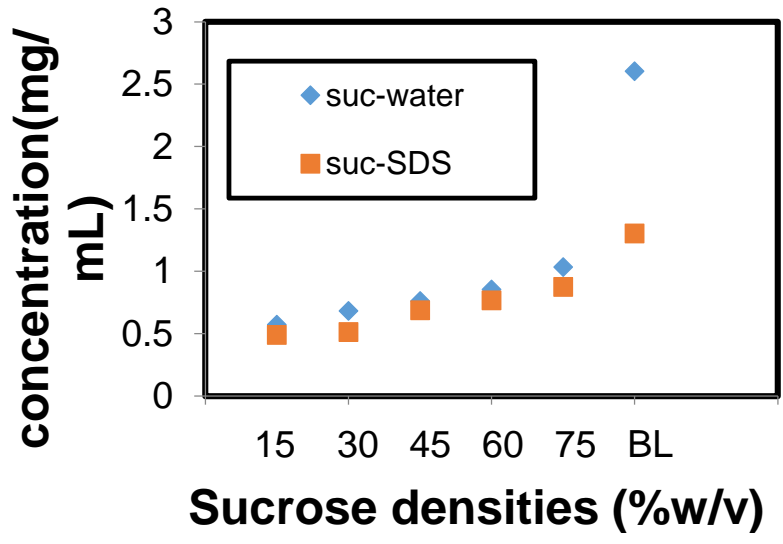


b)

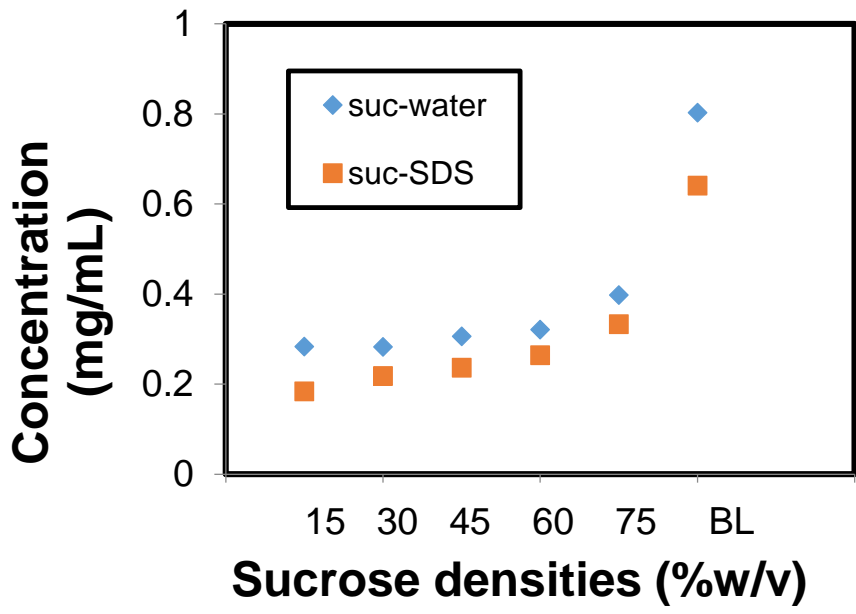


c)

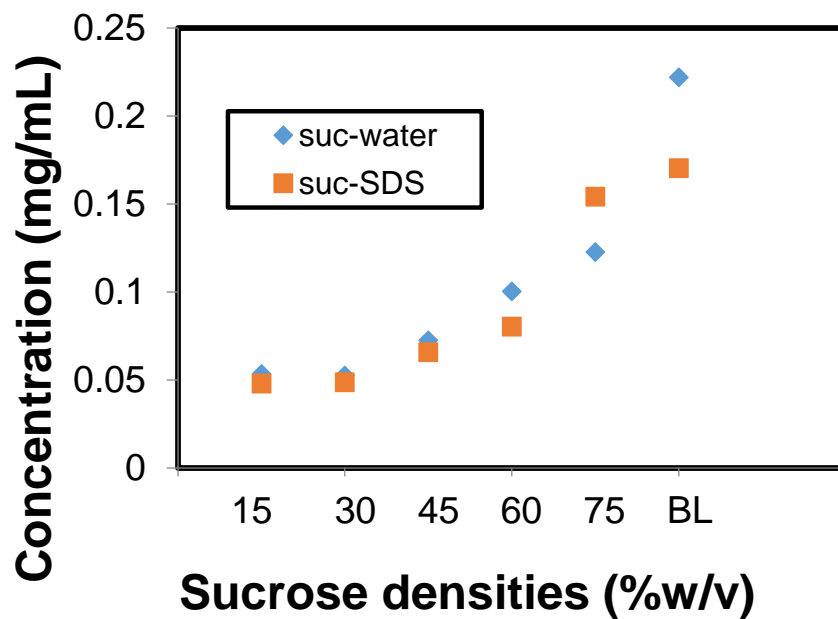
Figure 3.8: Effect of SWNT concentration on different sucrose densities with SDS and water at 600nm; a)-c) 5%-25% sucrose concentrations with water and SDS at 1mg/mL, 0.5mg/mL and 0.1mg/mL respectively.



a)



b)



c)

Figure 3.9: Effect of SWNT concentration on different sucrose densities with SDS and water at 600nm; a)-c) 15%-75% sucrose concentrations with water and SDS at 1mg/mL, 0.5mg/mL and 0.1mg/mL respectively.

Table 3.1: I_G/I_D ratios of Raman suspensions and deposits for 1mg/mL SWNT concentration.

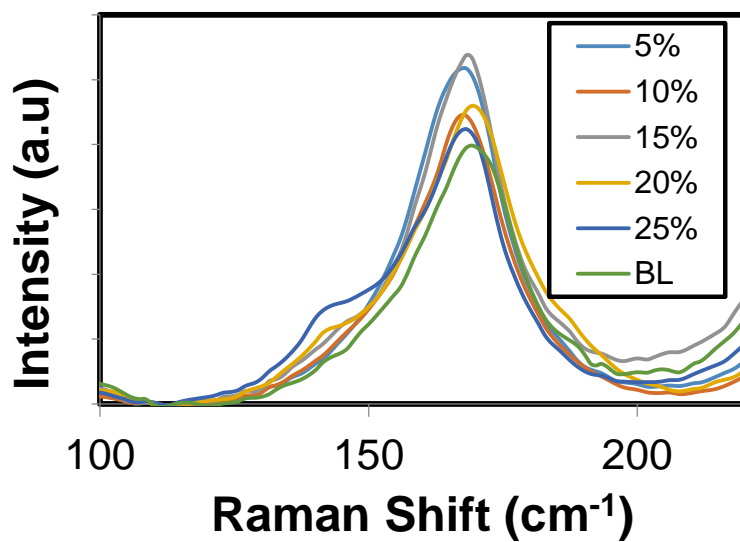
	5%	10%	15%	20%	25%	Bottom
Suspension	60.83±2.64	59.58±0.85	54.63±1.58	53.97±0.29	52.62±1.02	49.52±0.70
Deposits	69.09±4.64	68.46±15.3	65.41±19.72	64.27±2.56	63.66±4.17	55.71±13.78

Table 3.2: I_G/I_D ratios of Raman suspensions and deposits for 0.5mg/mL SWNT concentration.

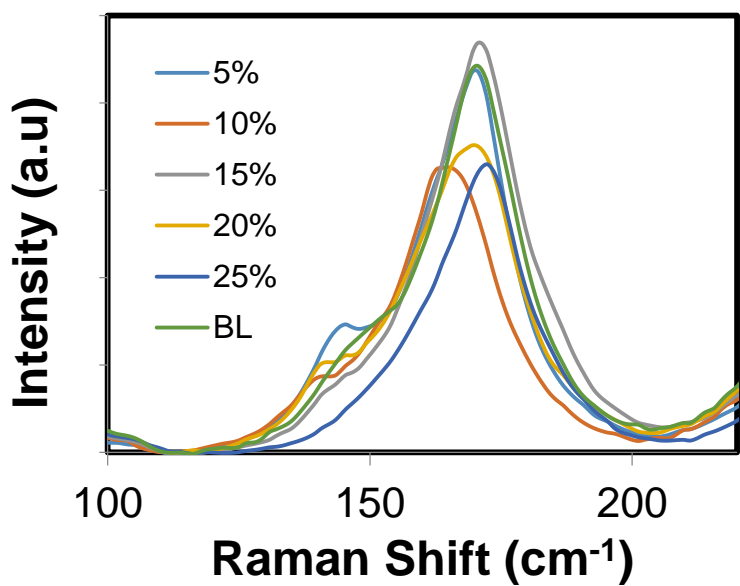
	5%	10%	15%	20%	25%	Bottom
Suspensions	58.14±1.71	57.68±2.51	57.39±0.97	55.23±2.05	54.07±1.81	52.37±0.74
Deposits	96.23±14.24	94.84±18.1	88.20±23.2	87.13±9.20	86.91±4.84	83.27±9.11

Table 3.3: I_G/I_D ratios of Raman suspensions and deposits for 0.1mg/mL SWNT concentration.

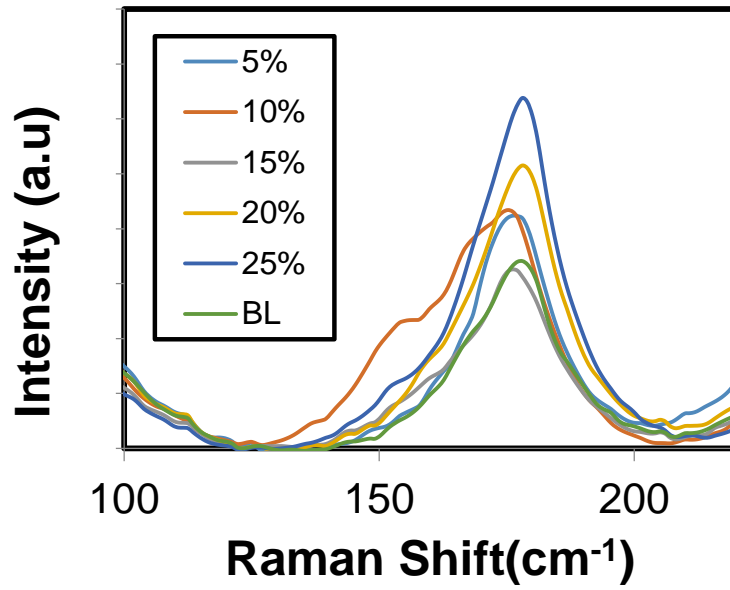
	5%	10%	15%	20%	25%	Bottom
Suspensions	31.92±1.12	29.82±1.4	29.22±0.6	28.93±2.05	28.04±0.31	27.74±1.14
Deposits	64.50±11.7	62.31±11.2	55.38±14.05	55.04±14.5	50.06±14.9	42.50±10.2



a)

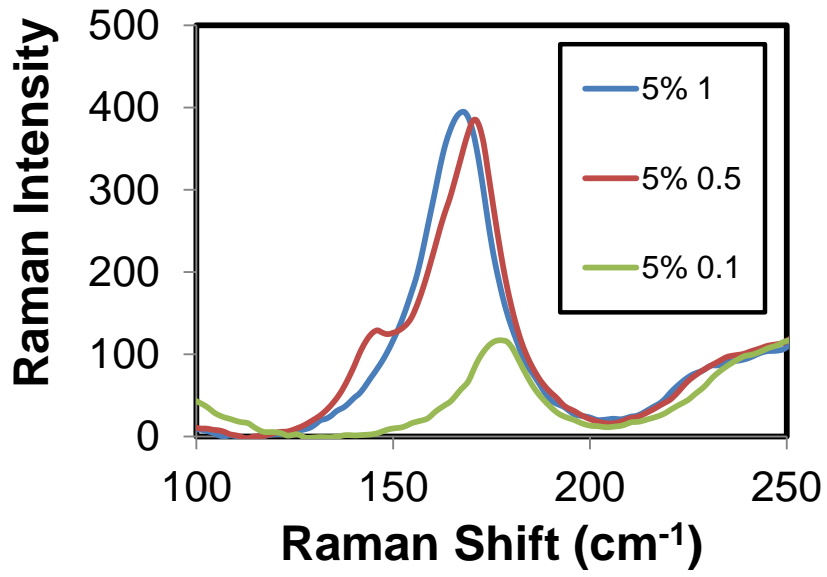


b)

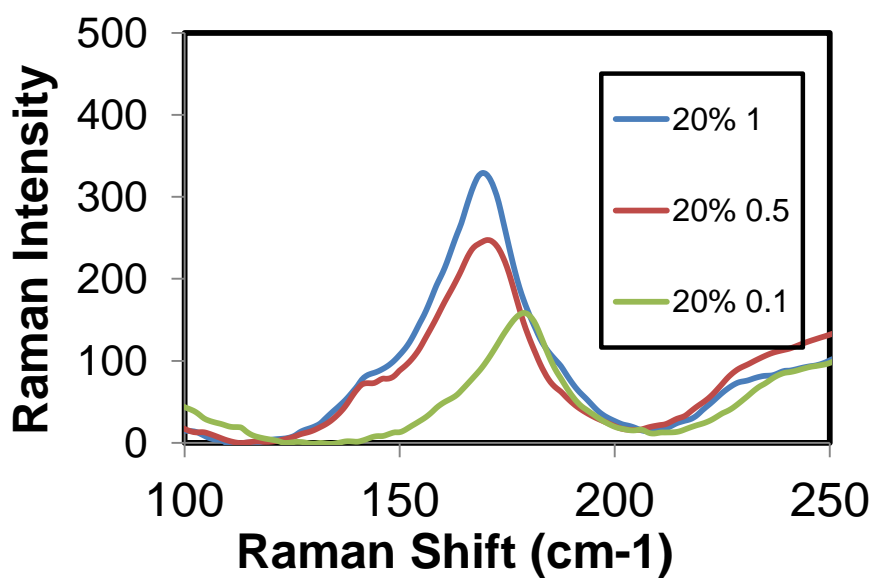


c)

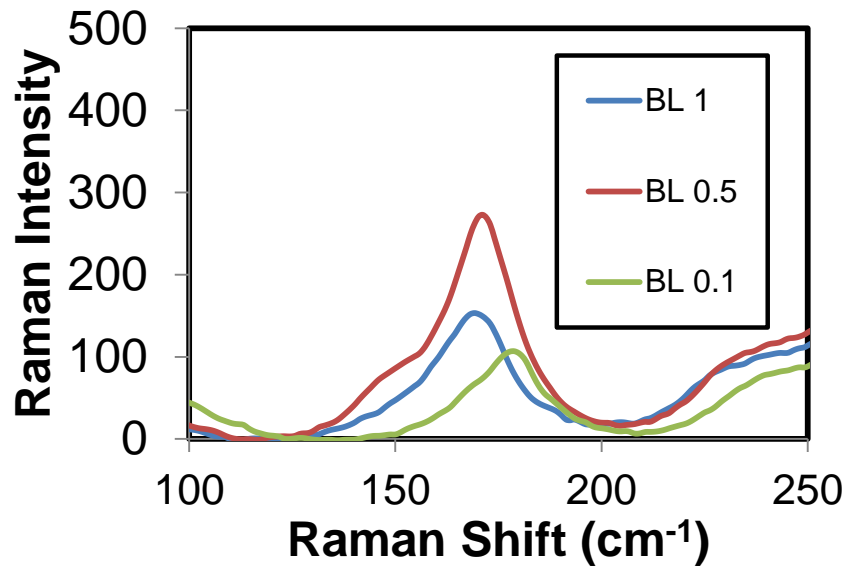
Figure 3.10: a) RBM spectra of the SWNT suspension at 1 mg/mL concentration suspension; b) RBM spectra of the SWNT suspension at 0.5 mg/mL concentration suspension; c) RBM spectra of the SWNT suspension at 0.1 mg/mL concentration suspension.



a)

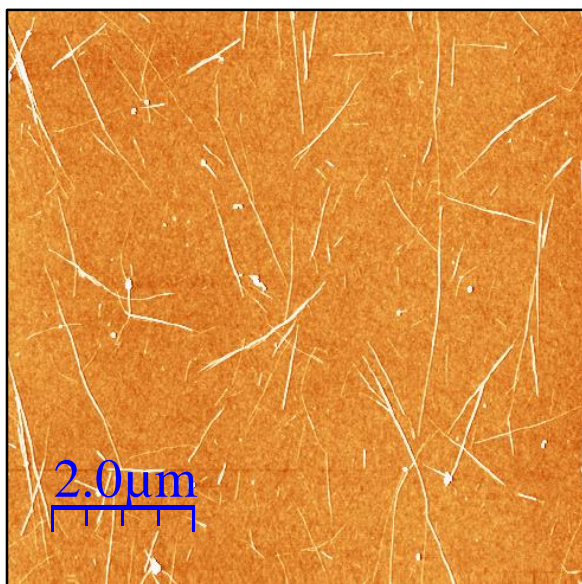


b)

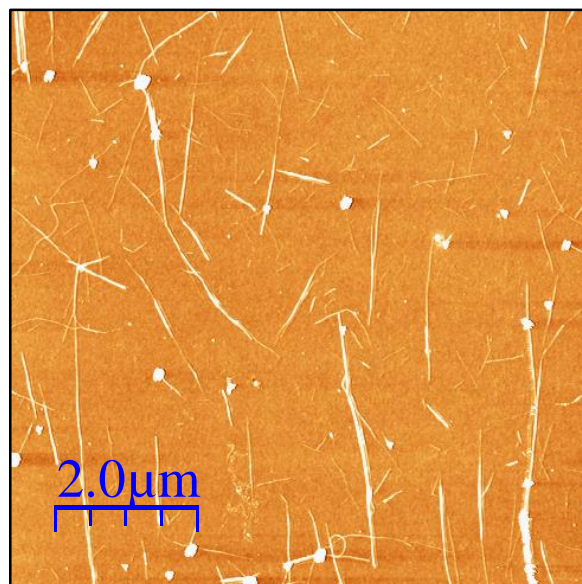


c)

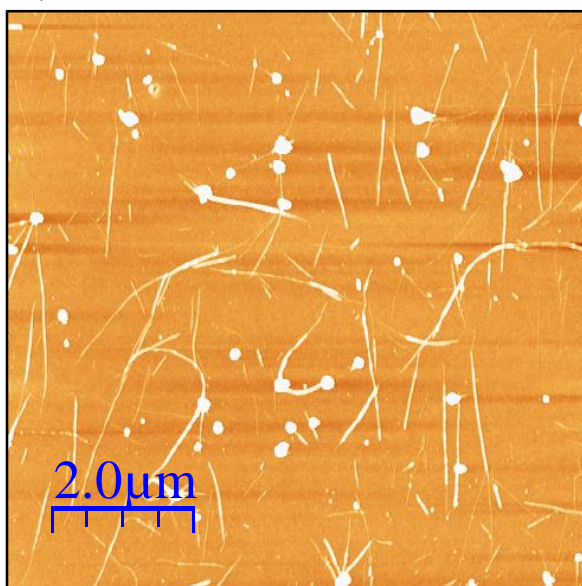
Figure 3.11: a) RBM region in Raman spectra of SWNT deposits of sucrose layers indicating peak shifts at 1mg/mL, 0.5mg/mL, and 0.1mg/mL; a) at 5%; b) at 20%; c) at the bottom layer.



a)



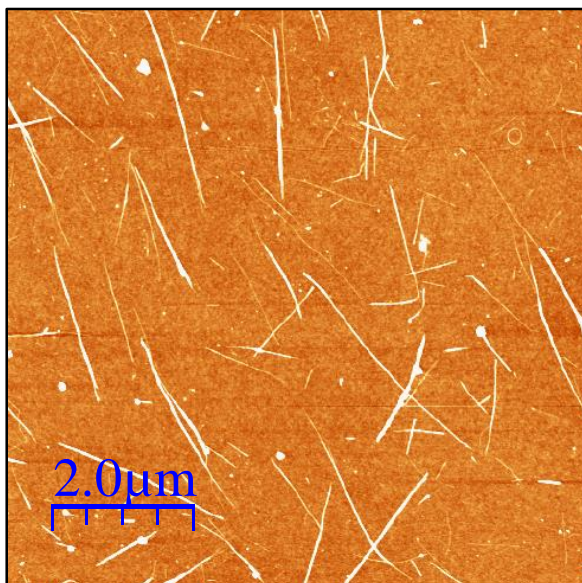
b)



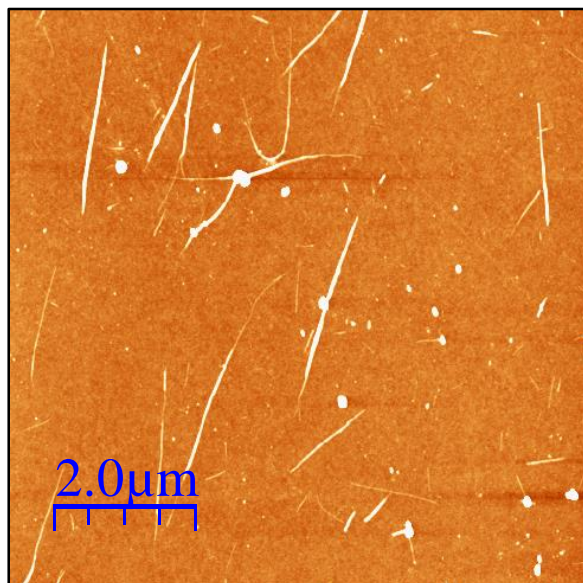
c)

Figure 3.12: Representative AFM images for SWNTs in each sucrose layers for 1 mg/mL SWNT concentration; a) 5% (w/v) with average height of 4.32 nm and density of 0.15 SWNT/ μm^2 ; b) 15% (w/v) with average height of 5.67 nm and density of 0.225 SWNT/ μm^2 ; c) Bottom layer shows more pelletization and less nanotubes has an average height of 8.45 nm and density of 0.178

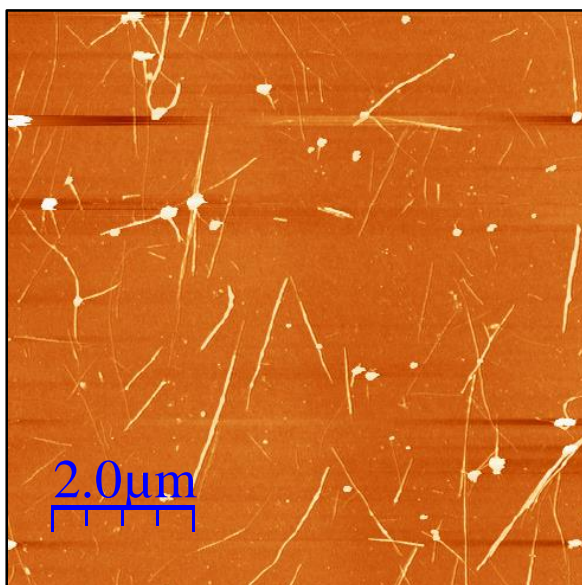
SWNT/ μm^2 The height increases with the increase in the sucrose layers indicating the SWTN solution is isolating at the bottom of centrifuge tube.



a)

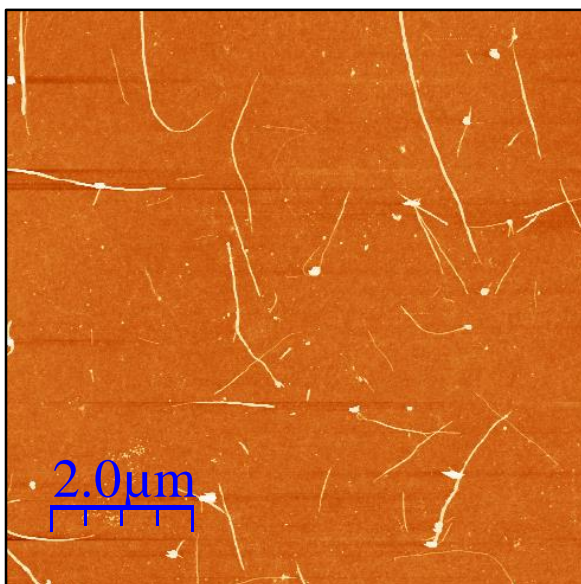


b)

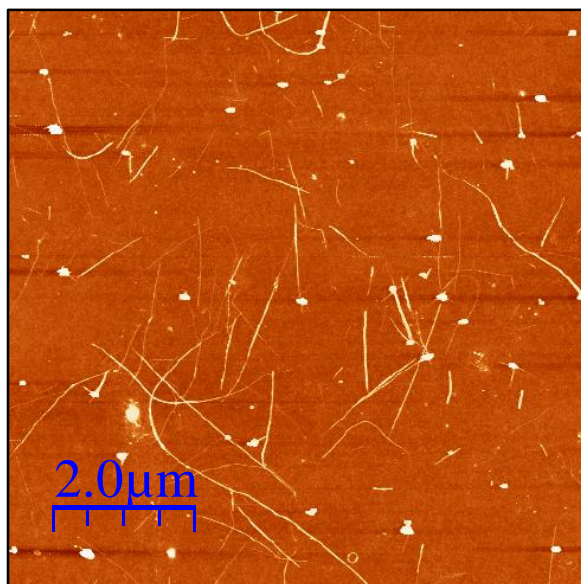


c)

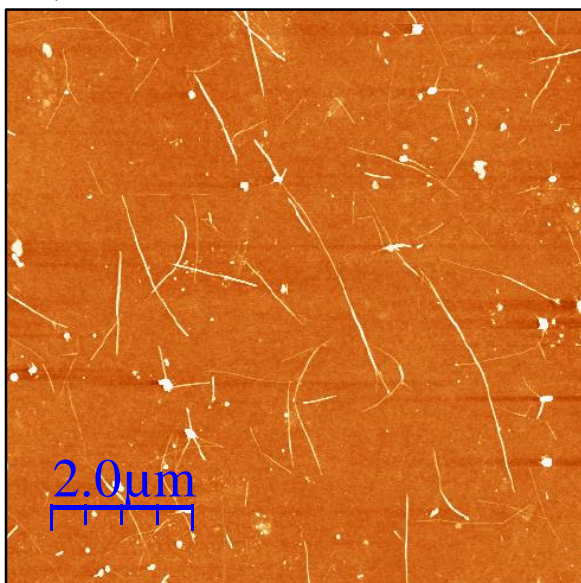
Figure 3.13: Representative AFM images for sucrose layers for 0.5 mg/mL SWNT concentration; a) 5% (w/v) with average height of 5.87 nm and density of 0.320 SWNT/ μm^2 ; b) 15% (w/v) with average height of 8.23 nm and density of 0.244 SWNT/ μm^2 ; c) Bottom layer with average height of 11.73 nm and density of 0.211 SWNT/ μm^2 .



a)

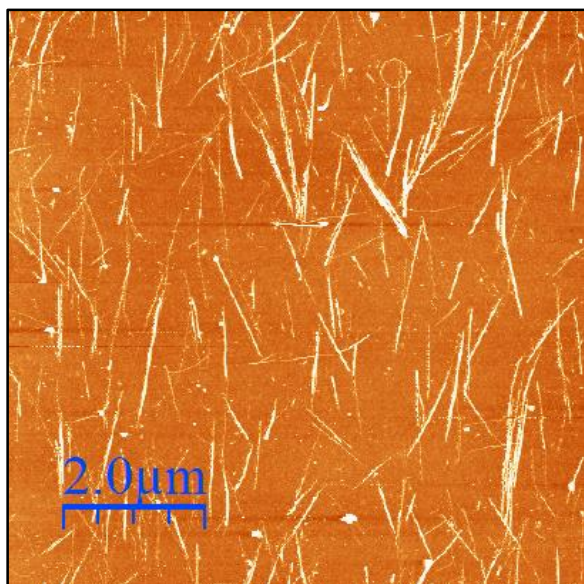


b)

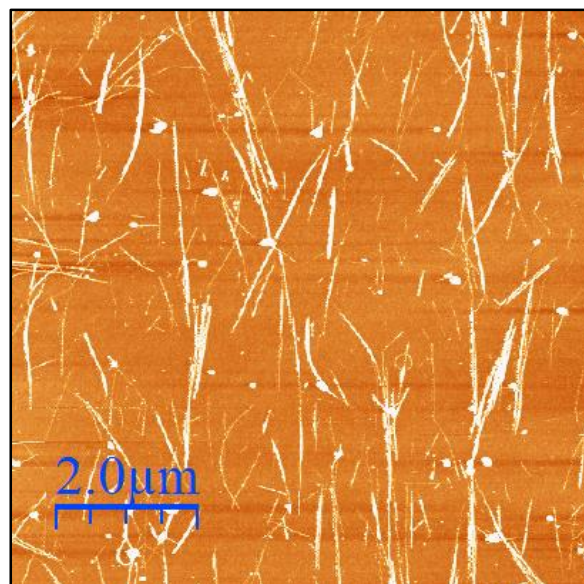


c)

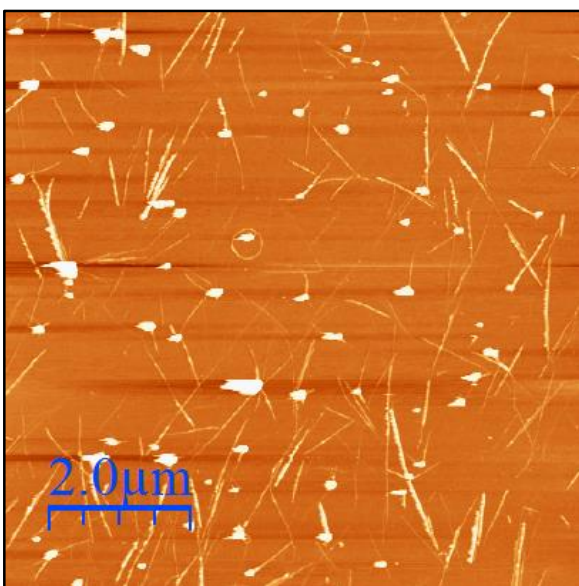
Figure 3.14: Representative AFM images for sucrose layers for 0.1 mg/mL SWNT concentration; a) 5% (w/v) with average height of 4.06 nm and density of 0.183 SWNT/ μm^2 ; b) 15% (w/v) with average height of 6.84 nm and density of 0.131 SWNT/ μm^2 ; c) Bottom layer with average height of 8.83 nm and density of 0.0807 SWNT/ μm^2 .



a)



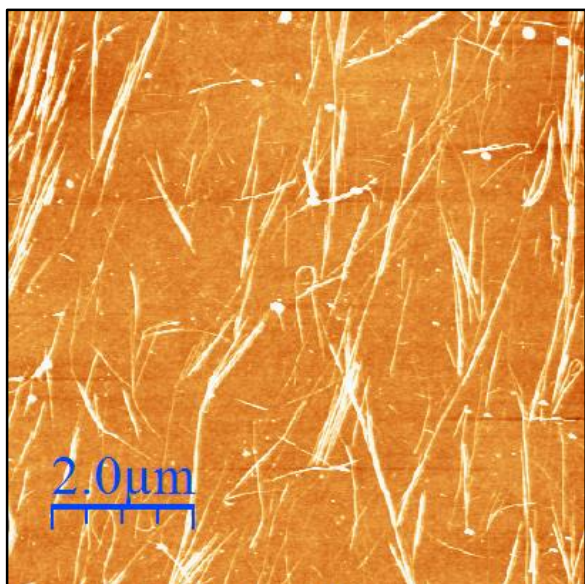
b)



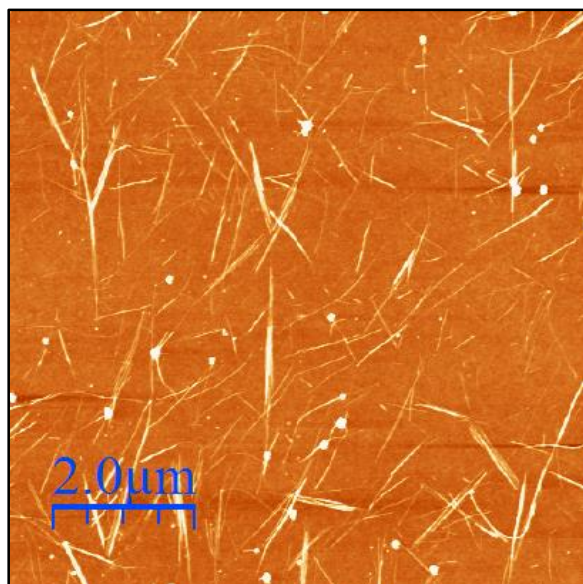
c)

Figure 3.15: Representative AFM images for SWNTs in each sucrose layers with SDS for 1 mg/mL SWNT concentration; a) 5% (w/v) with average height of 5.54 nm and density of 0.506 SWNT/ μm^2 ; b) 15% (w/v) with average height of 7.32 nm and density of 0.284 SWNT/ μm^2 ; c) Bottom layer which shows more pelletization and less nanotubes has an average height of 16.01

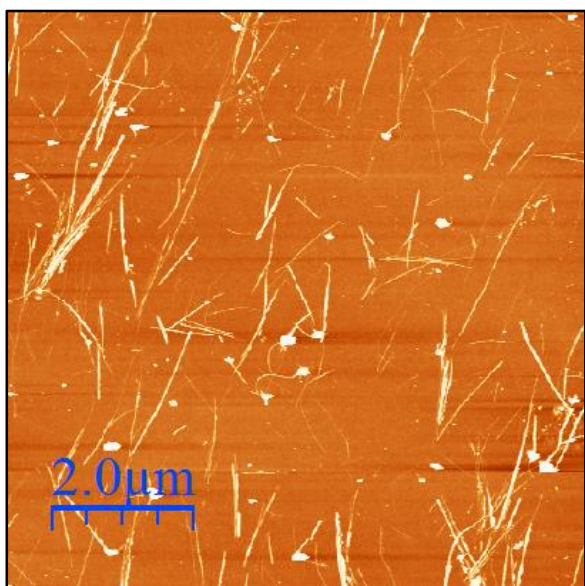
nm and density of $0.105 \text{ SWNT}/\mu\text{m}^2$. The height increases with the increase in the sucrose layers indicating the SWTN solution is isolating at the bottom of centrifuge tube.



a)



b)



c)

Figure 3.16: Representative AFM images for SWNTs in each sucrose layers with SDS for 1 mg/mL SWNT concentration; a) 15% (w/v) with average height of 3.69 nm and density of 0.281 SWNT/ μm^2 ; b) 45% (w/v) with average height of 5.04 nm and density of 0.187 SWNT/ μm^2 ; c)

Bottom layer with the least number of nanotubes has an average height of 8.65 nm and density of 0.119 SWNT/ μm^2 .

Table 3.4: AFM analysis on the effect of different SWNT concentration with sucrose gradients.

a) 1mg/mL, b) 0.5mg/mL, c) 0.1mg/mL

1mg/mL	5%	10%	15%	20%	25%	BL
Average Height (nm)	4.32±0.98	5.17±1.54	5.67±1.57	6.89±1.23	7.44±1.38	8.45±2.09
RMS	0.98±0.16	1.64±0.17	1.73±0.64	2.19±0.13	2.20±0.15	3.17±0.42
Length (µm)	1.77±0.27	1.48±0.43	1.32±0.39	1.24±0.57	1.18±0.53	1.08±0.58
Density (µm/SWNT ²)	0.415±0.049	0.282±0.060	0.225±0.048	0.206±0.030	0.203±0.261	0.178±0.033

a)

0.5mg/mL	5%	10%	15%	20%	25%	BL
Avg Height (nm)	5.87±0.99	7.70±2.02	8.23±2.88	8.43±1.93	10.03±2.49	11.73±4.34
RMS	1.59±0.35	1.89±0.048	1.81±0.49	2.10±0.28	2.24±0.30	2.57±0.37
Length (µm)	1.62±0.47	1.35±0.27	1.25±0.26	1.08±0.26	1.04±0.15	0.88±0.23
Density (µm/SWNT ²)	0.320±0.069	0.308±0.035	0.244±0.045	0.226±0.027	0.215±0.023	0.211±0.027

b)

0.1mg/mL	5%	10%	15%	20%	25%	BL
Avg Height (nm)	4.06±0.78	6.3±0.59	6.84±0.62	7.55±2.29	8.64±1.79	8.83±2.78
RMS	1.40±0.14	2.07±0.32	2.14±0.16	2.16±0.32	2.25±0.34	2.52±0.74
Length (μm)	1.36±0.34	1.10±0.34	0.988±0.22	0.965±0.38	0.915±0.14	0.883±0.19
Density (μm/SWNT ²)	0.183±0.034	0.178±0.023	0.131±0.041	0.117±0.031	0.0968±0.014	0.0807±0.007

c)

CHAPTER 4

EFFECT OF SELF ASSEMBLED MONOLAYERS (SAMs) ON THE ELECTRICAL PROPERTIES OF SINGLE-WALLED CARBON NANOTUBE NETWORK

Bhatt.N.P; Vichchualada; Lay.M.D. To be submitted to *Langmuir*

4.1 ABSTRACT

The interaction between different self-assembled monolayers (SAMs) and single-walled carbon nanotubes (SWNTs) were investigated to optimize the production of low density SWNT network. The ability to form low density SWNT network is of great importance for application in electronic devices. The low density network was formed using laminar flow deposition (LFD) at room temperature and the density of the SWNT network was verified by atomic force microscopy (AFM). Room temperature deposition method allows for separation, purification of SWNTs before deposition. LFD was used to form 2-D networks of SWNTs while preventing bundle formation during network growth. The pH treatment on the purified SWNT suspensions alter the density, average height of the SWNT network. The defects introduced due to the pH treatment were then analyzed by Raman spectroscopy. Different self-assembled monolayers were used to control purity of the deposit while measuring the electric properties during the deposition process.

4.2 INTRODUCTION

Since their discovery in 1991, single-walled carbon nanotubes have been extensively researched. Due to their novel structure and remarkable physical and chemical properties carbon nanotubes can be used in various fields throughout the electronic industry. Single nanotube devices have high mobilities, current carrying capacities of 10^9 A/cm²¹ and on/off ratio as large as 10^5 .² SWNT networks have been studied for quantum wires, thin film transistors,^{2,3 4} diodes,⁵ sensors, capacitors.⁶ For SWNT network, SWNT density is the major determining factor for macroscopic electrical properties. Depending on the density of the deposition, SWNT networks behave as semi-conductive when composed of low densities of unbundled SWNTs. When SWNTs are composed of high density bundled networks, the surface behaves as metallic. Low density SWNT networks are of significant interest because they can be tuned from semi conductive to metallic as the density increases.

The networks of carbon nanotubes can be in bundled or unbundled formation. The bundled⁷ and unbundled⁸ SWNT networks have very different properties and applications, so it is very important to develop a method that can control the purity of the deposit and degree of bundle formation in the network, which can help measure the electrical properties of the SWNT network. The thin film transistors containing large bundles show larger “off” current due to the high density of metallic nanotubes present on the SWNT network. Unbundled and bundled network have higher current drive than individual SWNT, since the current is proportional to the number of SWNTs in a network. Room-temperature routes to SWNT network formation will create new energy efficient electronic materials. Liquid deposition methods show tremendous potential by using non-oxidizing purification methods before network formation. Previous studies of the liquid deposition process include spray coating,⁹ dip-coating¹⁰ and laminar fluid-flow method.¹¹ It remains a great

challenge to produce controlled deposition of SWNT on different substrates. The deposition of SWNT network requires optimization of self-assembled monolayers (SAMs). SAMs are chemisorbed organic layers formed on metal substrate by adsorption of molecules with polar head groups, functional tail group and non-polar alkyl chain.

Self-assembled monolayers (SAMs) have attracted great attention since their discovery in the 1980's by Sagiv.¹² Large variety of self-assembly systems have been studied, including different alkanthiols on gold¹³, alkylsilanes on silicon,¹⁴ which is the most used combination in self-assembling molecules on substrates. Self-assembly is the assembly of atoms or molecules to form larger structures by H bond, π - π stacking, ionic interactions, and hydrophilic or hydrophobic interactions. SAMs present a versatile approach to surface functionalization due to simple instrumentation, high reproducibility, and reduced assembly time.¹⁵ The self-assembled monolayers are single layer of organic molecules adsorbed onto a solid substrate. They consist of three parts: the polar head group, non-polar alkyl chain, and functional tail group. The head group is responsible for anchoring the molecules to the substrate. The alkyl chain stabilizes the monolayer due to the van der Waals interactions between the chains. The tail group modifies the surface properties by introducing chemical functionality into the monolayer. This functionalization provides the properties like adhesion, conductivity in controlled manner as it offers effective tuning of these properties.¹⁵ Therefore, SAMs have been extensively used in manufacturing process in areas of nanomaterials, sensors,¹⁶ electronics.¹⁷

To form SWNT network on the substrate, self-assembled monolayers play an important role. It has been shown in previous literature that different self-assembled monolayers have a significant impact on the threshold voltage, source-drain current, field effect mobility, and I_{on}/I_{off} ratios.^{18, 19} It is easier to manipulate the SWNT network using different SAMs since they are ideal

sensor materials and are very responsive as they are composed of surface atoms.²⁰ The surface chemistry of the SWNT network can be altered by using different SAMs comprising of various functional groups. It has been shown before that the surface chemistry has an impact on the on current, I_{on}/I_{off} ratios, and as a result electrical properties of SWNT network can be tuned using SAMs.²¹ This report shows the effect of different SAMs on the electrical properties of SWNT networks. The effect of aminosilanes and aromatic functionalized silanes has been investigated as well. Since the amines can be protonated or deprotonated, the 3-APTES was used to deposit an acidic and basic SWNT suspension. This manuscript also provides a new method for controlling the purity of the deposit by using different self-assembled monolayers on the SWNT network and also use the chemistry on the silane to modify the electrical properties after deposition. This report presents the deposition on the SWNT networks by LFD, which has proven useful in the formation of low- density SWNTs network since LFD ensures that nanotube bundling does not occur during the deposition process.⁸ Each deposition cycle consists of density of aligned and orthogonal SWNTs.

4.3 EXPERIMENTAL PROCEDURE

4.3.1 Formation and Purification of SWNT suspensions

To form the suspensions, 1 mg/mL AP grade arc discharge soot (Carbon Solutions, Inc) was dispersed in 1% SDS (J.T.Baker) solution via 30 min. of probe ultrasonication (Fisher Model 500) at a power density of 0.4 W/mL, which imparted 21 kJ of energy to the suspension. Next, SWNT suspensions were distributed into 1.5 mL centrifuge tubes and centrifuged (Beckman Microfuge) for 45 min. at 18,000 G. After multiple centrifugation cycles, the upper 50% of the supernatant was carefully collected and the purified SWNT suspension was obtained.

4.3.2 Formation of Acidic and Basic SWNT suspension

To form an acidic pH SWNT suspension, sulfuric acid (J.T Baker) of molarity 18.1M was used as a stock solution to obtain a pH of 3. By using the dilution titration formula, 2.76 μL of the 18.1M stock was added to 50 mL of water to make 0.001M sulfuric acid yielding pH of 2.50. Next, 2 mL of the (pH 2.50) sulfuric acid solution was added to 2 mL of purified SWNT suspension to get to the final of pH 3.22 as shown in Figure 4.1. This solution was used to form SWNT network using deposition.

To form basic pH SWNT suspension, sodium hydroxide pellets (J.T Baker) weighing 0.1g was dissolved in 1 L of water with the molarity of 0.0025M and pH 11.35. Three mL of the stock solution was added to 2 mL of the purified SWNT suspension, to get to the final pH of 10.54. The pH of the above solutions were measured by the pH meter (Beckman 360) and pH probe (Fisher Scientific).

4.3.3 Formation of SWNT deposits via Laminar Flow Deposition (LFD)

The process of Laminar flow deposition has been explained in previous work. Briefly the Si/SiO₂ wafers were cleaned with compressed CO₂. Prior to SWNT deposition, the substrates were modified with different self-assembled monolayers for 45 min and then were immersed in a solution of 3-aminopropyl triethoxysilane (99%, Sigma Aldrich) in ethanol (99.5%, absolute 200 proof, ACROS). In order to ensure that only one monolayer of the silane remained, substrates were washed with copious amount of ethanol, water, and then dried in a stream of N₂ gas. Then, they were cleaned with compressed CO₂.

After substrate preparation, two deposition cycles, each using 90 μL of SWNT suspension, were used to form the low-density SWNT deposits in that would be used for AFM analysis as shown in Figure 4.1. The networks were aligned one direction following the two deposition cycle. For an acidic and basic SWNT suspensions, four deposition cycles with 90 μL each was used.

Each deposition cycle consisted of wetting the silane coated Si/SiO₂ wafer with the SWNT suspension, followed by quick drying in a stream of N₂ gas at a pressure of 60 psi. The wafers were then rinsed with copious amounts of nanopure water (>18.1 MΩ) and dried again under a stream of N₂ gas. The process was repeated using three other self-assembled monolayers: n-propyl triethoxysilane (97% Sigma Aldrich), phenyl triethoxysilane (Alfa Aesar 98%), and octadecyltrimethoxysilane (OTS) (Sigma Aldrich 90%).

Orthogonal networks were formed on SWNT substrate with deposition cycles in both directions (vertical and horizontal). This method of deposition resulted in more homogenous distribution of nanotubes on the surface. It maximizes the number of SWNT-SWNT junctions and allows for better determination of effect of self-assembled monolayers on the electrical properties. This type of network is expected to yield highest macroscopic conductivity with less loading of SWNTs compared to aligned deposits. It has proven in previous works that the random networks showed more consistent resistance measurements.⁸ This can prove efficient in formation of SWNT networks with more precision.

Before the SWNT network formation, two Ti electrodes were deposited using the Thermal evaporator on the Si substrate. The process has been explained in previous papers.²² Briefly, dual filament thermal evaporator (Thermionics), under high vacuum with pressure less than 1×10^{-6} Torr was used to deposit the Ti pellets (Kurt J. Lesker Company, 99.9995% pure 1/8" diameter pellets). Stainless steel stencil was placed between the deposition source and Si wafer. This would serve as a mask to deposit 2mm diameter circles 1cm apart. Ti deposited was ~0.5μm thick verified by AFM. Four different self-assembled monolayers (3-APTES, n-propyl triethoxysilane, phenyl triethoxysilane, and OTS) were deposited around the Ti electrodes and then SWNTs were deposited using orthogonal pattern, shown in Figure 4.2.

4.3.4 Characterization of SWNT deposits with different SAMs by AFM, and Raman Spectroscopy

AFM images were obtained via intermittent contact mode in air (Molecular Imaging, Pico Plus). AFM image analysis software (WSxM, v5.0)²³ was used to determine the effect of the different silanes on the average height, length of SWNTs, as well as the surface roughness. Additionally, the change in surface roughness was evaluated in order to determine the concentration of impurities remaining in an acidic and basic suspensions for the 3-APTES.

Raman spectroscopy (Thermo Scientific, DXR SmartRaman) was performed on suspensions in a sealed capillary tube and on SWNT deposits. A CCD detector was used to record spectra obtained using a 532 nm diode laser excitation source. The pH suspensions were analyzed with a 10 X objective and a source intensity of 10 mW at the sample, while for SWNT deposits, a 50 X objective with 7 mW intensity at the sample was employed.

A semiconductor characterization system (Keithley, 4200SCS) and probe station (Signatone, S-1160A) were used for electrical measurements. To determine the effect of self-assembled monolayers on the inter SWNT junction resistance, samples were examined using 2 point probe method for resistance measurements and I_{on}/I_{off} ratios was measured at -10V and +10V respectively for transistor response of the samples.

4.4 RESULTS AND DISCUSSION

4.4.1 Characterization of acidic and basic SWNT Suspension by UV-vis NIR Spectroscopy

The absorbance for the basic SWNT suspension and an acidic SWNT suspension is lower than the pristine SWNT suspension (Figure 4.3a). The absorbance for an acidic suspension is slightly lower than the basic, which is indicative of the presence of more impurities in the basic suspension compared to the acidic. The intensity of peak S₂₂ decreases (Figure 4.3b) with increase

in the pH. This result indicates that the change in the concentration of H^+ and OH^- causes electronic structure change in semiconducting SWNTs.²⁴

4.4.2 Analysis of Aligned Deposits on Different Self- Assemble Monolayers by Raman Spectroscopy

Raman spectroscopy is used for characterizing the relative purity of SWNT suspensions and deposits due to the high Raman scattering efficiency of both defect-free and disordered sp^2 hybridized carbon atoms. The graphite band (G-band), which occurs near 1590 cm^{-1} , is indicative of tangential phonons in the pristine nanotubes, while the disorder band (D-band), near 1370 cm^{-1} , is indicative of asymmetric stretching in amorphous sp^2 hybridized C.

For different self-assembled monolayers, I_G/I_D ratios for deposits (Table 4.2) decrease for an acidic and basic SWNT suspension compared to the pristine SWNT deposition. The ratios for the basic suspension is lower than an acidic suspension which indicates that more defects are introduced on the side walls of the nanotubes at higher pH. This was confirmed by the UV-vis NIR spectroscopy. At around pH 3, the level of the protonation was increased, resulting in a decrease in D band intensity compared to the intensity of G band which shows higher I_G/I_D ratios. The defects in the tubes were negatively charged at pH 3 and were strongly attracted to the surface. At pH 10, more tubes with defects were present on the substrate because the etched APTES layer created more defects in the tubes resulting in lower I_G/I_D ratios. At higher pH the self-assembled monolayer starts to destroy resulting in lower SWNT adsorption. This would have very important implications for SWNT-based transistors, especially controlling SWNT defects for future electrical applications. Among phenyltriethoxysilane and octadecyltrimethoxysilane, and n-propyltriethoxysilane, the I_G/I_D ratios for phenyltriethoxysilane is the highest, followed by OTS

and the lowest for n-propyltriethoxysilane (Table 4.1). This can be explained by the dominance of metallic tubes on the substrate with aromatic molecules.

4.4.3 Analysis of SWNT density by Atomic Force Microscopy (AFM): Effect of pH on aligned SWNT deposit

The density of the SWNT adsorbed on the surface reduced from pH 3 to pH 10 (Table 4.3). At low pH, the amines on the substrate become positively charged and the amine functional group on APTES convert to ammonium ions which interact with the negatively charged carboxylate defect groups in the SWNT suspension. The strong electrostatic attraction between the positively charged surface and the negatively charged SWNTs lead to high density of tubes on the surface. The decrease in the density of nanotubes from pH 3 to pH 10 can be explained by the weakening of electrostatic attractions due to the decrease in ammonium ions.²⁴ However, strong acids cut the carbon nanotubes into small pieces which decrease the aspect ratio of the nanotubes. The average height and RMS (root mean square) roughness of an acidic SWNT suspension is higher than the basic SWNT suspension because the bundle formation for an acidic suspension is more than the basic suspension which can be confirmed by the higher absorbance at 242nm for an acidic suspension. The absorbance at 242nm is due to both the carbonaceous impurities and the bundles in the SWNTs.^{25,26} The AFM image of the purified SWNT suspension shows longer tubes (Figure 4.4a) and less globular impurities compared to the ones treated with sulfuric acid and sodium hydroxide base (Figure 4.4b and 4.4c). This confirms that when suspension is treated with an acid or a base, it introduces defects into the side walls of carbon nanotubes along with the presence of carboxyl groups at the ends.

4.4.4 Effect of different Self-assembled monolayers on aligned SWNT deposit

AFM images in Figure 4.5 show SWNT deposits on different self-assembled monolayers. The average density of SWNTs deposited on phenyltriethoxysilane is the highest compared to the OTS and n-propyl silane. This can be explained by the fact that aromatic functionalized surfaces favor the metallic nanotubes.²⁷⁻²⁹ N-propyl has lower density of nanotubes, lower height than OTS and phenyltriethoxysilane. But the self-assembly process depends on the water content, the solvent, the age of the solution, the deposition time, the temperature, and the humidity of the room, which play an important role in the formation of the monolayer making the results challenging to compare.

4.4.5 Analysis of Orthogonal deposits on SWNT network

As mentioned earlier, orthogonal deposits lead to homogenous SWNT distribution on the SWNT network. Due to the random orientation, more inter-SWNT junctions are created leading to higher conductivity with the lowest loading of SWNTs. Same type of samples are used here as the ones for aligned deposits. The only difference is that, with orthogonal deposits the semi-conductive SWNT network was formed with the resistance around $1\text{M}\Omega$. Surfaces functionalized with aminosilanes (3-APTES) (Figure 4.7d) show selective absorption of semiconducting nanotubes. However it has been shown in literature that the phenyl-terminated silane (Figure 4.7c) bind selectively to metallic nanotubes. This selectivity is due to the fact that SWNT consists of π bonds that interact with other π system via π - π stacking. This is stronger with metallic nanotubes compared to the semiconducting ones due to the polarizability.²⁷⁻²⁹ Similarly, Table 4.4 shows $I_{\text{on}}/I_{\text{off}}$ ratios with resistance values and height measurements of SWNT suspension on different self-assembled monolayers. Comparing the $I_{\text{on}}/I_{\text{off}}$ ratios for OTS, phenyl and n-propyl silane, SWNT substrates functionalized with aromatic molecules have the lowest $I_{\text{on}}/I_{\text{off}}$ ratios since they

are dominated by metallic nanotubes. The ratios for 3-ATPES is the highest because they absorb everything (nanotubes/some impurities) when deposited on the surface due to the electron donating power of the amine group. OTS show highest ratios as compared to other two phenyl terminated and n-propyl terminated silane, this can be due to the extreme hydrophobicity. These results can work as a prerequisite step to achieving higher I_{on}/I_{off} ratios using different self-assembled monolayers which can be used in to tune electronic devices. This can be achieved by deposited copper nanoparticles on SWNT network.³⁰

Aminosilanes are used because they enhance the absorption of nanotubes and improve the performance of transistors. Papadimitrakopoulos and coworkers³¹ showed selective absorption of amines on semiconducting SWNTs. Dai and Hong³² demonstrated that the electron donating power of NH_2 groups causes significant change in the electrical conductance of semiconducting SWNTs, whereas the metallic SWNTs remained insensitive to the adsorbed amines. The I_{on}/I_{off} ratios for the substrates functionalized with 3-APTES is the highest than OTS, phenyltriethoxysilane and n-propyltriethoxysilane (Table 4.4). This corroborates the assertion that the APTES adsorb semiconducting nanotubes leading to higher on current and lower off current resulting in higher I_{on}/I_{off} ratios. Phenyl-terminated silane strongly binds to metallic nanotubes²⁷ leading to on/off ratios ~ 2 . Higher current capacity than the amine surface is indicative of the fact that phenyl surfaces are dominated by metallic nanotubes. The weak interaction between the substrate and SWNTs is due to the extreme hydrophobicity of OTS which gives poor adhesion leading to less adsorption of SWNTs on to the surface.

4.5 CONCLUSIONS

Two dimensional networks of unbundled SWNTs were deposited via laminar flow deposition from the aqueous suspensions of varying pH. The depositions on the SWNT network

were analyzed by atomic force microscopy and the defects were verified by Raman spectroscopy. The pH treatment on the purified SWNT suspensions with sulfuric acid and sodium hydroxide showed lower density and the height compared to the untreated SWNT suspension as the addition of acid and base in the SWNT suspension introduced defects into the sp^2 structure of the carbon nanotube thus changing the electrical properties of the network. Using different self-assembled monolayers with average density and height can be also used as a method in controlling the density and alignment of the deposited SWNT network. Semiconducting and metallic nanotubes can be isolated using 3-APTES and phenyltriethoxysilane respectively. This can serve as a route to tune and optimize device performance in some electronic devices.

4.6 REFERENCES

1. Yao, Z.; Kane, C.; Dekker, C. *Physical Review Letters* **2000**, 84, (13), 2941-2944.
2. Shiraishi, M.; Takenobu, T.; Iwai, T.; Iwasa, Y.; Kataura, H.; Ata, M. *Chemical Physics Letters* **2004**, 394, (1-3), 110-113.
3. Meitl, M. A.; Zhou, Y.; Gaur, A.; Jeon, S.; Usrey, M. L.; Strano, M. S.; Rogers, J. A. *Nano Letters* **2004**, 4, (9), 1643-1647.
4. Hu, L.; Hecht, D. S.; Grüner, G. *Nano Letters* **2004**, 4, (12), 2513-2517.
5. Kocabas, C.; Shim, M.; Rogers, J. A. *Journal of the American Chemical Society* **2006**, 128, (14), 4540-4541.
6. Masarapu, C.; Zeng, H. F.; Hung, K. H.; Wei, B. *ACS Nano* **2009**, 3, (8), 2199-2206.
7. Eda, G.; Fanchini, G.; Kanwal, A.; Chhowalla, M. *Journal of Applied Physics* **2008**, 103, (9), 093118.
8. Vichchulada, P.; Zhang, Q.; Duncan, A.; Lay, M. D. *ACS Applied Materials & Interfaces* **2010**, 2, (2), 467-473.
9. Gruner, G. *Journal of Materials Chemistry* **2006**, 16, (35), 3533-3539.
10. Jang, E. Y.; Kang, T. J.; Im, H. W.; Kim, D. W.; Kim, Y. H. *Small* **2008**, 4, (12), 2255-2261.
11. Zhang, Q.; Vichchulada, P.; Lay, M. D. *physica status solidi (a)* **2010**, 207, (3), 734-738.
12. Sagiv, J. *Journal of the American Chemical Society* **1980**, 102, (1), 92-98.
13. Ulman, A. *Chemical Reviews* **1996**, 96, (4), 1533-1554.
14. Wasserman, S. R.; Tao, Y. T.; Whitesides, G. M. *Langmuir* **1989**, 5, (4), 1074-1087.
15. Smith, R. K.; Lewis, P. A.; Weiss, P. S. *Progress in Surface Science* **2004**, 75, (1-2), 1-68.
16. Chaki, N. K.; Vijayamohanan, K. *Biosensors and Bioelectronics* **2002**, 17, (1-2), 1-12.

17. Aswal, D. K.; Lenfant, S.; Guerin, D.; Yakhmi, J. V.; Vuillaume, D. *Analytica Chimica Acta* **2006**, 568, (1–2), 84-108.
18. Possanner, S. K.; Zojer, K.; Pacher, P.; Zojer, E.; Schürerer, F. *Advanced Functional Materials* **2009**, 19, (6), 958-967.
19. Pernstich, K. P.; Haas, S.; Oberhoff, D.; Goldmann, C.; Gundlach, D. J.; Batlogg, B.; Rashid, A. N.; Schitter, G. *Journal of Applied Physics* **2004**, 96, (11), 6431-6438.
20. Lee, R. S.; Kim, H. J.; Fischer, J. E.; Thess, A.; Smalley, R. E. *Nature* **1997**, 388, (6639), 255-257.
21. Vosgueritchian, M.; LeMieux, M. C.; Dodge, D.; Bao, Z. *ACS Nano* **2010**, 4, (10), 6137-6145.
22. Zhang, Q.; Vichchulada, P.; Shivareddy, S.; Lay, M. *J Mater Sci* **2012**, 47, (7), 3233-3240.
23. Horcas, I.; Fernandez, R.; Gomez-Rodriguez, J. M.; Colchero, J.; Gomez-Herrero, J.; Baro, A. M. *Review of Scientific Instruments* **2007**, 78, (1).
24. Opatkiewicz, J. P.; LeMieux, M. C.; Bao, Z. *ACS Nano* **2010**, 4, (2), 1167-1177.
25. Bhatt, N. P.; Vichchulada, P.; Lay, M. D. *Journal of the American Chemical Society* **2012**, 134, (22), 9352-9361.
26. Priya, B. R.; Byrne, H. J. *The Journal of Physical Chemistry C* **2008**, 112, (2), 332-337.
27. LeMieux, M. C.; Roberts, M.; Barman, S.; Jin, Y. W.; Kim, J. M.; Bao, Z. *Science* **2008**, 321, (5885), 101-104.
28. Nish, A.; Jeong-Yuan, H.; Doig, J.; Nicholas, R. J. *Nature Nanotechnology* **2007**, 2, (10), 640-646.
29. Lu, J.; Lai, L.; Luo, G.; Zhou, J.; Qin, R.; Wang, D.; Wang, L.; Mei, W. N.; Li, G.; Gao, Z. *Small* **2007**, 3, (9), 1566-1576.

30. Asheghali, D.; Vichchulada, P.; Lay, M. D. *Journal of the American Chemical Society* **2013**, 135, (20), 7511-7522.
31. Chattopadhyay, D.; Galeska, I.; Papadimitrakopoulos, F. *Journal of the American Chemical Society* **2003**, 125, (11), 3370-3375.
32. Kong, J.; Dai, H. *The Journal of Physical Chemistry B* **2001**, 105, (15), 2890-2893.

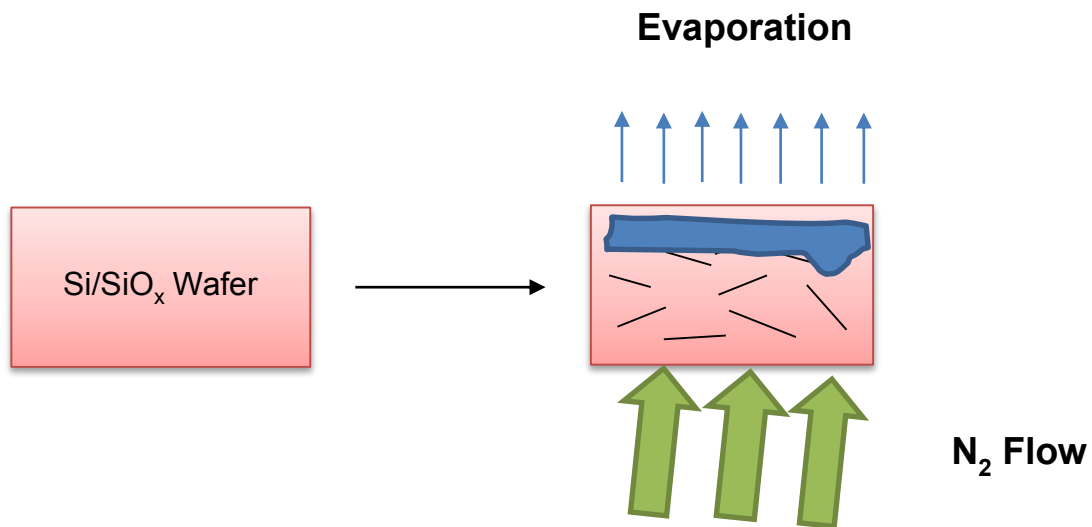


Figure 4.1: Laminar Flow deposition process to form SWNT network, where a unidirectional flow is applied to liquid/surface interface to effect the laminar flow of the suspension and resulting in drying of the substrate with nitrogen gas.

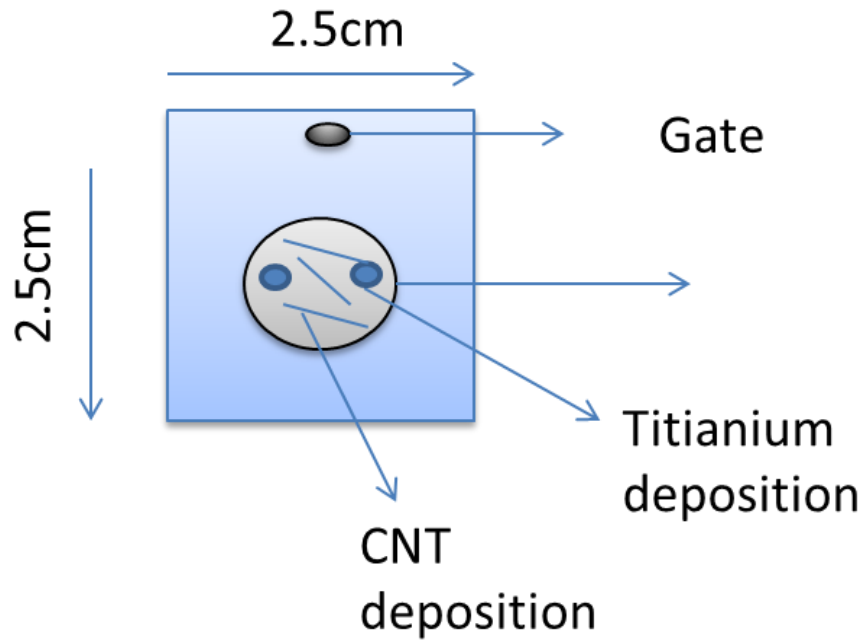
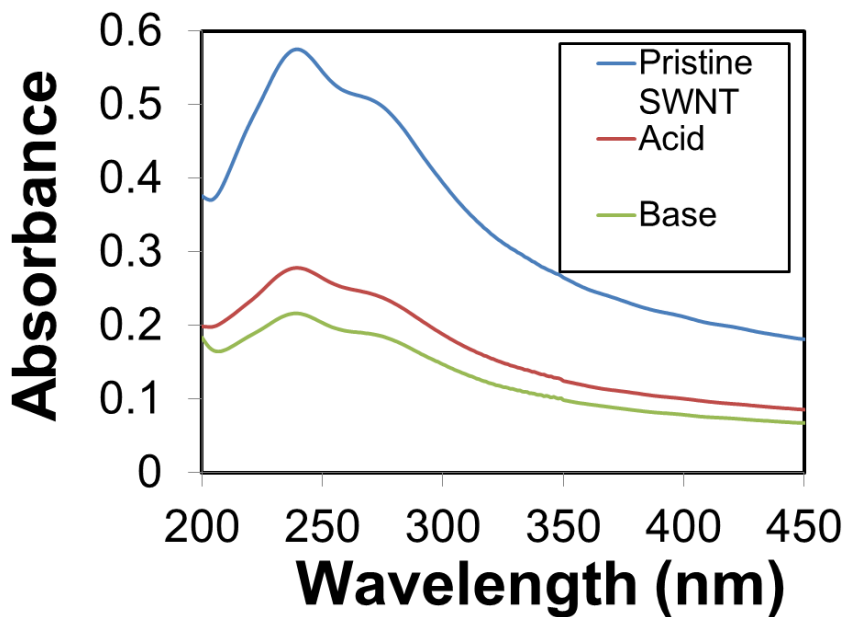
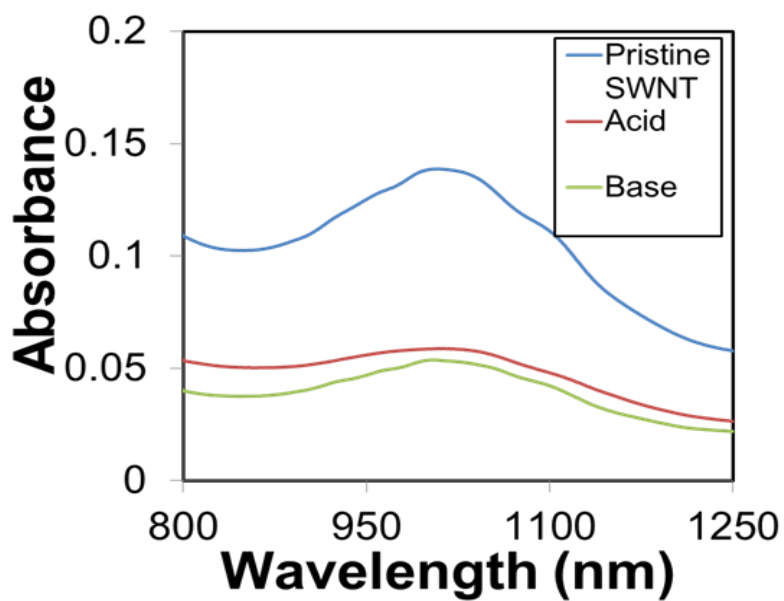


Figure 4.2: Schematic representation showing deposition of Titanium on Silicon substrate.

SWNTs are deposited in align and crossbar patterns.

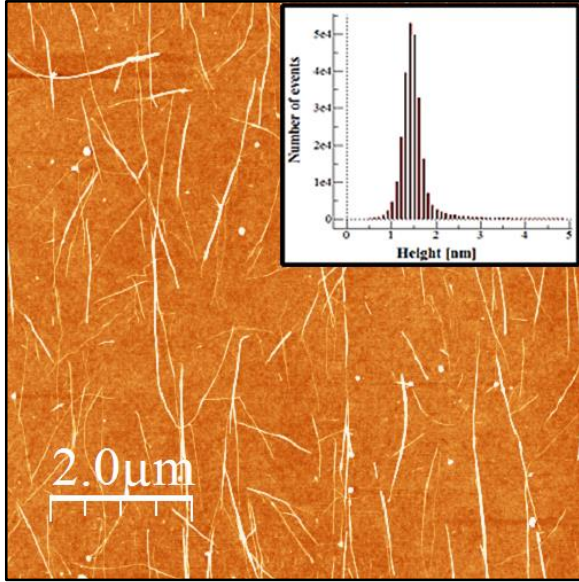


a)

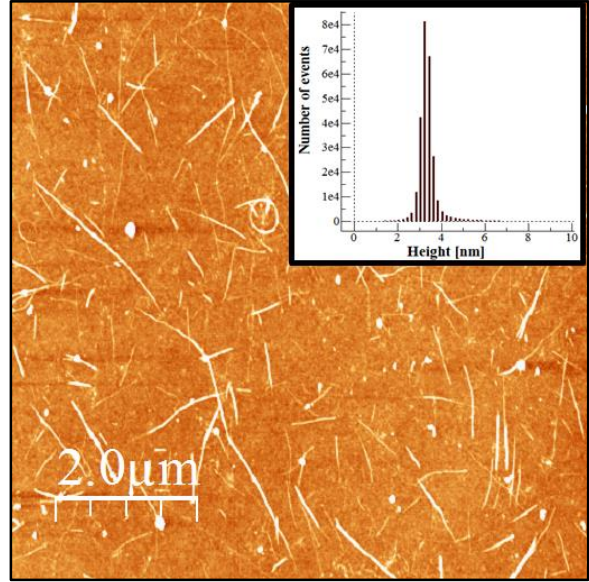


b)

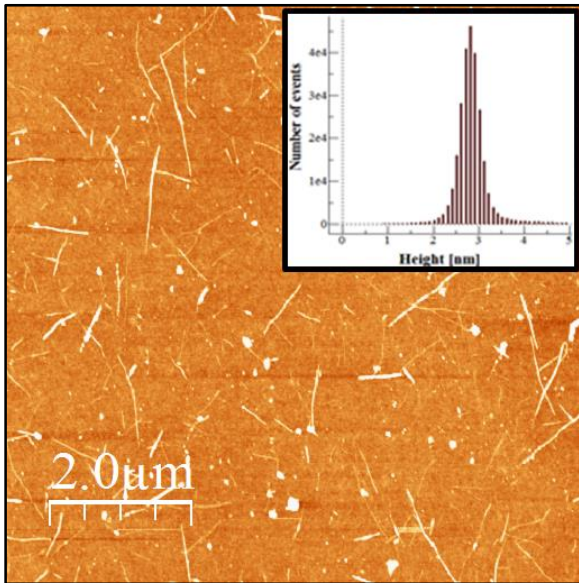
Figure 4.3: UV-vis/NIR spectra of pristine SWNT suspension, acid and basic suspension; a) the absorbance of the pristine SWNT suspension is higher than the acidic and basic; b) unbundling of SWNTs is confirmed by the NIR spectra around 1010nm.



a)

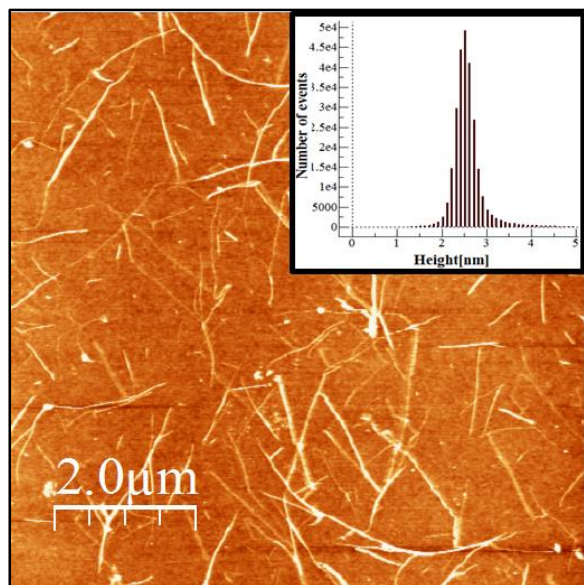


b)

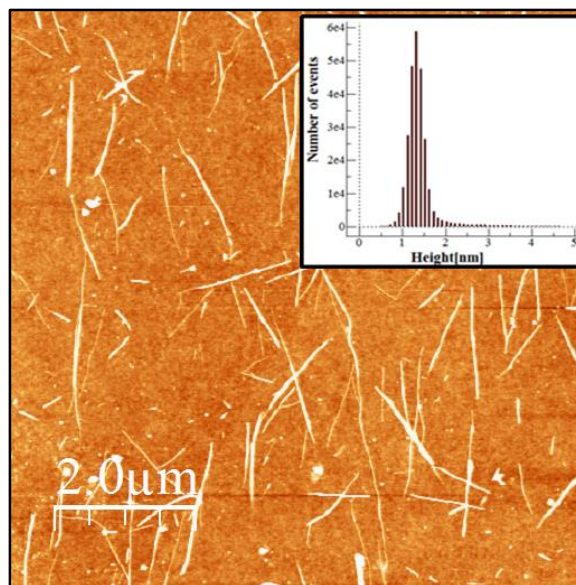


c)

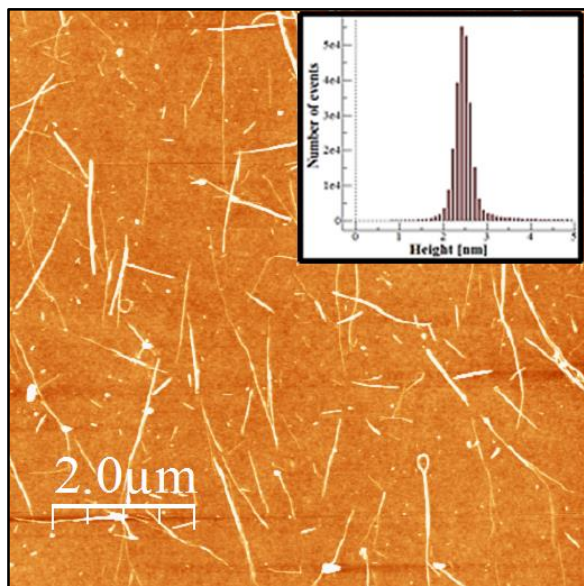
Figure 4.4: Representative AFM images ($8\mu\text{m} \times 8\mu\text{m}$) for deposits; a) pristine SWNT unbundled suspension with height around 1.69 nm; b) acidic suspension with height of 3.01 nm; c) basic suspension with height of 2.90 nm.



a)

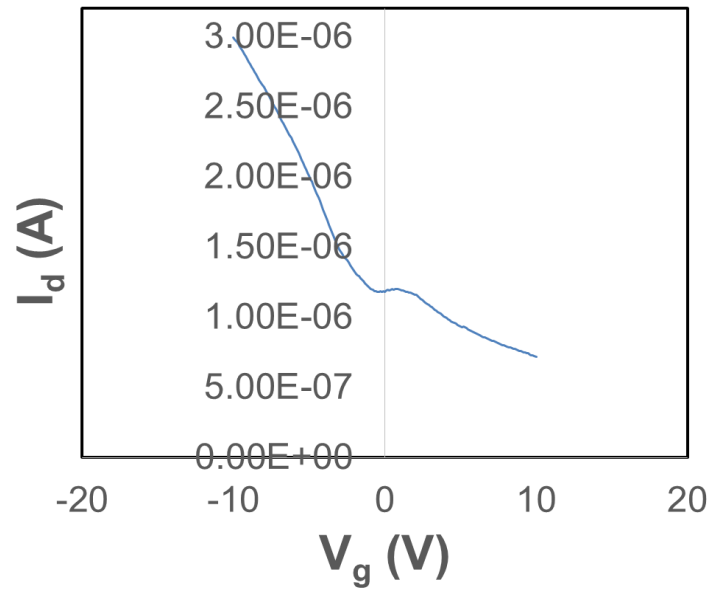


b)

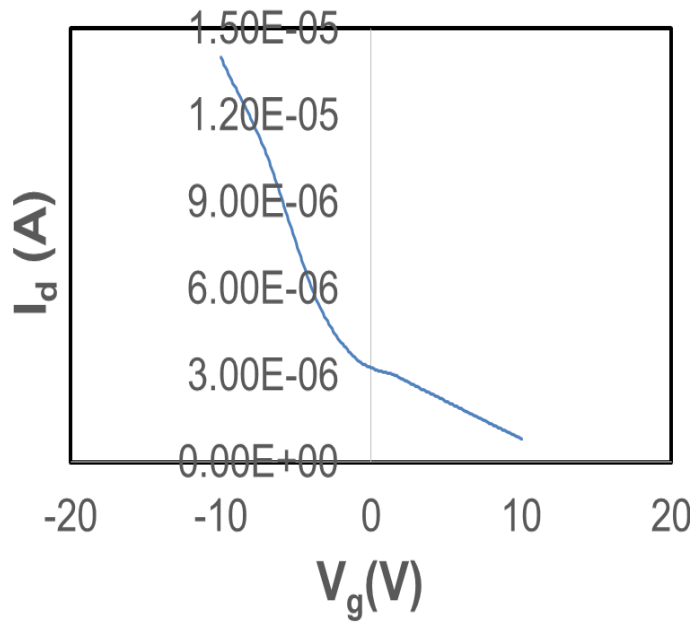


c)

Figure 4.5: Representative AFM images ($8\mu\text{m} \times 8\mu\text{m}$) for deposits; a) pristine SWNT suspension on OTS deposited substrate with height of 3.13 nm; b) pristine SWNT suspension on n-propyltriethoxysilane deposited substrate with height of 2.30 nm and; c) pristine SWNT suspension on phenyltriethoxysilane deposited substrate with height of 2.60 nm.



a)



b)

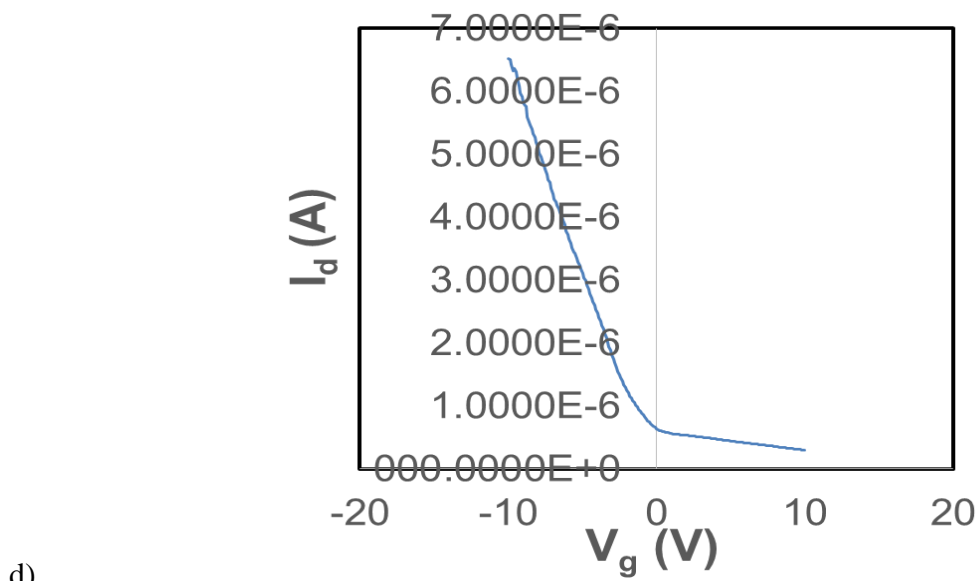
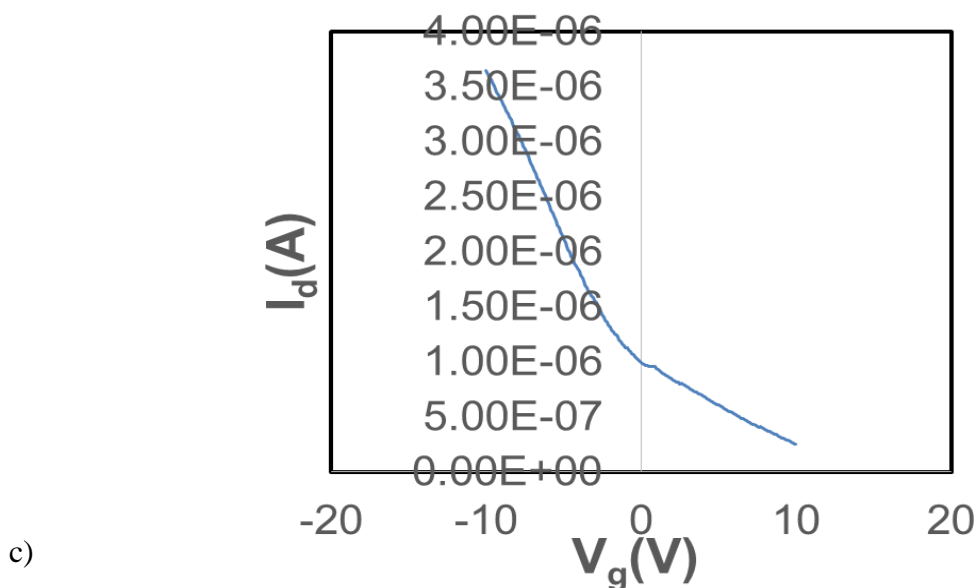
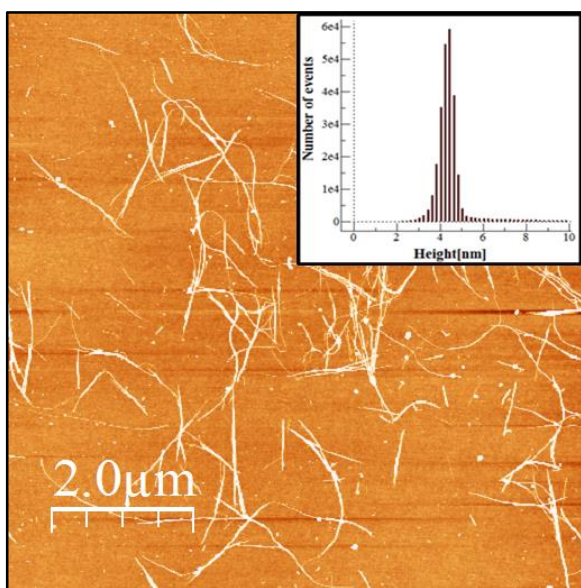
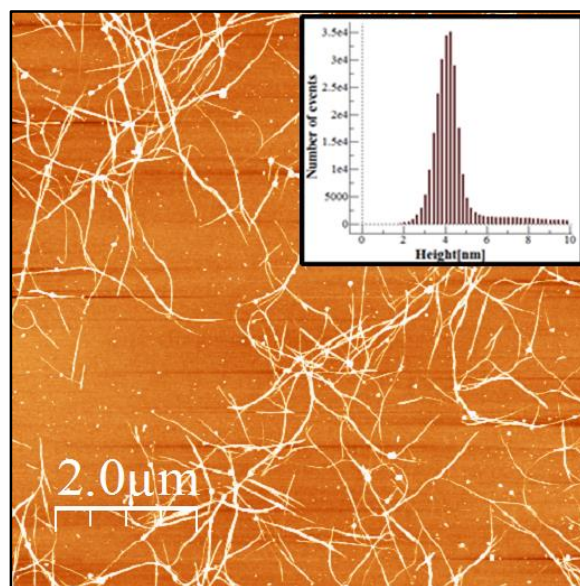


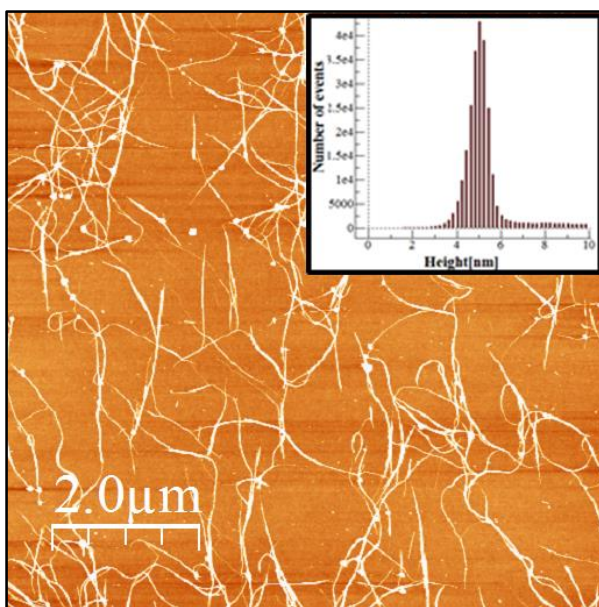
Figure 4.6: I_{on}/I_{off} ratios for purified SWNT suspensions using; a) OTS; b) Phenyltriethoxy silane; c) n-propyltriethoxy silane; d) 3-APTES. 3-APTES showed the highest on current and lower off current resulting in highest I_{on}/I_{off} ratio vs. lowest on current for Phenyltriethoxysilane resulting in lowest I_{on}/I_{off} ratios.



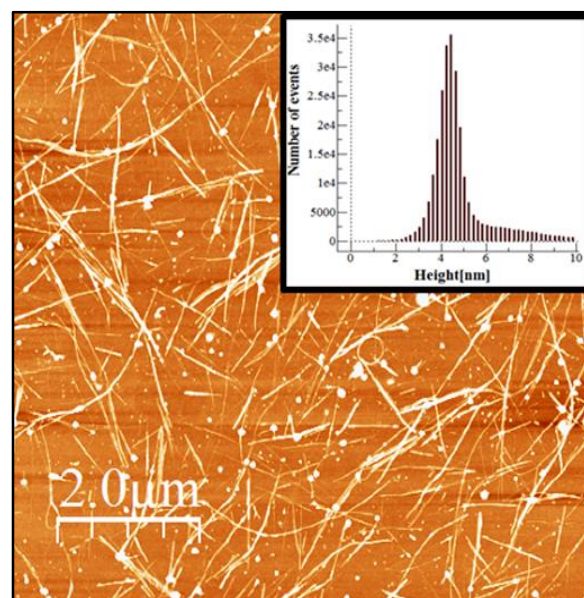
a)



b)



c)



d)

Figure 4.7: AFM images of SWNT network using different self-assembled monolayers; a) OTS showing height of 5.04nm; b) n-propyltriethoxy silane showing height of 5.44nm and; c) phenyltriethoxy silane showing height of 5.47nm; d) 3-APTES showing height of 6.14nm. SWNT network with 3-APTES shows increased height indicating adsorption of nanotubes plus

impurities onto the surface. Whereas decreased height of SWNT network with OTS is due to the less adsorption of SWNTs on to the surface.

Table 4.1: The average I_G/I_D ratios observed for different self-assembled monolayers for SWNT depositions.

	OTS	n-propyl	Phenyl
Deposition	111.94±11.25	102.31±12.72	115.69±14.2

Table 4.2: The average I_G/I_D ratios for SWNT deposits and suspension for acidic, basic, and pristine SWNTs.

I_G/I_D Ratios	Purified SWNT 3 APTES	Acidic SWNT 3 APTES	Basic SWNT 3 APTES
Suspension	75.02±2.23	69.4±2.53	50.49±5.87
Deposition	115.61±14.47	89.15±8.93	84.71±12.1

Table 4.3: AFM data of the effect of different silane on low density SWNT deposits.

	3-APTES	3-APTES (Acidic suspension)	3-APTES (Basic suspension)	OTS	n-propyl	Phenyl Silane
# SWNTs/ μm^2	0.790	0.369	0.328	0.416	0.375	0.422
Average Height (nm)	1.69 \pm 0.12	3.01 \pm 0.642	2.90 \pm 0.445	3.13 \pm 0.780	2.30 \pm 0.69	2.63 \pm 0.231
RMS Roughness	0.94 \pm 0.055	1.09 \pm 0.176	1.04 \pm 0.0679	0.77 \pm 0.170	0.69 \pm 0.095	0.83 \pm 0.064

Table 4.4: AFM analysis and I_{on}/I_{off} ratios for different silanes. The table describes the increase in I_{on}/I_{off} ratios for 3-APTES with decreased in R value as compared to the lowest I_{on}/I_{off} ratios for phenyltriethoxysilane with higher R value.

	3-APTES	OTS	Phenyl	n-propyl
Average Resistance	1.53 ± 0.92	1.85±0.062	2.04±0.040	1.71±0.042
Average I_{on}/I_{off} ratios	8.22±0.47	5.26±0.20	2.23±0.04	4.34±0.070
Average Height (nm)	6.14±0.78	5.04±0.47	5.44±0.65	5.47±1.36
Average RMS roughness	2.79±0.14	1.72±0.21	2.57±0.13	2.41±0.08

CHAPTER 5

EFFECT OF SONICATION ENERGY ON AQUEOUS SUSPENSIONS OF SINGLE- WALLED CARBON NANOTUBES (SWNTs)

Bhatt.N.P; Vichchualada; Lay.M.D. To be submitted to *Analyst (The Royal Society of Chemistry)*

5.1 ABSTRACT

This report presents the effect of sonication power on the average length of SWNTs in aqueous suspensions. Different sonication powers have been used to disperse SWNT bundles into the suspension and low g purification cycles for purifying the suspension. The low g centrifugation cycles produced SWNT suspensions (supernatant) without any bundles, amorphous carbon and catalyst nanoparticles. This allows for direct determination of effect of sonication power without the interference of impurities. The effect of the sonication power on the remaining bottom suspension was also analyzed. The supernatant was characterized by spectroscopic techniques. UV-vis and NIR measurements describes about the effect of sonication power on unbundling of SWNTs. Raman spectroscopy mentions about the defects density on the SWNTs due to sonication and atomic force microscopy shows the average length of SWNT network due to sonication.

5.2 INTRODUCTION

Single walled carbon nanotubes are emerging as potential candidates for wide range of applications due to their unique mechanical, electrical and physical properties. The ability to form suspensions is of critical importance in applications like transistors,¹ diodes,² sensors,³ capacitors etc. Control over average length and its concentration is very important in applications with low density network. However, as-produced soot presents a challenge as it consists mainly of amorphous carbon, catalyst particles and globular impurities. Due to this large heterogeneity in the material, the SWNTs are obtained in bundles and in varying purities. AP soot interacts strongly with one another through van der Waals forces and thus exist in large aggregates such as bundles. So they key challenge for the SWNTs is to obtain a homogeneous dispersion while maintaining its intrinsic properties.

The ability to disperse SWNTs has been demonstrated for different materials, including surfactants,⁴ polymers⁵ and organic materials.⁶ In the past decade, lots of efforts have been made to develop techniques to disperse in a surfactant. The techniques are categorized into covalent and non-covalent functionalization. In covalent functionalization, oxidation of carboxyl groups are formed on the SWNT surface, followed by the grafting of organic moieties onto the SWNTs.⁷ This disrupts the electrical, mechanical and optical properties.⁸ Non-covalent functionalization uses dispersants such as surfactants, organic solvents, polymers to disperse SWNT suspension, without interfering with the electronic properties of SWNTs.⁹

Dispersion of single-walled carbon nanotubes with the aid of surfactants is a common procedure for generating homogeneous carbon nanotube solutions. The tendency to remain in aggregates is a major hurdle and this is due to the van der Waals forces between nanotubes, in combination with their high surface area and high aspect ratio, often leads to significant

agglomeration. Sonication in presence of a surfactant is a common method to disperse carbon nanotubes in solution. Sonication in combination with surfactants is used frequently to disperse, break, or de-bundle SWNT aggregates.¹⁰ The unbundling of SWNTs in aqueous solution is due to the hydrophilic/hydrophobic interactions, in which the hydrophobic tail of the surfactant molecule adsorbs on the surface and hydrophilic head associates water for dissolution.¹¹ This allows for encapsulation of surfactant molecules forming either cylindrical or hemispherical micelles around the hydrophobic SWNTs.

Smalley and his group¹² obtained individual nanotubes, each encapsulated in a cylindrical micelle, by sonicating an aqueous dispersion in SDS and then centrifuging to remove bundles, ropes and residual catalysts. To form these individual nanotubes, they dispersed SWNTs via high probe sonication at 540W and ultracentrifuge at 122,000g for 4 hours. This led to the suspension of unbundled nanotubes with average length of 130nm.¹² This process works effectively in producing unbundled suspensions. Lot of studies in the literature have mentioned the sonication as a way to achieve exfoliation of SWNTs.¹³

Another report by Lu and his group indicated that the use of higher sonication power at 17W yields high concentration of defects such as bending and buckling, observed by electron micrographs. The further effect of ultrasound shows stripping of outer graphite layers thinning the nanotubes.¹⁴ Cheng Ma and coworkers¹⁵ reported defects in nanotubes using high probe sonication between 100-500 W. This was observed as a larger defect band in Raman spectroscopy. Using different sonication time have been shown as a parameter to assist in SWNT dispersion.^{16, 17} However, other literature works^{18, 19} reported that degree of SWNT dispersion is dependent on the sonication energy rather than the time. The sonication energy is defined in Watts/mL. Insufficient supply of sonication energy could lead to insufficient dispersion of SWNTs, while excessive

energy can lead to low aspect ratios nanotubes. So it is necessary to investigate the effect of sonication energy in surfactant assisted SWNT dispersion. So this report presents series of dilutions from the SWNT suspensions while using different power density at 0.1W/mL, 0.2W/mL, 0.3W/mL, and 0.4W/mL and then purifying it by using non-oxidative treatments. This method of using lower sonication power helps minimize the defects and can yield high aspect ratio nanotubes as a result. The suspensions were characterized with scanning probe and spectroscopic techniques. UV-vis and NIR showed the effect of unbundling in SWNT suspension, while Raman spectroscopy determines the defect damage at each sonication power. AFM analysis on the deposits was used to determine the average length of the nanotubes at each sonication power.

5.3 EXPERIMENTAL PROCEDURE

5.3.1 Formation of SWNT suspensions

A series of SWNT dilutions were made by dispersing 10mg of AP arc discharge soot (Carbon Solutions Inc.) in 10ml of 1% SDS (Sodium dodecyl sulfate) (J.T.Baker) via probe sonication for 30 min at different power density : 0.1W/mL, 0.2W/mL, 0.3W/mL, and 0.4W/mL which imparted 5kJ, 10kJ, 16kJ, and 21kJ of energy to the suspension respectively. The SWNT concentrations after dilutions were 0.01mg/mL, 0.025mg/mL, 0.05mg/mL, 0.075mg/mL and 0.1mg/mL. Each of these diluted SWNT suspensions at different concentrations were purified by four cycles for 45 min at 18,000G (Beckman, Microfuge). The solution was then characterized via spectroscopic techniques: UV-vis –NIR, Raman spectroscopy and AFM analysis.

5.3.2 Standard curve of suspensions

1mg/mL purified SWNT suspension was made in 1% SDS. The purified suspension was filtered through the 0.2 micron filter paper in a glass crucible. A series of dilutions were made from the purified suspension with SWNT concentration of 0.01mg/mL, 0.025mg/mL, 0.05mg/mL, 0.075mg/mL and 0.1mg/mL. A calibration curve will be used to accurately determine the extinction coefficient of the purified SWNTs.

5.3.3 Effect of Sonication power on SWNT suspensions via UV-vis NIR, Raman spectroscopy and AFM analysis

UV-Vis-NIR spectroscopy (Cary, 5000) was performed using a quartz cell with a path length of 1 mm. Raman spectroscopy (Thermo Scientific, DXR SmartRaman) was performed on suspensions in a sealed capillary tube and on SWNT deposits. A CCD detector was used to record spectra obtained using a 532 nm diode laser excitation source. Suspensions were analyzed with a 10 X objective and a source intensity of 10 mW at the sample, while for SWNT deposits, a 50 X objective with 7 mW intensity at the samples at different concentrations. To analyze the effect of sonication power on the average length, height and RMS roughness on the surface, deposits were formed using the Si/SiO₂ wafer by the process of Laminar Flow deposition explained in previous works.²⁰ Briefly, the Si/SiO₂ wafers were cleaned with compressed CO₂. Prior to SWNT deposition, the substrates were modified with different self-assembled monolayers for 45 min, firstly immersing the substrates in a solution of 3-aminopropyl triethoxysilane (99%, Sigma Aldrich) and ethanol (99.5%, absolute 200 proof, ACROS). In order to ensure that only one monolayer of the silane remained, substrates were washed with copious ethanol, water, and then dried in a stream of N₂ gas. Then, they were cleaned with compressed CO₂.

5.4 RESULTS AND DISCUSSION

The UV-vis spectra obtained for different sonication powers were similar in appearance. The absorbance of all the concentrations increase with increase in the sonication power. The starting concentration of all the solutions was 1mg/mL (SWNT soot). The solution sonicated at the highest power density (0.4W/mL imparting 21kJ of energy) had the highest absorbance for all the SWNT concentrations. Whereas, the ones treated with 0.1W/mL (5kJ energy) sonication power had the lowest absorbance. The increase in absorbance with sonication power indicates that the increase in sonication energy which helps SWNTs disperse and exfoliate. The NIR region shows the unbundling of SWNTs as the spectral features become more resolved. The interband transitions were evident when NIR region was normalized at 1010nm for 21kJ. The peaks were observed between 900nm (M_{11}) and 1150nm (S_{22}) for all the sonication powers. The peaks increase in size with the increase in sonication energy for SWNT 0.1mg/mL. Similar trend is observed for the other four (0.01, 0.025, 0.05, and 0.075 mg/mL) SWNT concentrations. However, at 0.1W/mL (5kJ energy) the peak is relatively smaller as compared to the 10, 16, and 21kJ as shown in Fig 5.1. This indicates that may be the lowest sonication power is insufficient to unbundle SWNTs for larger volumes.

In addition to showing quantitative measurements, UV-Vis NIR was also used to calculate the SWNT concentration at a 600nm. To determine the concentration of each SWNT suspension after purification, several standard solutions of known SWNT concentrations were analyzed. An absorbance at 600 nm yields a linear relationship between SWNT concentration and absorbance. This is due to the lower scattering efficiency at 600 nm and also that it falls between the metallic and semiconducting bands for SWNTs. The extinction coefficient is the slope of the Beer's law plot constructed for diluted SWNT concentrations. The graph of concentration before

centrifugation vs. concentration after centrifugation is linear (Fig 5.2). This indicates that the concentration of purified suspension is in direct proportion with the starting concentrations. This holds true of all the sonication powers. The slope is the fraction of SWNTs left after centrifugation. The slope increases with the increase in the energy (from 0.066 at 5kJ to 0.141 at 21kJ) at four centrifugation cycle. This indicates that lower percent of bundles remain in the solution after four processing steps at 5kJ as compared to 21kJ.

5.4.1 Effect of sonication power on Raman Spectroscopy measurements

The Raman spectra of SWNTs is similar to the spectra for graphite since both species are composed of sp^2 hybridized carbon; both display a G-band around 1500 cm^{-1} . The disorder band, which can be observed around 1300 cm^{-1} , is caused by defects in the C lattice. The I_G/I_D ratios measure the quality of SWNT suspensions with the change in sonication power. The intensity of the G band increases with the higher sonication power, indicating greater dispersibility of nanotubes in the suspension. However, the D band also increases with greater sonication power indicating that defects are introduced with higher sonication energy (Figure 5.3). Therefore the ratio of I_G/I_D eventually decreases as the power density increases therefore increases the energy imparted to the suspension. At 5kJ, 10kJ, 16kJ, and 21kJ the I_G/I_D ratios increases from the lowest SWNT concentration to the highest (0.025mg/mL to 0.1mg/mL) for all the centrifuge cycles. This is due to the fact that bundles are isolated towards to the bottom of the centrifuge tube, leaving the supernatant with unbundled and high aspect ratio SWNTs. But the I_G/I_D ratios at 5kJ are higher compared to the 21kJ indicating that the lowest power density produced least defects on the SWNTs (Table 5.1). This can be confirmed by UV-vis NIR spectroscopy, which shows that the unbundling of the SWNTs was the lowest at 5kJ.

The length and density of SWNTs affects the electronic properties of SWNT network. The formation of these networks is dependent on the ability to form unbundled high aspect ratios SWNT suspension with average length's and densities. AFM is an indispensable technique that shows the quality of SWNT formed during the deposition process. The future work will be to perform AFM analysis of the SWNT substrate and observing the effect of sonication power on length and density of SWNTs.

5.4.2 Determination of extinction coefficient for purified SWNTs

UV-vis spectroscopy has proven to be an efficient analytical method for monitoring SWNT concentration in SDS solution. The extinction coefficient for purified SWNTs was determined by the Beer's law calibration curves. The calibration curve for AP (as produced) soot and purified filtered SWNTs have a different slope as shown in Fig 5.4. This indicates that the concentration of SWNTs changed since absorptivity is constant for SWNTs at same wavelength. So the actual concentration of filtered SWNTs is calculated using the calibration curve equation of AP soot. The slope of the graph is 0.0878 (constant change factor). It can also be calculated by dividing the filtered SWNT slope by AP soot slope ($0.4312/4.909$). This indicates that only 8% of the SWNT material remained as unbundled nanotubes after the filtration process.

5.5 CONCLUSIONS

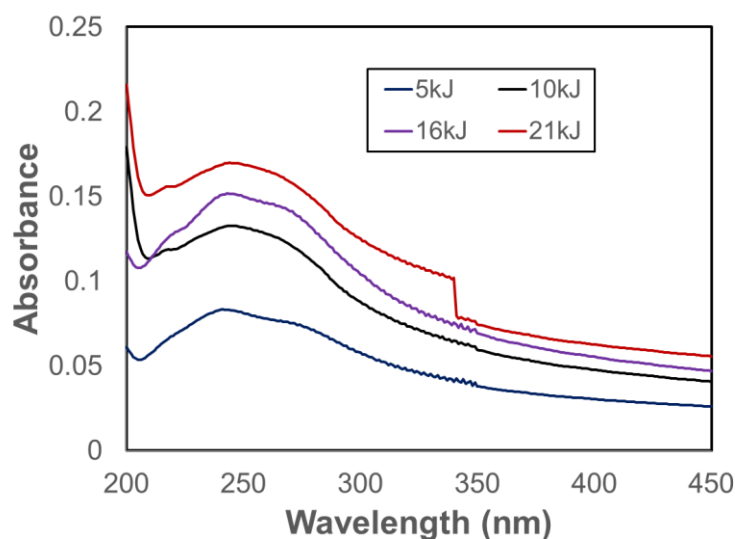
As-produced SWNTs consists of bundles which are held together by Van der Waals forces. Sonication energy is required to break those bundles in the suspension and allow the SWNTs to disperse in surfactants without any mechanical damage to the nanotubes. The report showed that lower sonication power is insufficient to unbundle nanotubes, whereas highest sonication power showed unbundled nanotubes in the NIR region, but Raman spectroscopy showed damage to the SWNTs yielding lower I_G/I_D ratios. The calibration curve from the series of dilutions for purified

SWNTs allowed us to accurately determine the extinction coefficient of filtered SWNTs. This can be used as a standard curve of suspensions formed from purified suspensions. This can be used in future for studying the concentration of SWNTs in any suspension.

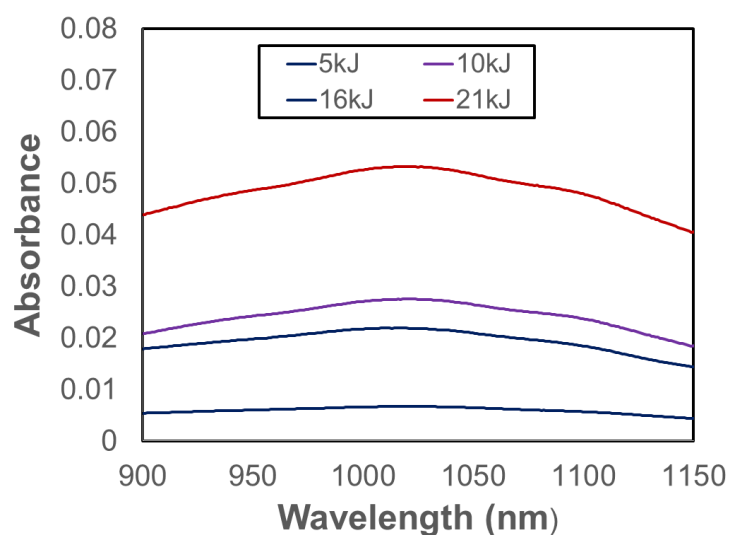
5.6 REFERENCES

1. Zhou, C.; Kong, J.; Dai, H. *Applied Physics Letters* **2000**, 76, (12), 1597.
2. Lee, J. U. *Applied Physics Letters* **2005**, 87, (7), 073101-073101-3.
3. Zhao, Q.; Gan, Z.; Zhuang, Q. *Electroanalysis* **2002**, 14, (23), 1609-1613.
4. Vaisman, L.; Wagner, H. D.; Marom, G. *Advances in Colloid and Interface Science* **2006**, 128–130, (0), 37-46.
5. Park, C.; Ounaies, Z.; Watson, K. A.; Crooks, R. E.; Smith Jr, J.; Lowther, S. E.; Connell, J. W.; Siochi, E. J.; Harrison, J. S.; Clair, T. L. S. *Chemical Physics Letters* **2002**, 364, (3), 303-308.
6. Ausman, K. D.; Piner, R.; Lourie, O.; Ruoff, R. S.; Korobov, M. *The Journal of Physical Chemistry B* **2000**, 104, (38), 8911-8915.
7. Yamamoto, T.; Noda, S.; Kato, M. *Carbon* **2011**, 49, (10), 3179-3183.
8. Barone, P. W.; Baik, S.; Heller, D. A.; Strano, M. S. *Nat Mater* **2005**, 4, (1), 86-92.
9. Star, A.; Liu, Y.; Grant, K.; Ridvan, L.; Stoddart, J. F.; Steurman, D. W.; Diehl, M. R.; Boukai, A.; Heath, J. R. *Macromolecules* **2003**, 36, (3), 553-560.
10. Islam, M. F.; Rojas, E.; Bergey, D. M.; Johnson, A. T.; Yodh, A. G. *Nano Letters* **2003**, 3, (2), 269-273.
11. Wang, H. *Current Opinion in Colloid & Interface Science* **2009**, 14, (5), 364-371.
12. O'connell, M. J.; Bachilo, S. M.; Huffman, C. B.; Moore, V. C.; Strano, M. S.; Haroz, E. H.; Rialon, K. L.; Boul, P. J.; Noon, W. H.; Kittrell, C. *Science* **2002**, 297, (5581), 593-596.
13. Grossiord, N.; Regev, O.; Loos, J.; Meuldijk, J.; Koning, C. E. *Analytical Chemistry* **2005**, 77, (16), 5135-5139.

14. Lu, K. L.; Lago, R. M.; Chen, Y. K.; Green, M. L. H.; Harris, P. J. F.; Tsang, S. C. *Carbon* **1996**, 34, (6), 814-816.
15. Ma, P.-C.; Siddiqui, N. A.; Marom, G.; Kim, J.-K. *Composites Part A: Applied Science and Manufacturing* **2010**, 41, (10), 1345-1367.
16. Matarredona, O.; Rhoads, H.; Li, Z.; Harwell, J. H.; Balzano, L.; Resasco, D. E. *The Journal of Physical Chemistry B* **2003**, 107, (48), 13357-13367.
17. Moore, V. C.; Strano, M. S.; Haroz, E. H.; Hauge, R. H.; Smalley, R. E.; Schmidt, J.; Talmon, Y. *Nano Letters* **2003**, 3, (10), 1379-1382.
18. Yang, Y.; Grulke, E. A.; Zhang, Z. G.; Wu, G. *Journal of Applied Physics* **2006**, 99, (11), 114307.
19. Yu, J.; Grossiord, N.; Koning, C. E.; Loos, J. *Carbon* **2007**, 45, (3), 618-623.
20. Bhatt, N. P.; Vichchulada, P.; Lay, M. D. *Journal of the American Chemical Society* **2012**, 134, (22), 9352-9361.



a)



b)

Figure 5.1: a) UV- vis spectra of SWNT suspension at different power density with different joules of energy, indicating an increase in absorbance with sonication power; b) For NIR spectra, of S_{22} transition for semiconducting SWNTs, the SWNTs suspension was normalized at 1010nm for 21kJ. The resolved peaks with higher energy due to interband transitions is quite evident, indicating unbundled SWNTs in a suspension.

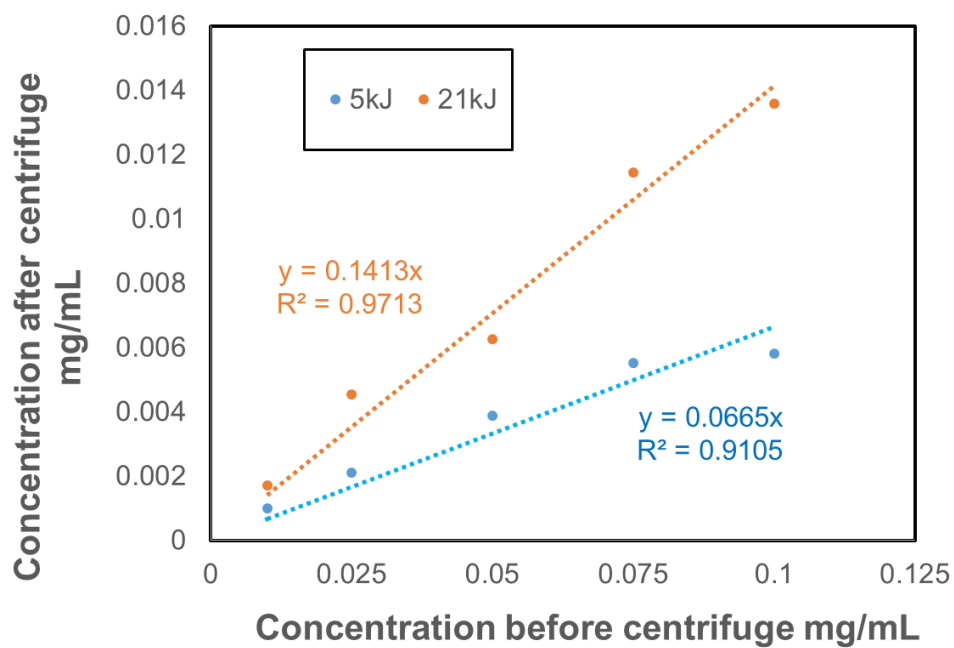


Figure 5.2: UV-vis spectroscopy was used to determine the concentration of SWNT suspension.

The plot of concentration of purified suspension vs. uncentrifuge suspension at 3W and 12W showed the fraction of SWNT remained after purification.

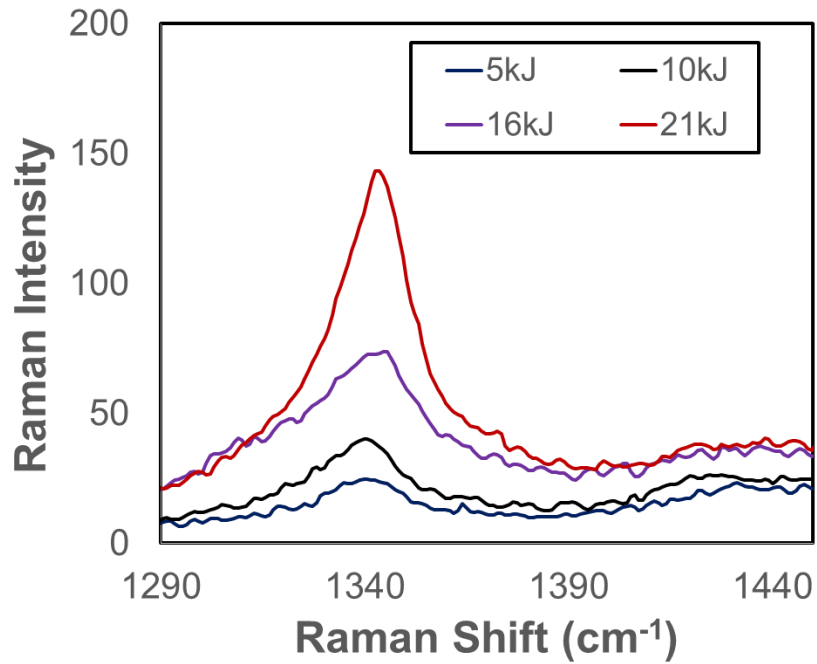


Figure 5.3: D-band of the Raman spectra showing increase in defect density as the sonication power increased, indicating more defects are introduced at higher sonication power leading to lower I_G/I_D ratios.

Table 5.1: I_G/I_D ratios of SWNT deposit at different sonication power.

I_G/I_D Ratios	3W	6W	9W	12W
0C	57.29±1.22	55.72±2.55	43.38±3.03	34.44±1.42
4C	102.19±5.58	94.34±6.76	90.628±0.789	85.69±4.67

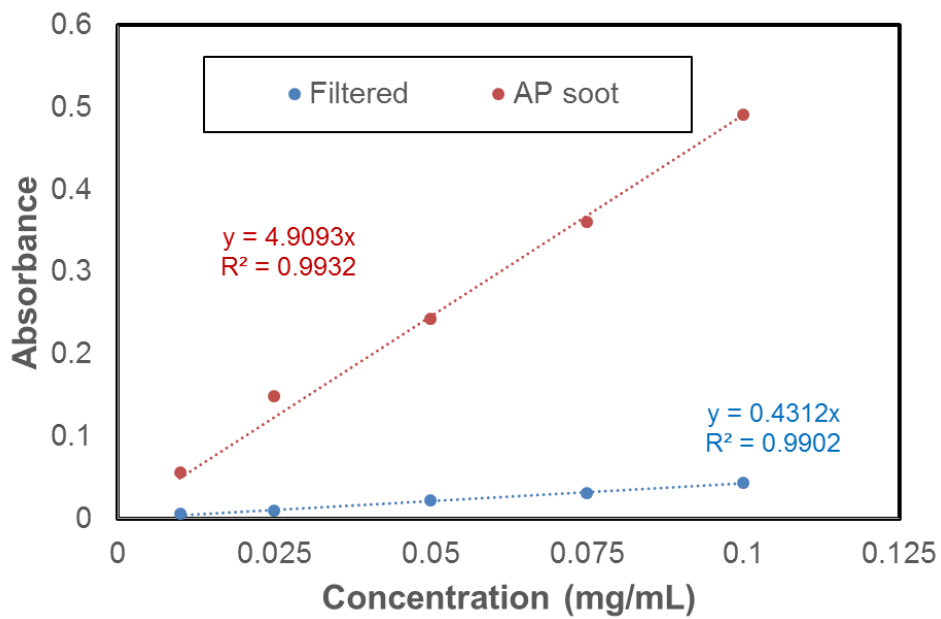


Figure 5.4: Calibration curve using Beer's Law of purified filtered SWNT suspension and as-produced (AP) soot.

CHAPTER 6
CONCLUSIONS AND FUTURE WORK

6.1 CONCLUSIONS

SWNTs play an important role in nanotechnology research due to their unique properties. Depending on their chirality, they can be seen as either semi conductive or metallic conductors. Single-walled carbon nanotubes are been extensively used in many electrical applications, but their impurities have shown deleterious effect on the performance of electronic devices. So studies presented in this dissertation were to obtain the understanding of using different purification techniques for SWNTs (low g centrifugation and density gradient purification) and measuring the electrical properties of SWNT network using different self-assembled monolayers. The studies were investigated by spectroscopy and scanning probe microscopy.

Non-destructive, non-oxidizing purification technique using low g centrifugation cycle was demonstrated. Two important challenges were addressed: To remove residual catalyst nanoparticles and amorphous carbon without damaging SWNTs. To form suspensions with unbundled high aspect ratio SWNTs knowing average length and density. High aspect ratio nanotubes with average length in excess of $2\mu\text{m}$ was achieved. AFM images showed that iterative processing method yielded unbundled, long SWNTs with the average height of 1.31nm , which is consistent with the height of one SWNT. Relative purity of SWNTs was observed by measuring the ratio at $A(242\text{nm})/A(600\text{nm})$. The ratios increased with increase in the processing step, indicating that the SWNT suspension is enriched by removing impurities and small bundles. Raman Spectroscopy showed that the purity of SWNT deposit on the substrate was higher as compared to the suspension, due to the greater translational diffusion coefficient of shorter nanotubes leaving them in the suspension leading to higher I_G/I_D ratios for the deposits.

Density gradient studies use additional reagents for the purification process, which are difficult to remove; a requirement for electrical applications. So using sucrose as a density gradient

medium does not require any reagents and was used in the place of iodixanol. Sucrose density gradient along with one step purification process produce higher yield of SWNTs. The level of purification was similar to the ones observed with multiple centrifugation cycles. Individual nanotubes were observed for SWNT suspension with sucrose solutions (water) vs. bundled nanotubes were obtained for the sucrose solutions made with SDS. This is due to the higher viscosity of SDS in sucrose solution, leading to agglomeration. SWNT with high aspect ratios with lengths close to $2\mu\text{m}$ was observed. Long, purified, unbundled SWNTs were obtained with just one processing step. So density gradient studies can be used in near future to produce large scale purified SWNT solutions, which can help improve applications in many fields.

Aligned and orthogonal SWNT networks were investigated by depositing carbon nanotubes on self-assembled monolayer substrates. SWNT networks were formed by Laminar Flow Deposition and characterized by AFM and Raman spectroscopy. Electrical measurements were obtained by the transistor response curve using the semiconductor analyzer system. The $I_{\text{On}}/I_{\text{Off}}$ ratios show that aminosilanes favor the semiconducting nanotubes due to the electron donating amine group, whereas phenyltriethoxysilane favor metallic nanotubes due to aromatic ring structure. Pristine, homogenous and well-ordered SWNT arrays can be used in many electrical applications because they can maintain their intrinsic properties.

Lastly, to understand the dispersing of SWNT in SDS aqueous suspension, a series of SWNT suspensions were studied. Various sonication power were used during the SWNT dispersion. UV-Vis and Raman spectroscopy was used to characterize the suspensions. Lower power yields less bundles as compared to the highest power. The density of defect was higher at 12W than 3W due to the fact that the greater sonication power introduces defects in SWNTs.

Further work will be done by observing the effect of length on sonication power using AFM analysis.

6.2 FUTURE WORK

Studies on SWNT purification has been performed and are still flourishing. Using long unbundled SWNT suspension on SWNT network-based electronic devices have been used a lot. The studies presented herein lays the foundation for various future prospects involving SWNTs. The future of the research will be depositing SWNT network array on substrates which would result in reproducible high quality 2D networks. The efficiency of using SWNTs in electronic devices can be achieved by depositing nanoparticles on the SWNT network. The nanoparticles improve the overall performance of the device by reducing the effect of metallic SWNTs in network. This can also be achieved by observing the effect of varying the functional groups of the silane used to anchor the SWNTs to the surface. Electrostatic Force Microscopy or conductive AFM studies can be used to map the electrical pathways of 2D SWNT network.

Future research will also be focusing on improving techniques for SWNT dispersion especially with density gradient. This will be achieved by using different surfactants which can separate SWNTs better at lower concentrations. Further work will be on the effect of SWNT length with varying sonication power, so that we can achieve the goal of fabrication of clean reproducible SWNT networks. Other work will be varying the SDS concentration and observing the effect of SDS concentration on dispersion of SWNTs.